Check for updates

Aluminum–air batteries: current advances and promises with future directions

Bharti Rani, [ID] Jitendra Kumar Yadav, [ID] Priyanka Saini, [ID] Anant Prakash Pandey and Ambesh Dixit [ID] *

Owing to their attractive energy density of about 8.1 kW h kg^{-1} and specific capacity of about 2.9 A h g^{-1}, aluminum–air (Al–air) batteries have become the focus of research. Al–air batteries offer significant advantages in terms of high energy and power density, which can be applied in electric vehicles; however, there are limitations in their design and aluminum corrosion is a main bottleneck. Herein, we aim to provide a detailed overview of Al–air batteries and their reaction mechanism and electrochemical characteristics. This review emphasizes each component/sub-component including the anode, electrolyte, and air cathode together with strategies to modify the electrolyte, air-cathode, and even anode for enhanced performance. The latest advancements focusing on the specific design of Al–air batteries and their rechargeability characteristics are discussed. Finally, the constraints and prospects of their use in mobility applications are also covered in depth. Thus, the present review may pave the way for researchers and developers working in energy storage solutions to look beyond lithium/sodium ion-based storage solutions.

1. Introduction

The ever-growing energy demand, which is inherently coupled with the pressing need to address climate change, has propelled the world towards clean and green energy sources. However, although these renewable energy sources such as solar and wind are abundant and environmentally friendly, their

Advanced Material and Devices Laboratory (A-MAD), Department of Physics, Indian Institute of Technology, Jodhpur, Rajasthan, 342030, India. E-mail: ambesh@iitj.ac.in

intermittent nature poses a challenge in integrating them seamlessly into the existing energy grid.[1–4] In this scenario, electrochemical energy storage devices have emerged as the crucial missing link in the energy demand and supply chain. These devices may bridge the gap between generation and consumption, storing excess energy from renewable sources and releasing it when needed to ensure grid stability and reliability.[5–9] These electrochemical energy storage systems include various devices such as supercapacitors and rechargeable batteries.[10–13] Rechargeable lithium-ion (Li-ion) batteries

Bharti Rani is a PhD student, working under the supervision of Prof. Ambesh Dixit, in the A-MAD research group, Department of Physics, Indian Institute of Technology Jodhpur, India. She obtained her MSc Physics (2020) degree from Maharaja Ganga Singh University, Bikaner, India and her BSc Hons. Physics (2018) from University of Delhi (DU), New Delhi, India. She is currently engaged in the fabrication and characterization of energy storage systems that can be promising for post-lithium technology. Her current focus is mainly on aluminum-based storage systems including Al-ion batteries.

Bharti Rani

Jitendra Kumar Yadav is a 4th year doctoral student, working at Prof. Ambesh Dixit's research group (A-MAD laboratory), Indian Institute of Technology Jodhpur, India. He obtained his Master's Degree in Physics from Malaviya National Institute of Technology Jaipur, Rajasthan, India, in 2020 and his Bachelor's Degree specialised in Mathematics from Central University of Rajasthan, Ajmer, India, in 2018. His work is mainly focused on clean and green energy storage systems including batteries and supercapacitor, especially Fe-ion batteries.

Jitendra Kumar Yadav

have shown their potential and dominate the energy storage market, especially portable electronics and hybrid/electric vehicles, due to their high energy density and relatively low-weight characteristics.[14–16] However, their reliance on lithium, a limited resource, has spurred interest in multivalent metal-ion batteries, which use ions such as iron, magnesium, calcium, and aluminum, offering a higher charge density and potentially lower cost.[17–19] Nevertheless, both technologies are associated with many challenges, as follows: Li-ion batteries face safety concerns related to dendrite formation and thermal runaway, while multivalent metal-ion batteries grapple with electrode material limitations, electrolyte compatibility issues, and lower electrical conductivity.[20–22] Overcoming these hurdles will require innovative approaches in materials science,

electrolyte design, and manufacturing processes to unlock the full potential of both Li-ion and multivalent metal-ion rechargeable batteries for future energy storage applications.[20–25]

More interestingly, due to the high theoretical capacity and energy density of metal–air batteries, they have shown potential as alternatives to the currently dominating Li-ion batteries. Furthermore, the weight of metal–air batteries is also one of the exciting factors given that oxygen from air acts as the cathode material. Thus, in principle, this reduces the need for a cathode in these energy storage systems.[26–28] Generally, these batteries are equipped with metal as the anode and an air-penetrating current collector to complete the circuit.[29,30] The battery is vitalized with a suitable electrolyte between the metal and current collector to provide a medium for efficient ionic conduction. Presently, various metal–air batteries are the subject of research, aiming to find better alternatives to the existing Li-ion energy storage solutions.[31–33] Firstly, lithium has the highest theoretical energy density compared to conventional batteries, *i.e.* the lithium–air (Li–air) battery has an energy density of 13000 W h kg^{-1} but suffers from numerous challenges despite being rechargeable, unlike other air batteries. Furthermore, the operation of Li–air batteries is not convenient in a humid environment, which makes them unstable. Another challenge is the blockage of their porous current collector from residue. Moreover, there is still a lack of understanding of how catalysts work in the rechargeability of Li–air batteries. The penetration of CO_2 leads to the formation of alkali carbonate residues, which is another complex issue that needs to be addressed with these energy storage systems.[34–37] However, Li–air batteries have a significantly

Priyanka Saini

Priyanka Saini received her BSc from Pandit Deendayal Upadhyaya Shekhawati University (Rajasthan, Sikar) in 2018 and her MSc from Maharshi Dayanand Saraswati University (Rajasthan, Ajmer) in 2021. She is currently a Doctoral student at the Indian Institute of Technology Jodhpur (Rajasthan, Jodhpur), working under the supervision of Prof. Ambesh Dixit. Her current research focuses on fabricating nano-engineered materials for energy storage applications.

Anant Prakash Pandey

Dr Anant Prakash Pandey completed his undergraduate studies, graduate studies, and PhD at Banaras Hindu University. He currently works at IIT Jodhpur as a Post Doctoral Fellow. His area of expertise is the synthesis of 2-D materials and porous carbonaceous materials for electrochemical and hydrogen storage technologies. His current areas of focus are hybrid supercapacitors and metal-ion batteries due to their improved power density and storage capacity.

Ambesh Dixit

Ambesh Dixit is a Professor at IIT Jodhpur, India, and has more than 15 years of experience in computational and experimental functional materials physics. His particular emphasis is on the development of functional materials for various technologies, including energy, water, and health together with next-generation electronic devices such as resistive random access memories (RRAM) for neuromorphic computing, chemical, biological, and nuclear sensors. His current interest in energy includes hydrogen generation/storage, lithium/sodium and beyond lithium/sodium electrochemical energy storage for mobility applications. He is the first one in the scientific community to show that iron vanadate ($FeVO_4$) is an intrinsic multiferroic system. He has co-authored (i) Nanotechnology for Defence Applications (Springer) and (ii) Nanotechnology for Rural Development (Elsevier) and co-edited three books on Solar Energy (Springer). He is an Editorial Board member of "Vacuum" Elsevier.

higher energy density than their lithium-ion counterparts, translating to a longer range for electric vehicles and extended runtime for electronics. Nevertheless, the associated challenges remain the same, thus limiting their commercial use to date. These batteries utilize reactive lithium metal anodes and require open designs for air intake, raising safety concerns. Additionally, issues related to the electrolyte stability, cathode clogging, and overall cycle life hinder their practical use. In this scenario, switching from Li–air batteries is crucial for sustainable future energy technology.[29,38–41]

Another metal–air battery that has emerged as an attractive alternative is the zinc–air battery due to its non-toxic nature and ease-of-fabrication under normal conditions. However, it is also associated with some challenges, such as dendrite formation in the zinc anode during multiple charge–discharge cycles, non-uniform dissolution due to precipitation of zinc residue, limited solubility of oxygen, and high overpotential.[42–47] Similarly, Fe–air batteries have also been explored due to their many advantages, including the abundance of iron and low cost, making them potentially cost-effective for large-scale energy storage applications. However, Fe–air batteries face certain challenges such as limited rechargeability, low efficiency due to the sluggish oxygen reduction kinetics, and issues related to iron anode degradation and electrolyte management.[48–50]

Recently, Al–air batteries have been widely explored due to the enormous advantage of the aluminum metal anode. Firstly,

aluminum is one of the most abundant elements in the Earth's crust, making it an attractive and sustainable choice for large-scale energy storage applications.[51–54] Secondly, aluminum has a higher energy density than zinc and iron, potentially surpassing existing metal–air batteries in specific energy and power (comparison of different metal anodes and metal–air batteries shown in Fig. 1 and Table 1, respectively). These attractive features make Al–air batteries promising for application in electric vehicles, grid-scale energy storage, and other critical areas due to their high energy density, potential for longer battery life, and environmental advantages over existing technologies. Thus, due to their potential as an alternative to existing battery technologies, Al–air batteries are the primary focus of this review.[55,56] Additionally, Al–air batteries have the potential to be more environmentally friendly, given that aluminum is readily recyclable and poses fewer environmental concerns compared to other metals.[57,58]

Aluminum-based batteries have undergone significant development since their inception, with notable milestones including the introduction of Al–MnO₂ batteries around the 1960s and subsequent efforts to improve their efficiency and applicability. Initially, Al was employed as an anode in the Buff cell in conjunction with a carbon cathode around 1857, then went on a long journey to the current form of Al-based energy storage systems, further explored based on Al–MnO₂ batteries, and later extended by Zaromb et al. to Al–O₂ batteries.[66] The
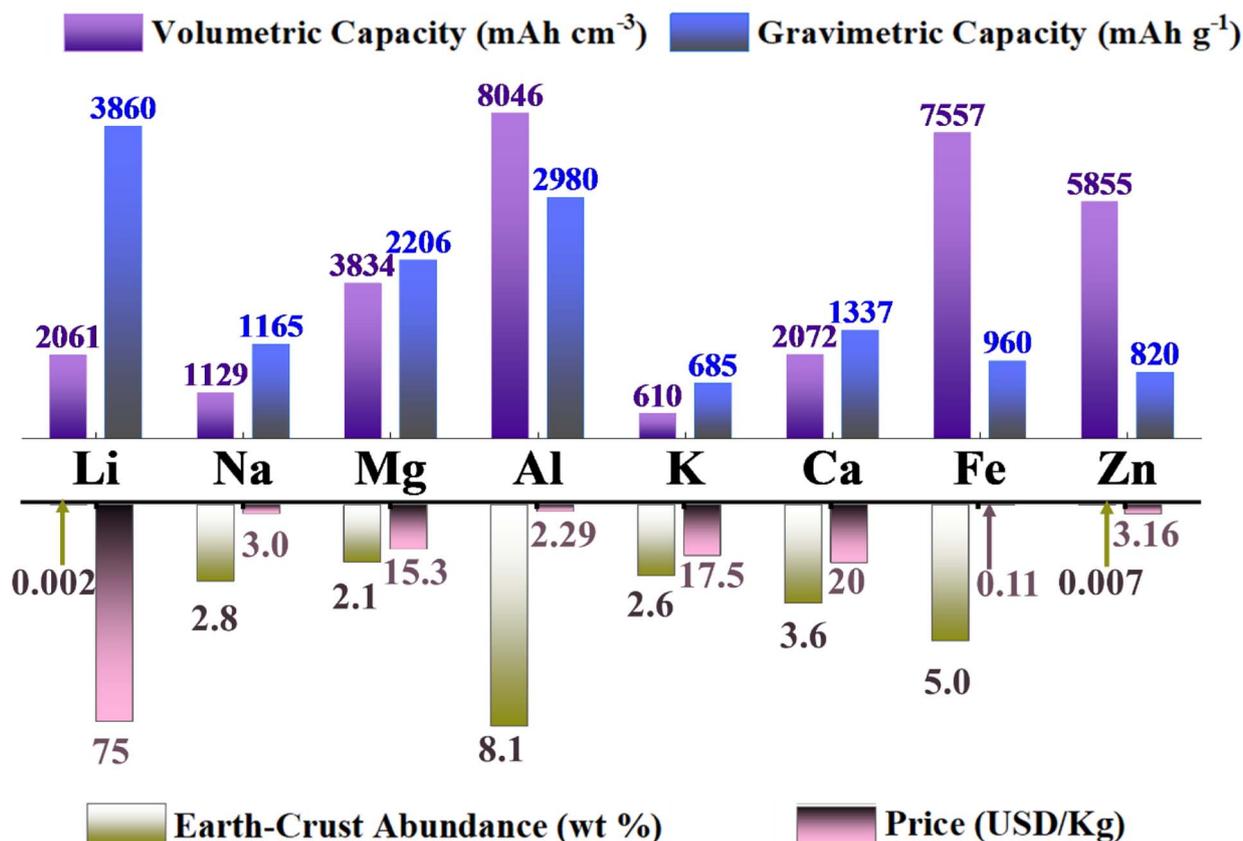

Fig. 1 A comparison of the gravimetric and volumetric capacity, Earth-crust abundance and cost of metal-anodes.

Table 1 Various metal–air battery systems and corresponding redox reaction with electrochemical parameters including O_2 intake

S. N.	Battery system	Redox reaction	Battery type	Theoretical OCP (V)	Practical OCP (V)	Theoretical specific energy (W h kg^{-1})	Ref.
1	Li–air	$2Li + O_2 \leftrightarrow Li_2O_2$	Secondary	2.96	2.4–2.8	3500	59
2	Na–air	$Na + O_2 \leftrightarrow NaO_2$	Secondary	2.27	2.2–2.3	1108	60
3	Al–air	$4Al + 3O_2 + 6H_2O \rightarrow 4Al(OH)_3$	Primary	2.71	1.2–1.6	2784	61 and 62
4	Mg–air	$2Mg + O_2 + H_2O \rightarrow 2Mg(OH)_2$	Primary	2.77	1.2–1.4	2848	61 and 63
5	Zn–air	$2Zn + O_2 \leftrightarrow 2ZnO$	Secondary	1.65	1–1.2	1086	63 and 64
6	Fe–air	$3Fe + 4O_2 \leftrightarrow Fe_3O_4$	Secondary	1.28	0.6–1.0	764	65

development over time is schematically summarized in Fig. 2(a).[67] To date, continuous efforts have been devoted to processing Al–O_2 batteries under ambient conditions, where ambient O_2 can be utilized as an efficient cathode in these systems. Recently, Al–air batteries have attracted attention for their use in strategic fields, i.e., marine and military applications, because of their high energy density. Given that their working mechanism is somewhat comparable to that of fuel cells, researchers have also started looking into that direction as well.[68,69] Nowadays, companies such as Phinergy and Alcoa are devoting their efforts to employing Al–air batteries for e-vehicles.[70,71] However, despite the reported advances, there are various constraints associated with these batteries, which should be addressed to make Al–air batteries fully-efficient for large-scale systems and mobility applications.[72–74]

The Al–air battery has been the subject of intense research for the past few decades, as has been observed from previous discussions related to its journey and timeline. Fig. 2(b) illustrates the publication trend and timeline of aluminum-based batteries sourced from the *Web of Science* database.[75] However, its associated issues such as corrosion, non-reversible reactions, stability, and self-discharge in a non-use state still prevent its successful transition from the laboratory to end-use. Aluminum corrosion in aqueous electrolytes is the biggest barrier in the application of the Al–air battery, which needs to be managed effectively for its potential use. The Al–air battery tends to form a passive oxide layer as a result of corrosion in the aqueous electrolyte, which is the main reason for its limited effective use even after various attempts have been made since Zaromb's research (i.e. from the early 60's) to date.[66,76–80] Therefore, various methodologies have been introduced in the literature to minimize its corrosion such as alloying of Al, surface coatings, introducing an additive in the electrolyte, and using water-in-salt and non-aqueous, such as different electrolyte media. Thus, this review provides a comprehensive analysis, including the underlying functioning mechanism and electrochemical interactions, to mitigate some of these issues. A thorough and detailed review is presented, emphasizing the current status of each constituent of the Al–air battery, including its anode, electrolyte, and catalyst. In addition, the potential rechargeability of Al–air batteries is also highlighted together with their geometrical structures/designs for efficient performances. The focus is the current prevailing obstacles and future prospects for Al–air batteries.

2. Aluminum: from material to vital component in batteries

Unlike lithium, aluminum, a non-noble metal, is not classified as critical in the reserves-to-production ratio. It is primarily extracted from bauxite, with concentrations in raw materials exceeding that of lithium by more than double, leading to significant volumes of soil being transported for mining.[73,81] The physical parameters for Al are listed in Table 2. The abundance of Al makes the effective use of Al anodes in different energy storage systems desirable. Al is commonly used as an efficient current collector in electrical energy storage systems, including lithium-ion batteries and supercapacitors. Although its mining process requires a large amount of energy, early implementation of a recycling infrastructure was undertaken to effectively reduce the energy consumption associated with aluminum production. The bond dissociation energy of the Al–O bond is $\sim$512 $\pm$ 4 kJ mol^{-1}, while that for the Al–Al bond is $\sim$186 kJ mol^{-1}.[82–84] Therefore, it is possible to achieve a 95% reduction in energy usage for the entire aluminum production process using aluminum scrap. Currently, recycled-secondary aluminum accounts for 35% of the total aluminum demand.[85,86]

Aluminum forms a crystal in the $Fm\bar{3}m$ space group, with the lattice parameter of $a = 4.04$ at ambient temperature and pressure.[73] The inherent structural integrity of Al and its extensive crystal structures make it an attractive candidate as the negative electrode in batteries. Additionally, its ability to form intermetallic phases with a wide range of crystal structures further enhances its potential for battery applications.[66,68,69,72–74,87–89]

One of the primary obstacles associated with the use of aluminum as a material for active batteries pertains to its strong affinity to oxygen, resulting in the oxidation of the newly formed aluminum surface when exposed to oxygen, water, or other oxidizing agents. Under standard conditions, the enthalpy of solid oxide formation is around 1675 kJ mol^{-1}, exceeding the enthalpy of the oxidation reaction of iron (Fe) to Fe_3O_4, which is around 1121 kJ mol^{-1}, and to Fe_2O_3 of $\sim$822.2 kJ mol^{-1}.[96,97] However, aluminum can rapidly generate a thin, uniform, and continuous amorphous Al_2O_3 surface layer of a few nanometers, i.e., $\sim$2 to 10 nm thickness.[87] According to Yang and team, the dielectric and amphoteric oxide layer exhibits liquid-like behavior when subjected to stress, hence demonstrating self-healing capabilities. The oxide layer exhibits compression
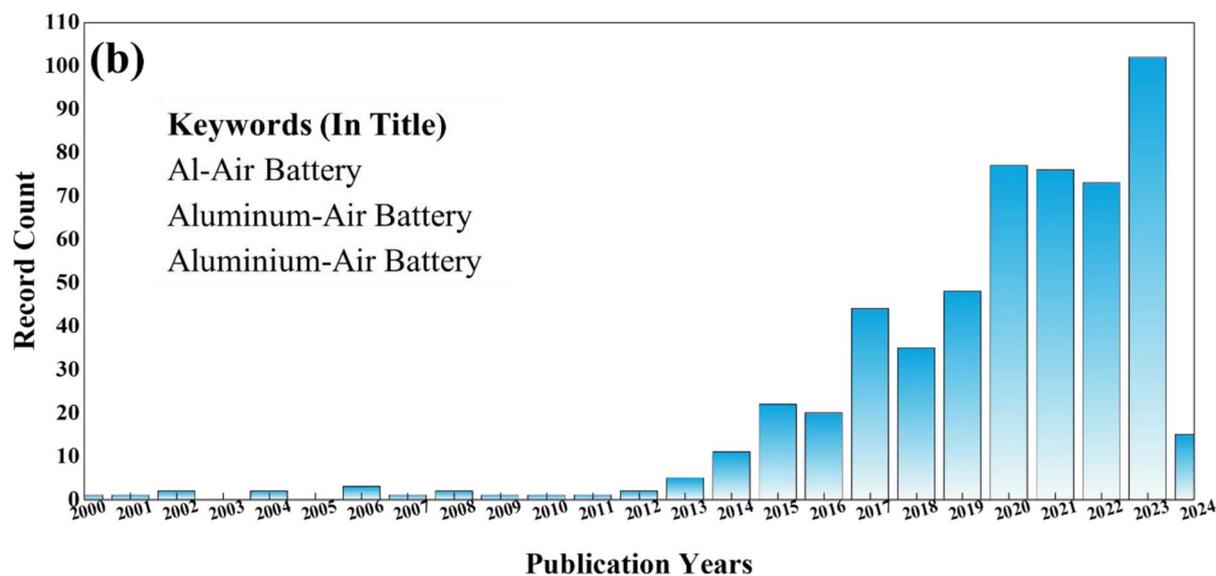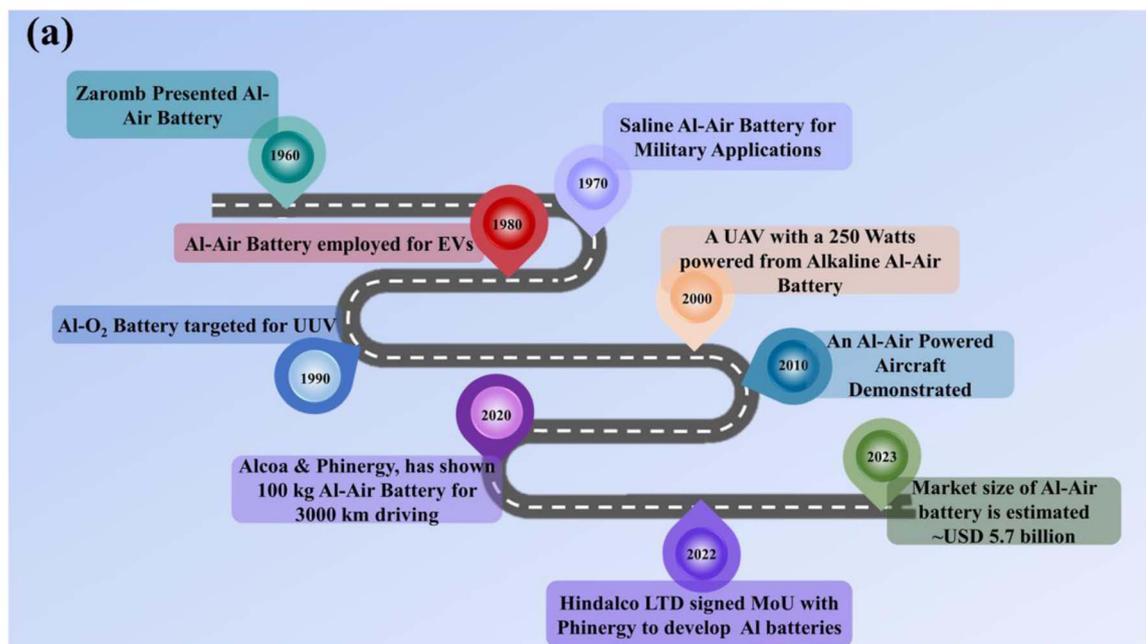
Fig. 2   (a) Timeline of aluminum-based batteries explaining the development of Al−air batteries with time. (b) Publication trend with the year for Al−air battery (source: https://www.webofscience.com/).[75]

relative to the underlying aluminum, which can withstand deformation without experiencing fracture.[98] This is why it provides several advantages when used as a current collector in lithium and other batteries. The formed oxide layer does not behave as a complete dielectric, but still provides electric conduction due to the tunneling effect even after adding up the contact resistance of the order of kΩ. Conversely, it creates an obstacle for the solvation of aluminum, which presents a difficulty in utilizing aluminum metal as a negative electrode.[80] Therefore, this inherent oxide impacts the electrochemical characteristics, specifically the overpotential of aluminum as an anode.[99] Typically, a secondary layer is created on the oxide layer

by reacting with the surrounding gases and liquids. The continuous oxide layer closest to the metal surface transforms into a hydroxylated film at the interface between the solid and gas. This becomes a barrier if the aluminum battery is intended to be electrically rechargeable.[100] Ultimately, the abundance, structural integrity, and ability to form intermetallic phases of aluminum make it a compelling candidate for battery applications despite challenges such as oxidation and oxide layer formation. Accordingly, addressing these challenges is crucial for realizing the full potential of aluminum-based batteries in industrial-scale energy storage solutions including both Al-ion and Al−air batteries.

Table 2 The physical/chemical characteristics of aluminum metal

Al-characteristics (parameters)	Value	Reference
Abundance (wt%)	8.1	90
Melting point (°C)	660.4	91
Atomic radius (Å)	1.431	48
Ionic radius (Å)	0.53	92
Covalent radius (Å)	1.25	93
$E°$ vs. SHE (V)	−1.66	91
HER onset potential vs. SHE (V)	−0.47	91
Bond dissociation energy Al–O (kJ mol^{-1})	512	82
Bond dissociation energy Al–Al (kJ mol^{-1})	186	82
Al–H bond energy (kJ mol^{-1})	285	91
Theoretical energy density (W h kg^{-1})	8100	94
Theoretical specific capacity (mA h g^{-1})	2980	95
Cost (US$ per kg)	1.9	92

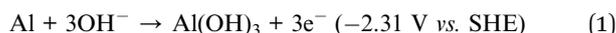# 3. Components of Al–air battery and reaction mechanism

The Al–air battery, as an energy storage system, consists of three major components, that is, anode, cathode, and electrolyte. In a battery, both electrodes are made up of solid materials, whereas in a fuel cell, the electrodes are gases. Alternatively, metal–air batteries such as Al–air batteries are a combination of both battery and fuel cell components. In these batteries, the anode consists of a solid metal electrode (Al), while the cathode utilizes the oxygen present in the air. Additionally, a current collector is required to complete the circuit from the cathode end, which is typically made of a porous mesh-like conductor. A catalytic layer is introduced on the surface of the current collector to accelerate the reaction mechanism.[101–104] Given that CO_2 from the ambient air reacts with alkaline electrolyte to form carbonate, which is detrimental to enhancing the potential, that's why a gas diffusion layer (GDL) is necessary to minimize this issue.[105] This layer prevents CO_2 while allowing O_2 to pass through to take part in the reaction. In contrast to the limitations associated with ambient air, purging with pure oxygen serves as a superior cathode. In this case, the battery is referred to as an Al–O_2 battery. This prevents carbonate formation and the entry of other impurities into the battery.[106–108] Besides, the electrolytes employed in these batteries are generally in liquid or semi-solid from, which can be ionic, aqueous, or polymer-gel.[109–111] The detailed description studies related to these components are discussed in the later sections/sub-sections. Here, in the following sub-sections, the electrochemical behavior and related reactions are explained to understand the mechanism of the Al–air battery.

3.1 Al anode corrosion and electrochemical reactions

The working mechanism of an Al–air battery is schematically explained in Fig. 3, with the associated chemical reactions at the respective electrodes and overall chemical reaction. Al–air batteries are metal–air batteries that utilize aluminum as the anode and ambient oxygen as the cathode. The anodic and cathodic half–cell reactions are summarized in eqn (1) and (2), respectively, together with the corresponding overall reaction in eqn (3). The corresponding electrochemical potential with respect to the standard

hydrogen electrode (SHE) potential is also mentioned next to these equations and seems feasible. However, several significant challenges are associated with the use of aluminum as the anode. The primary concern with aluminum as an anode is its tendency to undergo corrosion in an aqueous electrolyte. This corrosion process during the battery operation is essential given that it liberates electrons during the electrochemical reaction. However, excessive corrosion may lead to the fast degradation of the anode material, reducing the efficiency and lifespan of the Al–air battery. Further, a passivation layer of aluminum oxide (Al_2O_3) is formed on the surface of the anode during the corrosion process.[76] Although this passivation layer can protect the underlying aluminum from further corrosion, it also acts as a barrier to electron transfer, somewhat hindering the performance of the battery.[112] Additionally, the formation of a thick and non-conductive passivation layer can limit the accessibility of the electrolyte to the active aluminum surface, further reducing the efficiency of the battery. Aluminum hydroxide ($Al(OH)_3$) is a byproduct during the corrosion reaction between the aluminum anode and the hydroxide ions present in the alkali electrolyte media (eqn (1)). The hydroxides of aluminum will dissolve in the electrolyte in the presence of excess OH^- and may form aluminate gel. The dissolution of aluminum hydroxide can lead to the loss of the active anode material, resulting in capacity fading and reduced battery performance over time. Thus, controlling the dissolution of aluminum hydroxide and preventing the loss of the active material are crucial for maintaining the stability and longevity of Al–air batteries. The complete cell reaction in an Al–air battery undergoes the following reactions (1)–(3):[62]

Anodic half-cell reaction:

$$Al + 3OH^- \rightarrow Al(OH)_3 + 3e^- \ (-2.31 \text{ V } \textit{vs. } SHE) \quad (1)$$

Cathodic half-cell reaction:

$$O_2 + 2H_2O + 4e^- \rightarrow 4OH^- \ (0.40 \text{ V } \textit{vs. } SHE) \quad (2)$$

Overall reaction:

$$4Al + 3O_2 + 6H_2O \rightarrow 4Al(OH)_3 \ (2.71 \text{ V } \textit{vs. } SHE) \quad (3)$$

An aqueous alkaline electrolyte medium increases the likelihood of the hydrogen evolution reaction (HER), leading to the rapid depletion of the Al anode due to undesirable features.[79] HER causes Coulombic loss during discharge by the evolution of hydrogen gas from the anode surface, as mentioned in eqn (4) and (5). Usually, the aluminum anode in alkali solutions faces two significant problems, besides HER. The initial stage involves the formation of a passive oxide layer, which causes a reduction in the operational cell voltage, and later increases both the mass and charge transfer resistance, decreasing the open circuit potential (OCP).[111] Consequently, the realistic energy density and cell voltage are restricted. Another problem related to aluminum anodes is the rapid corrosion rate caused by removing the oxide layer. The theoretical OCP of 2.74 V has been observed practically in the range of 1.2 to 1.6 V due to corrosion and the formation of a passivating layer.[74] During an
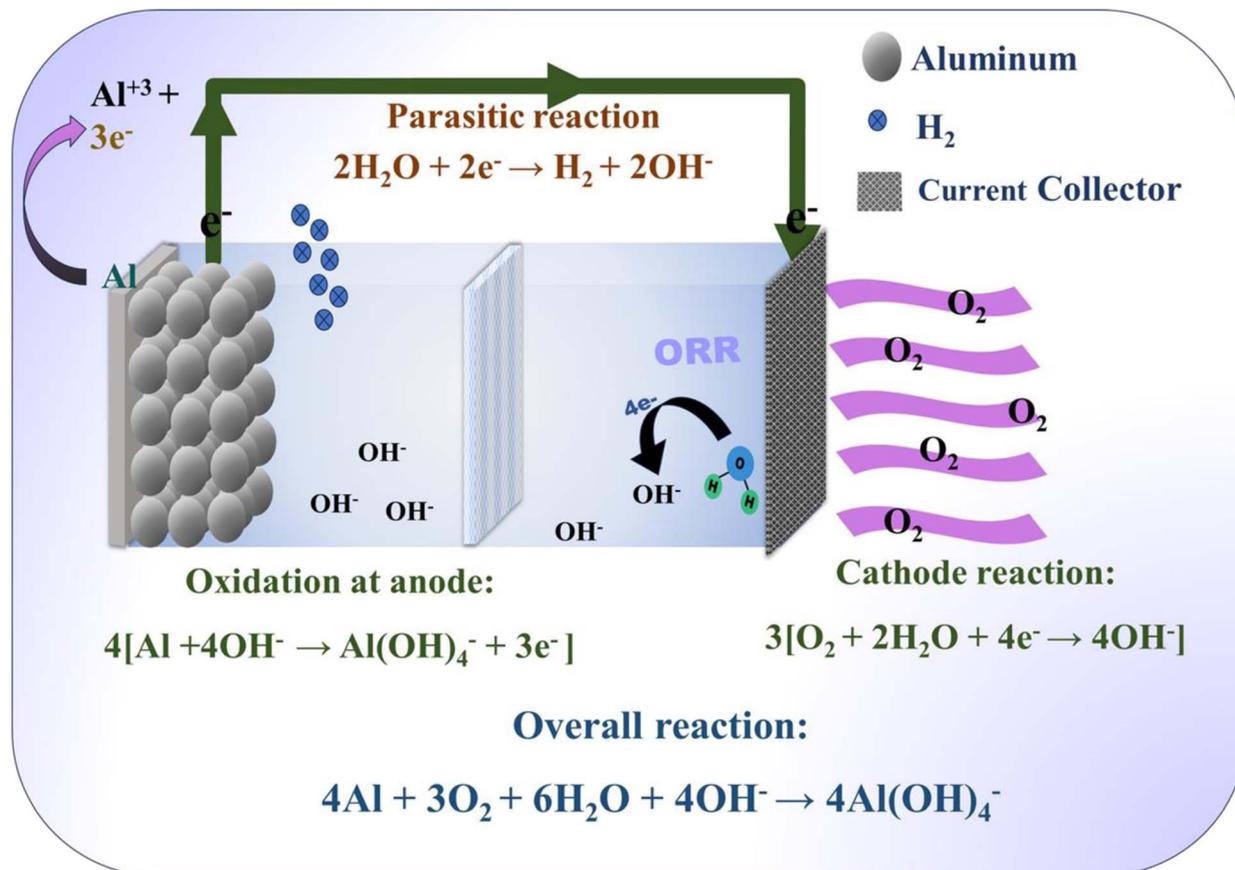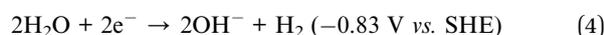
Fig. 3 Schematic representation of the working mechanism of a complete Al–air battery with the respective electrodes and overall reaction.

open circuit, the reduction of water and the occurrence of self-corrosion can be understood with eqn (4) and (5), as follows:[113]

Water reduction reaction:

$$2H_2O + 2e^- \rightarrow 2OH^- + H_2 \ (-0.83 \ V \ vs. \ SHE) \quad (4)$$

Self-corrosion reaction:

$$2Al + 2H_2O + 2OH^- \rightarrow 2Al(OH)_4^- + 3H_2 \ (1.48 \ V \ vs. \ SHE) \ (5)$$

The corrosion problem was initially addressed using two approaches, as follows: (i) modification of the aluminum anode and (ii) selection of a compatible electrolyte. Anode modification was performed using either an aluminum alloy or applying a protective layer, modifying anode grain size and crystal orientation. Also, alkali electrolytes are widely explored with numerous modifications, such as adding additives, changing the medium from aqueous to ionic, forming a gel/solid electrolyte, dual electrolyte systems, and oil displacement. Each type of electrolyte has advantages and disadvantages.[111,114] More details about the different types of electrolytes are discussed in the following section, as well as their impact on the overall performance and efficiency of Al–air batteries.

3.2 Reactions on the cathode

The cathode serves as the interface where oxygen molecules from ambient air are transformed and activate the reaction. The electrochemical mechanisms drive the energy conversion and storage capacity of Al–air batteries. The oxygen evolution reaction (OER) and oxygen reduction reaction (ORR) occur simultaneously at the cathode, despite their different kinetics and mechanisms. The OER process involves the oxidation of water molecules, which results in the release of oxygen, protons, and electrons. Alternatively, ORR promotes the reduction of oxygen molecules by removing electrons and protons, which leads to the production of water. The air cathode is a combination of catalyst, current collector, and GDL, where the electrolyte and ambient oxygen govern the reaction kinetics of the battery. The overall battery performance can be enhanced by understanding the cathode reaction mechanism and optimizing the catalyst design, electrolyte composition, and operating conditions. In the subsequent subsections, the underlying reaction mechanisms of ORR, OER, and other associated processes are explained to understand the complete electrochemical process of Al–air batteries.

3.2.1 Oxygen reduction reaction (ORR). ORR is the process of reducing oxygen molecules (usually from O_2 in the air) to produce water in an electrochemical system. Oxygen molecules in the atmosphere undergo reduction by accepting electrons and protons. This process typically occurs either through 4-e^- transfer or 2-e^- transfer. The process of e^- transfer and inter-mixed reactions can be influenced by both the pH of the electrolyte and the structure of the catalyst. In essence, O_2 coming
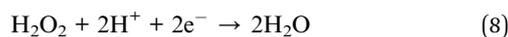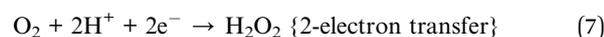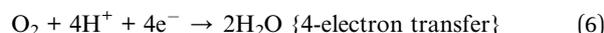
from the surrounding atmosphere traverses the GDL to engage in the reaction subsequent to its interaction with the catalyst. The presence of an active catalyst is essential for the functioning of both OER and ORR in the battery. Thus, the catalyst plays a crucial role in ensuring the durability, stability, and optimal efficiency of the battery.

However, the sluggish ORR in the Al–air battery limits the potential of this battery and complicates the process.[115] The intermediate steps, together with the activation of oxygen, removal of oxides, and bonding of oxygen atoms should considered to understand the complete mechanism.[116]

The ORR mechanism is different in acidic (eqn (6)–(8)) and alkaline media (eqn (9)–(13)), which are mentioned in the following reactions:[57,102]
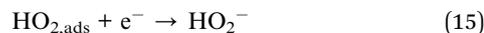
ORR in acidic medium:

$$O_2 + 4H^+ + 4e^- \rightarrow 2H_2O \text{ \{4-electron transfer\}} \tag{6}$$

$$O_2 + 2H^+ + 2e^- \rightarrow H_2O_2 \text{ \{2-electron transfer\}} \tag{7}$$

$$H_2O_2 + 2H^+ + 2e^- \rightarrow 2H_2O \tag{8}$$

ORR in alkali medium (9)–(12):[117]

$$X + O_2 + H_2O + e^- \rightarrow XOOH + OH^- \tag{9}$$

$$XOOH + e^- \rightarrow XO + OH^- \tag{10}$$

$$XO + H_2O + e^- \rightarrow XOH + OH^- \tag{11}$$

$$XOH + e^- \rightarrow X + OH^- \tag{12}$$
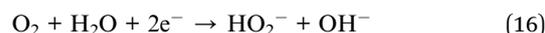
Overall reaction:

$$O_2 + 2H_2O + 4e^- \rightarrow 4OH^- \tag{13}$$

There is one more possibility of oxygen and the catalyst interacting for the ORR process, which occurs perpendicular to the surface. In this situation, two-electron transfer occurs during the process and hydroperoxides are evolved during the intermediate steps, as shown in the following reactions (14)–(16):[57,102,117]

$$O_2 + H_2O + e^- \rightarrow HO_{2,ads} + OH^- \tag{14}$$

$$HO_{2,ads} + e^- \rightarrow HO_2^- \tag{15}$$

Overall reaction:

$$O_2 + H_2O + 2e^- \rightarrow HO_2^- + OH^- \tag{16}$$

After undergoing the previously indicated two-electron reaction, hydroperoxide has the potential to undergo either a further two-electron reduction or chemical disproportionation, as depicted in the following equation:[74]
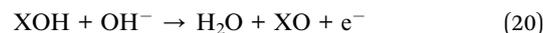
$$HO_2^- + H_2O + 2e^- \rightarrow 3OH^- \tag{17}$$

$$2HO_2^- \rightarrow 2OH^- + O_2 \tag{18}$$
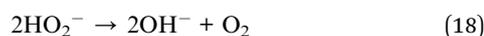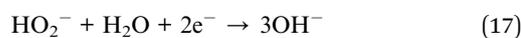
Eqn (17) indicates the process of hydroperoxide reduction, and eqn (18) shows hydroperoxide disproportionation during the 2-e⁻ transfer mechanism. The orientation of the catalyst is crucial for enhancing the efficiency of ORR, given that it is a kinetically sluggish process under normal conditions and can undergo either a 2- or 4-e⁻ transfer process.
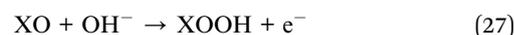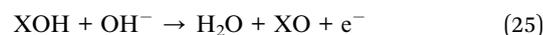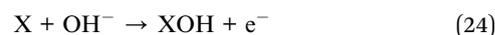
Although Al–air batteries rely on ORR at the cathode, the kinetics of this reaction have to be a 4-e⁻ transfer process to work effectively, particularly in alkaline electrolyte. The 2-e⁻ transfer process in ORR will make the battery less efficient given that it will undergo the formation of peroxide ions (according to eqn (14) and (15)). Considering this, when testing ORR, the number of electrons involved in the mechanism should be close to 4. Thus, improving the efficiency and kinetics of ORR is crucial for maximizing the overall performance and energy density of Al–air batteries.[118] Noble metal catalysts including platinum-based materials and their alloys are generally considered active catalysts to promote ORR. However, the high cost of these noble metals limits their use in Al–air batteries and large-scale application.[119] Thus, alternatives to noble metals have been explored recently, and their further discussion will be presented in Section 6.
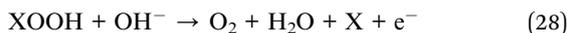
3.2.2 Oxygen evolution reaction (OER). OER is the process of liberating oxygen gas from water or another oxygen-containing material by applying an external electrical potential. In this context, the oxidation process results in the generation of O_2, H^+, and e^-. OER and ORR demonstrate contrasting orientations. The efficiency of the OER process relies on the pH level of the electrolyte. The electrocatalytic OER process is widely acknowledged as a heterogeneous reaction, wherein other proposed methods exhibit comparable intermediates such as XOH and XO, as outlined in eqn (19)–(28). This process involves a series of sequential stages, where intermediate entities such as hydroxyl radicals (OH*) and other oxygen-containing intermediates are generated prior to the ultimate liberation of O_2. The OER mechanisms can explained in both alkali and acidic mediums using the following reactions:[120]

In acidic medium:

$$X + H_2O \rightarrow H^+ + XOH + e^- \tag{19}$$

$$XOH + OH^- \rightarrow H_2O + XO + e^- \tag{20}$$

$$2XO \rightarrow O_2 + 2XO \tag{21}$$

$$XO + H_2O \rightarrow H^+ + XOOH + e^- \tag{22}$$

$$XOOH + H_2O \rightarrow H^+ + O_2 + X + e^- \tag{23}$$

In alkali medium:

$$X + OH^- \rightarrow XOH + e^- \tag{24}$$

$$XOH + OH^- \rightarrow H_2O + XO + e^- \tag{25}$$

$$2XO \rightarrow 2XO + O_2 \tag{26}$$

$$XO + OH^- \rightarrow XOOH + e^- \tag{27}$$

$$XOOH + OH^- \rightarrow O_2 + H_2O + X + e^- \quad (28)$$

To improve the efficiency of OER, a catalyst is employed to decrease the overpotential, which is crucial in the determination of the overall efficiency and OER performance of Al–air batteries. This is because it directly impacts the discharge characteristics, energy density, and battery stability. Efficient OER kinetics provide increased oxygen availability at the air electrode, which helps to enhance the power output of the battery at higher discharge currents. The maintenance of an alkaline environment within the battery is critical to facilitate appropriate electrochemical processes and prevent passivation of the Al anode. Efficient OER can contribute to this objective, which also enhances the probability of the activation of reversibility of the Al–air battery. Thus, the selection of OER catalysts that exhibit high activity and stability is important to optimize the overall performance and feasibility of Al–air batteries.

3.2.3 Electrocatalytic behaviour analysis.
The electrochemical test in a three-electrode system, which consists of a reference, counter, and working electrode, is used to evaluate the employed material as a catalyst. Cyclic voltammetry (CV) is commonly employed to assess the electrocatalytic performance of OER to determine the precise position and size of the reduction peak current. Linear sweep voltammetry (LSV) is employed to determine the kinetic current for a catalyst, disregarding the mass transfer effect and number of electrons using a rotating disc electrode (RDE). RDE is an extensively used hydrodynamic electrode because of its well-defined characteristics. In this electrode, both diffusive and convective transports are treated as one-dimensional processes. It assists in understanding the diffusion kinetics of the electrocatalyst. However, to avoid any false prediction, the area of the applied electrocatalyst must be considered equal to the geometric surface area of the electrode.[121,122] The responding total flux of the electroactive species, j, is directly proportional to the rotation speed of the electrode (ω) in reactions governed by both diffusion and kinetics at the rotating disc electrodes. This relationship is defined by eqn (29), which is also called the Koutecky–Levich equation.[103,123]

$$\frac{1}{J} = \frac{1}{J_k} + \frac{1}{J_L} = \frac{1}{J_k} + \frac{1}{B\omega^{1/2}} \quad (29)$$

$$B = 0.62nFAC_{O_2}D_{O_2}^{2/3}\nu^{-1/6} \quad (30)$$

where J_k represents the kinetic current density, J_L is the diffusion-limited current density, which can be calculated using ω (angular velocity), and B^{-1} refers to the slope of the Koutecky–Levich plot that is in between J^{-1} vs. $\omega^{-1/2}$. J_L also depends on F, which is the Faraday constant, C_{O_2} and D_{O_2} are the dissolved oxygen concentration and diffusion coefficient, respectively, ν is the kinetic viscosity coefficient of the solution and A is the area of the electrode.[103]

The ORR properties can further be investigated with the help of a rotating-ring disc electrode (RRDE). The following two eqn (31) and (32) are used to obtain the e⁻ transfer number during the process and H_2O_2 yield curves.[124,125]

$$n = \frac{4 \times I_d}{I_d + \frac{I_r}{N}} \quad (31)$$

$$H_2O_2\% = 200 \times \frac{\frac{I_r}{N}}{I_d + \frac{I_r}{N}} \quad (32)$$

where the variable I_d represents the disc current, N represents the collection efficiency (ranging from 0.24 to 0.5), and I_r represents the ring current. These equations can also be utilized to ascertain the efficiency of collection (N) and the proportion of oxygen transformed into hydrogen peroxide. A lower H_2O_2 yield (close to zero) signifies the better catalytic activity.[126]

Tafel analysis can also be employed to investigate the ORR polarisation, which examines the relationship between J_k and overpotential (η). This relationship can be mathematically expressed as the following eqn (33).[127,128]

$$\eta = a + b \log(J_k) \quad (33)$$

where η is the reaction overpotential. The Tafel slope and Tafel constant are expressed as 'b' (V dec⁻¹) and 'a', which are related to the exchange current density (J_0). The reaction overpotential η can be expressed as eqn (34) using the Butler–Volmer equation.[57]

$$\eta = \frac{RT}{\alpha nF} \times \ln(J_0) + \frac{RT}{\alpha nF} \times \ln(J) \quad (34)$$

where the symbol R represents the ideal gas constant, T denotes the temperature, α signifies the transfer coefficient, and J represents the current exchange density. The equation is expressed concisely as eqn (35).[57,129]

$$\log(J_0) = -\alpha \times \frac{2\alpha F}{2.31RT} \quad (35)$$

Thus, the overpotential η can be calculated by subtracting the reference electrode potential from the observed half-wave potential ($E_{obs} - E_{ref}$).

Thus, the calculated electrochemical potential can be converted into the scale of reversible hydrogen electrode using eqn (36).[130]

$$E_{RHE} = E_{ref(obs)} + E_{ref}^0 + 0.059 \times pH \quad (36)$$

where $E_{ref(obs)}$ is the observed potential while experiment is performed, the commonly used reference electrodes are Ag/AgCl, Hg/HgO, Ag/AgNO₃ etc., to be chosen according to the pH of electrolyte. E_{ref}^0 is potential of reference electrode vs. normal hydrogen electrode NHE, i.e. 0.198 V is taken for Ag/AgCl (in 3 M KCl) and 0.098 V for Hg/HgO electrodes.[131]

3.3 Hydrogen evolution and Al–air battery test

Hydrogen evolution is a crucial parameter in determining the performance of the Al–air battery. A higher evolution of hydrogen signifies the lower efficiency of the battery. The typical setup employed to test the hydrogen evolution rate is
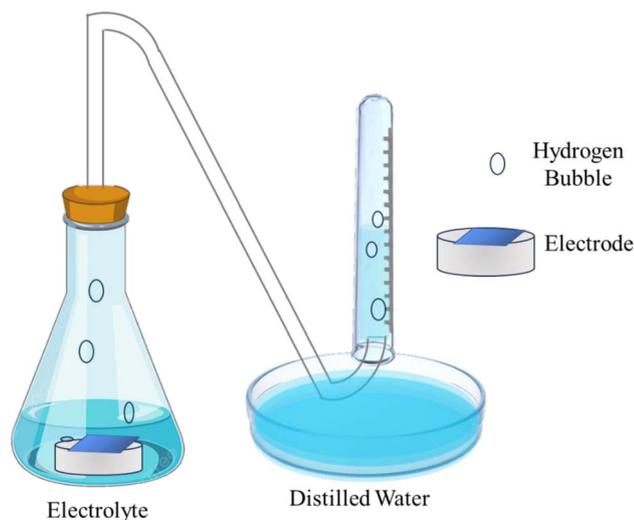
Fig. 4 Schematic demonstration of the setup to determine the hydrogen evolution rate.[115]

demonstrated in Fig. 4, which includes a conical flask and a gas guide attached to an inverted burette. Generally, the exposed area of the electrode inside the conical flask that is filled with electrolyte is considered 1 cm² for ease of calculation. The evolved hydrogen is passed from the gas guide and the displaced liquid is measured in the burette drainage, which can be used to determine the H_2 evolution rate in mL cm^{-2} min^{-1}. The following eqn (37) and (38) are generally used to evaluate the hydrogen evolution rate (R_{H_2}) and corrosion current density (i_{H_2}):[132,133]

$$R_{H_2} = \frac{V_{H_2}}{A \times T} \quad (37)$$

$$i_{H_2} = \frac{2p V_{H_2} F}{R T_E A T} \quad (38)$$

where A denotes the surface area of the aluminum alloy sample (cm²), T represents the duration of immersion (minutes), V_{H_2} represents the volume of H_2 released (mL), p represents the atm pressure (Pa), F designates the Faraday constant, and R & T_E relate to the gas constant and temperature at which analysis is performed (Kelvin), respectively.

The battery efficiency of the Al–air cell is tested in a complete cell composed of an Al anode, a catalyst supported with a current collector, and electrolyte. The main physical quantities to test the efficiency of a complete cell are specific capacity, i.e., capacity per unit mass consumed (Q), Al anode utilization amount (U_a) in percent, and energy density (W), calculated according to eqn (39)–(41):[134,135]

$$Q = \frac{It}{3600\Delta m} \quad (39)$$

$$U_a = \frac{It}{\Delta m F/9} \times 100\% \quad (40)$$

$$W = \frac{EIt}{3600\Delta m} \quad (41)$$

where I indicates the current flow throughout the process, t denotes the reaction duration, m represents the weight change, F is the Faraday constant, and E is the nominal discharge voltage.

Further, to analyse the performance of the battery, i.e., parameters such as specific capacity and energy density are crucial. These physical parameters will assist in understanding whether the fabricated battery is efficient. The main attributes such as discharge current, operating voltage, discharge time, and consumed mass of the anode are used to understand the battery performance. The specific capacity is calculated in units of mA h g^{-1}. The discharge current, operating voltage, and discharge time are measured during the controlled battery discharge measurement. Further, to measure the consumed mass, the byproduct from the discharged anode needs to be etched with proper care, which is essential for the precise measurement of specific capacity and energy density. There are various techniques reported in the literature, i.e., etching with strong bases such as NaOH and KOH, chromium oxide, and silver nitrate.[111,136,137] Linjee and Ren et al. used 2 wt% Cr_2O_3 and 5 wt% H_3PO_4 with DI water at 80 °C for a few minutes to remove the corrosive products.[138,139] Some reports also followed the ASTM-G-03 standard, where the consumed anode is rinsed to separate the corrosive byproducts.[140,141] However, the used etchant can also etch some of the non-consumed aluminum during the removal of byproducts. Also, the formed byproducts are usually $Al(OH)_3$ or aluminates, which may stick to the surface of Al and increase the mass of the anode. These aspects will tend to provide false interpretations for the measured specific capacity, and thus the measured energy density may not reflect the correct energy density. Thus, it becomes necessary to innovate a particular method for the complete removal of byproducts from the discharged anode to accurately determine the anode utilization, specific capacity, energy density, and other related parameters.

4. Alloying of aluminum anode

Electrochemical measurements have shown that alloying metals with aluminum may provide several advantages, such as reduced corrosion and enhanced stability in alkaline or acidic electrolyte. When pure aluminum is alloyed/surface modified with various metals through a bulk mixing, coating or doping process, its corrosion resistance characteristics are enhanced. The commercially available aluminum alloys, such as Al 1200, Al 8011, Al 6061, Al 7XXX (i.e., alloys of Al 7000 series with major alloying of zinc), and Al 2XXX (major alloying of copper), have been examined for their use as the anode in Al–air batteries.[142–144] According to the literature, the use of aluminum alloy effectively reduces the corrosion rate and enhances the anodic potential, as evidenced by several reports. Additionally, using various elements such as Ti, Zn, Mg, Bi, and Pb in the alloy may also improve the electrochemical performance.[33,99,143–146] Various electrochemical tests have been performed on these Al alloys, including hydrogen evolution rate, self-corrosion, anodic dissolution, polarization, and other tests. Discharging electrochemical test analysis showed that

alloying alters the surface characteristics compared to the pure Al anode. These results suggest that alloying improves the electrochemical performance by significantly altering the corrosion resistance. The commercial grade alloys have various ratios of Mn, Cu, In, Mg, Si, In, Zn, Ti, Cr, and Fe. The discharging at lower and higher current rates is greatly influenced by alloying. When pure Al is used as the anode, the surface is initially oxidized, forming Al_2O_3, which is converted into an $Al(OH)_3$ layer in the presence of the electrolyte. During this process, electron charge transfer occurs as three e^- are liberated, and simultaneously Al^{3+} species are formed and $Al(OH)^{4-}$ and $Al(OH)_3$ are automatically formed as corrosion products. The anode releases an e^- and dissolves, resulting in the formation of the above-mentioned compound as a byproduct. The parasitic corrosion reaction also occurs during this procedure. The primary problem is the development of passive oxide films, which function as a barrier to aluminum breakdown.[98,147]

Reboul *et al.* proposed a dissolution–redeposition method, aiming to address the issue of passive oxide film formation by utilizing aluminum alloying. This method involves the simultaneous dissolution and oxidation of individual elements in the Al matrix, producing cations in the electrolyte, which are subsequently deposited back on the Al surface through electrochemical reactions, which help break the compact oxide layer and activate the Al surface, as presented in Fig. 5(a). It has been suggested that elements with low-temperature eutectic should be selected to fully realize and comprehend multi-element alloying. The separated oxide coating produced by the eutectic development on the Al surface acts as an active site for the breakdown of the alloy. When complexes with cations are formed, the production of eutectic increases the adsorption of anions, which results in pitting corrosion. The amount of amalgam and other eutectic formed on the surface of the Al matrix is of the utmost importance for activation (see Fig. 5(b)). The surface structure of Al alloys during alloying exhibits nonuniformity due to

Fig. 5 (a) Schematic diagram explaining the dissolution–redeposition mechanism in Al-alloys proposed by Reboul *et al.* (b) Schematic diagram showing the eutectic mechanism.[77,148]

unpredictable processes such as eutectic development, shrinkage, segregation, and imperfections. This non-uniformity may lead to uneven corrosion reactions on the Al surface.[77,148] As a result, the surface of Al may experience an uneven corrosion reaction. In addition to other phenomena that may negatively impact the electrochemical performance of the battery, the local corrosion will worsen. Thus, to prevent this, numerous researchers are currently reintegrating the structure of aluminum alloy using an additional element distribution state, and some recent studies are tabulated in Table 3.

Pino *et al.* investigated commercially available Al-alloys, Al 2024, Al 7475, and Al 1085, as anode for Al–air batteries in both clad and unclad states. The abbreviation used for clad and unclad Al 7475 is Al7C and unclad Al7U, respectively. Similarly, the terms Al2C and Al2U are used in Fig. 6(a) and (b) for the clad Al 2024 and unclad Al 2024 samples, respectively. Fig. 6(a) and (b) illustrate the galvanostatic discharge curves and electrochemical performance in realizing the effect of using alloys in the clad and unclad states as an Al anode, respectively.[144] The clad alloys exhibited a superior current discharge at lower current rates. Al 7474 is a commercial alloy, mainly doped with Zn and Mg, which showed improved ability to dissipate current, even at higher discharge currents. The underlying mechanism for this phenomenon is the galvanic coupling between Al and metallic alloying, which influences its surface reactivity with the electrolyte. The alloying of gallium shows acceleration in the active dissolution of the Al anode with Mg and Sn, as described by Wu *et al.*[154] Furthermore, adding indium causes discharge products (such as In and $In(OH)_3$) to emerge, preventing the self-corrosion reaction. Thus, Al–Mg–Sn–Ga–In alloy-based anodes are promising at higher discharge rates for Al–air batteries in brine electrolytes. The polarization curve is shown in Fig. 6(c) for the Al–Mg–Sn–Ga–In alloy in 2 M NaCl electrolyte. Alloys 1, 2, 3, and 4 mentioned in Fig. 6(c) are the combination of Al–0.5Mg–0.1Sn, Al–0.5Mg–0.1Sn–0.05In, Al–0.5Mg–0.1Sn–0.05Ga, Al–0.5Mg–0.1Sn–0.05Ga–0.05In, respectively.[154] Ren *et al.* investigated three different Al–Sn, Al–Mg, and Al–Mg–Sn alloys and compared them with pure Al. The results of the self-corrosion test, *i.e.*, potentiodynamic polarization and galvanostatic discharge curves, suggest that alloying resulted in a better battery performance than pure Al. The self-corrosion was maximum for pure Al, followed by Al–Sn, Al–Mg–Sn, and Al–Mg alloys, showing lower self-corrosion with minimal self-corrosion for the Al–Mg alloy. The capacities were 2563 mA h g^{-1} for pure Al 4N6, 2569.5 mA h g^{-1} for Al–Sn, 2723.7 mA h g^{-1} for Al–Mg, and 2661.1 mA h g^{-1} for the Al–Mg–Sn alloy anodes.[155] Further, doping with manganese (Mn) increased the specific capacity to 1500 mA h g^{-1} by reducing the self-corrosion, resulting in an improved working potential and energy density for ~50% anode consumption. The corresponding polarization curve is shown in Fig. 6(d). The alloying process involves bonding two distinct metals, modifying their structural integrity and enhancing their electrochemical performance.[146,155] This is achieved by carefully selecting the doped metal composition in a proportional ratio based on the desired objective of either preventing self-corrosion or achieving simultaneous current discharging performance.
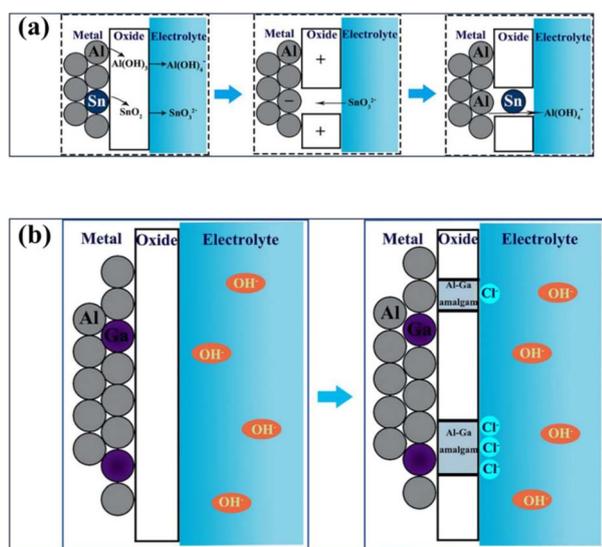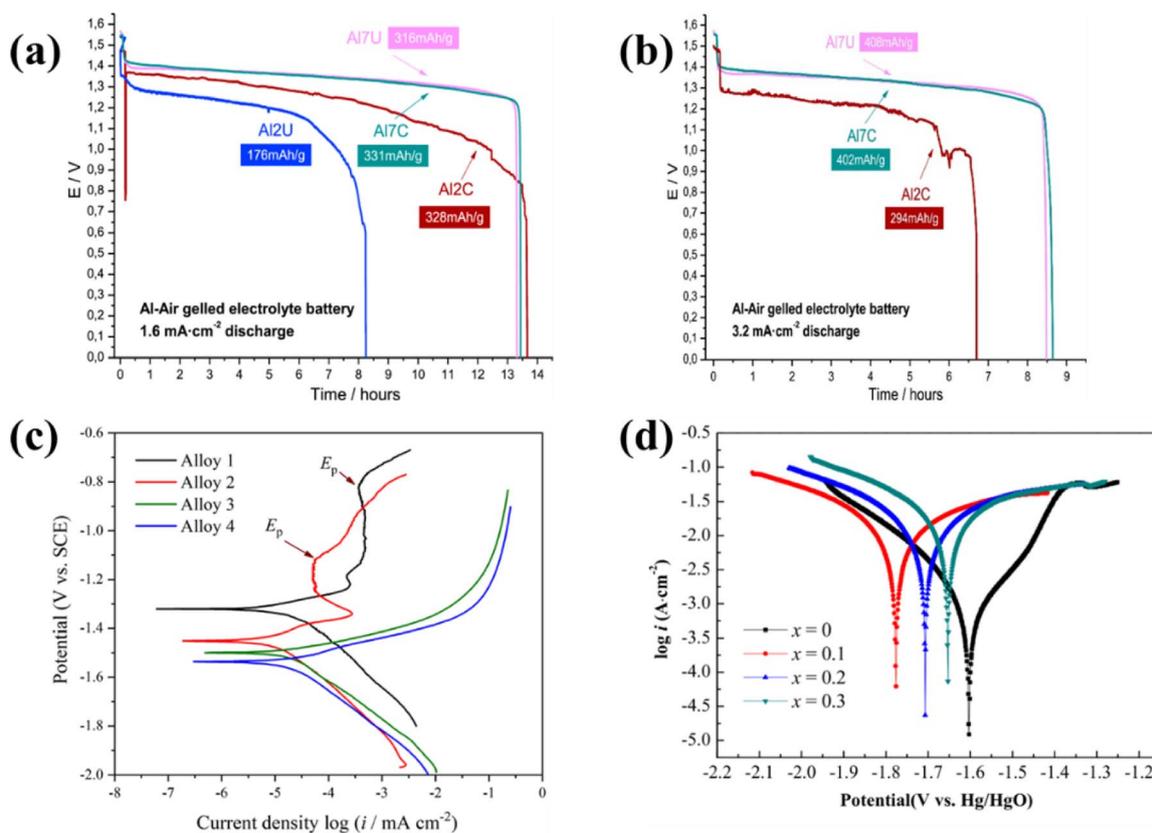
Table 3 Some recent studies on alloys and comparison of the corresponding hydrogen evolution rate, corrosion potential (E_{corr}), corrosion current density (j_{corr}), and Al–air battery-specific capacity with anodic efficiency

S. N.	Alloy	H$_2$ evolution rate (mL min^{-1} cm^{-2})	E_{corr} (V)	j_{corr} (A cm^{-2})	Performance (mA h g^{-1})	At current density (mA cm^{-2})	Anodic efficiency (%)	Ref.
1	Al–Ga	0.061	−2.023	2.45	2584.1	5	61.5	149
2	Al–In	0.006	−1.980	0.263	3343.2	5	73.1	
3	Al–Sn	0.001	−1.857	0.37	3267.6	5	86.3	
4	Al–1Zn–0.1In–0.1Sn–0.5Mg–0.1Mn	0.128	−1.776	0.0032	1481	20	49.75	146
5	Al–1Zn–0.1In–0.1Sn–0.5Mg–0.2Mn	0.227	−1.707	0.0010	1347	20	45.23	
6	Al–1Zn–0.1In–0.1Sn–0.5Mg–0.3Mn	0.313	−1.653	0.015	1212	20	40.70	
7	Al 6061	—	−1.386	0.126	624.77	2.6	—	142
8	Al 8011	—	−1.386	0.141	628.41	2.6	—	
9	Al 1200	—	−1.420	0.073	1096.84	2.6	—	
10	Al–0.1Sn–0.08Ca	0.142	−1.832	0.0036	2495.75	40	83.75	150
11	Al–Mn–Sb	—	−1.736	0.00137	2797	120	93.8	151
12	Al–Mg–Sn–In	—	−1.57	0.0026	—	—	42.7	152
13	Al 6061	0.3928	−1.380	0.168	—	—	—	153
14	Al 8011	0.2771	−1.450	0.144	—	—	—	

Fig. 6 (a) Galvanostatic discharge at 1.6 mA cm^{-2} and (b) galvanostatic discharge at 3.2 mA cm^{-2} of the Al 2024 and Al 7475 alloys in the clad and unclad states, respectively.[144] (c) Polarization curves of alloys in 2 M NaCl electrolytic solution of alloy 1–4 at 0.167 mV s^{-1} for 30 min.[154] (d) Potentiodynamic polarization curves of the Mn-doped alloy (Al–1Zn–0.1In–0.1Sn–0.5Mg–xMn) anodes in 4 M NaOH solution at 1 mV s^{-1} for 60 min.[146]

Thus, a suitable alloying composition is essential to achieve the optimal performance of Al–air batteries. Thus, alloying of aluminum anodes offers promising advancements for Al–air batteries, and the ongoing research efforts are aimed at optimizing the alloy compositions and structures for improved electrochemical performances.

5. Electrolyte

The electrolyte is an essential component of the Al–air battery to facilitate the reactions at the anode (aluminum) and cathode (air). The electrolyte also aids in regulating the pH balance in the battery. Al–air batteries require an alkaline environment

with a high pH to facilitate specific electrochemical reactions and minimize the creation of byproducts, which are undesirable and may harm the battery components. The composition and concentration of the electrolyte can influence the electrochemical reaction rate on both sides of the electrodes.[92,110] The composition of the electrolyte affects the formation and passivation layers on the aluminum anode surface. Thus, an appropriate electrolyte formulation and its optimization for a given solvent can help prevent excessive passivation, ensuring continuous electrochemical activity throughout the operation together with an optimal battery capacity and energy density.

5.1 Aqueous electrolyte

The behavior of aluminum in aqueous medium can be understood by the Pourbaix (E_H-pH) diagram, as shown in Fig. 7, which is calculated using the Nernst equation.[156] Aluminum is likely prone to corrosion, as already discussed in the previous section/ sub-section(s), which is similar to the rusting of iron, due to the potential driving force that hinders the formation of a protective (passive) oxide layer. Regions (I), acidic medium, and (III), alkaline medium, in Fig. 7, i.e., both acidic and alkaline conditions, favor the consumption of aluminum, showing an amphoteric nature, and likely the evolution of hydrogen gas (eqn (4)). However, in the intermediate pH (in region (II)), where H_2O remains in the stable phase, the passivation works effectively, and aluminum oxide (Al_2O_3) is formed, which is resistant to corrosion and exhibits an extremely low potential.[91] This illustrates negligible or no aluminum corrosion in pure water. In certain circumstances, aluminum exhibits immunity to corrosion due to the zero or presence of an opposing (i.e., negative) voltage force. The corrosion of aluminum can occur due to the presence of a potential driving force, which hampers the development of a durable oxide layer on its exposed area, indicated as region (IV) in Fig. 7. One possible explanation for the absence of corrosion in aluminum is the phenomenon known as 'passivation', which occurs when an oxide layer is formed on the exposed area, despite the presence of a potential driving force.[157] The effectiveness of this layer as a corrosion barrier remains uncertain. This phenomenon has also been proven to be beneficial for aluminum, which is employed as a potential current collector in batteries and supercapacitors. However, it cannot be ignored that a rechargeable Al-ion battery using aluminum metal as the anode in an aqueous system is not feasible due to the inability to plate aluminum at both low and high pH levels. It is also not solvable at medium pH. Hence, it is only possible to implement primary battery systems with aqueous electrolytes.

The various types of electrolytes are explored in the aqueous medium of different pH for Al–air batteries. The most common electrolytes are alkaline-based aqueous medium to promote ORR, as discussed in Sub-section 3.2.[158] Efforts are devoted to changing the pH with additives, which will mitigate the limitations associated with alkaline-electrolytes. These alkaline aqueous electrolytes in Al–air batteries are widespread due to their superior ionic conductivity. The stability of a metal is mostly constrained in acidic environments, which is why either alkaline or neutral electrolyte is preferred in the metal–air batteries. Both alkaline and neutral media have been suggested given that they have similar reaction pathways for oxygen redox activities (as discussed in Sections 3.2 & 3.3). However, it has been observed that the kinetics of these processes are relatively slower in neutral electrolyte, which poses a considerable constraint on the performance of Al–air batteries. The most well-known electrolytes for Al–air batteries are KOH and NaOH in alkaline electrolyte.[159,160] KOH is also preferred over NaOH due to its faster kinetics, better conductivity, and higher diffusion coefficient. However, NaOH is mainly used because KOH solution hinders recycling via the Hall–Héroult process.[161]

KOH and NaOH electrolytes exhibit a reduced voltage and current output with time compared to NaCl electrolyte. The initial OCP for the alkaline medium is relatively higher; however, it degrades very quickly. As the number of OH^- ions in the electrolyte increases, the anode will generate more metal oxide. Consequently, electrolyte with a higher OH^- concentration will experience rapid depletion compared to that with a lower concentration of OH^- ions.[162,163] Thus, saline water is considered relatively safer due to its neutrality. However, this is also prone to higher polarization, which causes severe corrosion. The presence of chloride will eventually help in reducing the polarization potential by the absorption of Cl^- ions on the anode side.[164] However, this will not sustain for a longer duration, and that is why other salts can be employed as an additive, such as sodium hydrogen carbonate and sodium sulphate. These additives will precipitate the gel of aluminum hydrate, which is the main culprit in reducing ionic conduction inside the electrolyte. In the case of crewless underwater vehicles, the choice of electrolyte is seawater itself, given that it is economically viable and requires low maintenance. However, in addition to the aluminum anode, other sub-components of the battery, such as the current collector and housing materials, may be susceptible to corrosion in seawater, which contains Cl^- ions, forming acidic byproducts.[165] Some of the recent studies related to the electrolytes and additives in aqueous and hydrogel media are tabulated in Table 4.
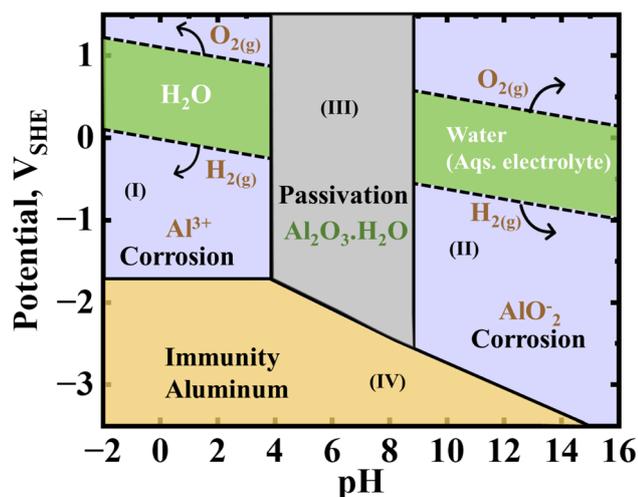

Fig. 7 Pourbaix diagram for aluminum, which is used to understand its possible corrosion, passivation, and immune regions in water medium.[73]

Table 4 The potential electrolytes and additives for the respective aqueous electrolytes with their corresponding hydrogen evolution rate, ionic conductivity, and Al–air battery specific capacity at a given discharge current density

S. N.	Electrolyte	Additive element	H$_2$ evolution rate (mL min^{-1} cm^{-2})	Ionic conductivity (mS cm^{-1})	Specific capacity (mA h g^{-1})	At current density (mA cm^{-2})	Ref.
1	4 M KOH	2 M sucrose	0.178	34.98	2330	10	166
2	4 M NaOH	20% glycerol	0.042	86.00	2564	10	167
3	4 M NaOH	10 mM ZnSO$_4$ + 1 g per L sodium alginate	0.174	13.82	267.41 mA cm^{-2} (capacity density)	30	162
4	4 M NaOH	ZnO/glucose	0.097	—	2271	20	52
5	4 M KOH	10% v/v 0.5 M Ba-acetate	0.042	—	2817	10	168
6	4 M NaOH	1.6 g per L zinc oxide + 1.0 mM 8-aminoquinoline	0.211	—	2703	20	169
7	4 M KOH	13 M (CO(NH$_2$)$_2$)	0.019	390.00	2330	35	170
8	6 M KOH	ZnCl$_2$	0.039	—	2322	20	171
9	4 M NaOH	4 mM-hexadecyl-3-methylimidazolium hexafluorophosphate (HMIH)	0.437		2128	20	172
10	4 M KOH	10 mM 4-amino-6-hydroxy-2-mercapto pyrimidine and 4 mM zinc oxide	0.134	—	785	20	173
11	4 M KOH	0.05 M Na$_2$SnO$_3$ and 4 mM ellagic acid	0.366	—	2439	50	174
12	4 M NaOH	1 mM dodecyl dimethyl betaine and 4 mM sodium dodecylbenzene sulfonate	0.110	—	2548	40	175
13	KF and KOH (hydrogel)	PAA	0.990	371.00	2199	10	176
14	Agar hydrogel	0.5 M Zn^{2+}	0.990	215.4	2592	10	177
15	KOH hydrogel	(NH$_4$)$_2$S$_2$O$_8$ in PAA	0.019	397.00	2377	10	178

The common problem faced by electrolyte in aqueous medium is that they tend to dissolve CO_2, resulting in the formation of carbonate, which hinders the efficiency of the battery.[101] These limitations must be mitigated to achieve the maximum anode efficiency. The Al anode naturally tends to form a protective oxide layer when exposed to oxygen and moisture in aqueous medium, which suppresses the overall performance of the battery. Thus, to overcome this, other media such as ionic and gel electrolytes are also explored for use in Al–air batteries.

5.2 Non-aqueous/ionic electrolyte

In an Al-ion battery, the popular non-aqueous electrolyte is $AlCl_3$ in 1-ethyl-3-methylimidazolium chloride (EMImCl).[179] Due to the reversible nature of the $AlCl_3$ electrolyte based on Lewis acid–base chemistry in the ionic medium, this battery exhibits potential rechargeability. Electrolytes with chloroaluminate salt were among the initial options examined for aluminum-based batteries. The feasibility of electrodepositing aluminum from chloroaluminate ions was established decades ago.[180] The aluminum valence electron shell is completed through the dimerization of two $AlCl_3$ molecules. This leads to the formation of a molecular liquid when the Al_2Cl_6 molecule melts, wherein the chlorine from each molecule forms a covalent bond with aluminum through one of its lone pairs of electrons. This liquid exhibits low ionic conductivity but demonstrates significant Lewis acid properties.[181] Consequently, it undergoes reactions with various halogen compounds, forming ionic liquids known as chloroaluminates. Revel *et al.* fabricated an Al–air cell using $AlCl_3$/EMImCl (1.5 : 1) electrolyte. This cell was evaluated at a low current, *i.e.*, 0.1 mA cm^{-2}, exhibiting a capacity of 71 mA h g^{-1} at an operating voltage of 0.6 V. However, the Al–air cell suffered from stability issues, given that its overpotential is higher than the potential at which the electrolyte remains stable, and thus rechargeability is not feasible for this battery.[179] Choi *et al.* used the same electrolyte to soak the aluminum anode and expose it for 24 h. Since then, a film of Al_2O_3 was developed, which resulted in an enhanced battery performance. Here, the ionic liquid solution worked as a Lewis acid and galvanic corrosion occurred. The exposed oxide layer facilitated the easy intercalation/deintercalation of Al^{3+} ions.[182]

Gelman and group used 1-ethyl-3-methylimidazolium oligo-fluoro-hydrogenate (EMIm (HF)$_{2.3}$F) and tested its use in a primary Al–air battery. This material was chosen due to its proven potential in silicon–air battery applications. The electrochemical potential range is the disparity between the limits of the cathodic and anodic peaks, representing the potential values at which oxidation and reduction appear. Finally, the number of electrons (*n*) was taken 2.3 due to the demonstrated hygroscopicity at *n* < 2.3. In addition to its stability in moisture and water, this ionic liquid possesses additional beneficial characteristics, such as electrical conductivity of approximately 100 mS cm^{-1} and low viscosity. Unlike other organic solvent electrolytes, EMIm (HF)$_{2.3}$F electrolyte can activate aluminum by disrupting its passive oxide layer through a specific species.

Ferrocene/ferrocenium (Fc/Fc$^+$) was employed as the reference electrode, which is compatible with the ionic liquid electrochemistry. The experimental findings (−1.1 V for aluminum anode and 1 V *vs.* Fc/Fc$^+$ for cathode) demonstrated a cell potential of 2.1 V for the Al–air battery. Linear polarisation tests were performed to evaluate the corrosion current density in EMIm (HF)$_{2.3}$F. The current density of ∼25 μA cm^{-2} is insignificant compared to the corrosion current density recorded in aqueous alkaline electrolyte. The results of the discharge studies conducted at current densities in the range of 0.1–1.5 mA cm^{-2} indicated that the aluminum foil anode exhibited a max charge capacity of 160 mA h, which is lower than the calculated capacity of 227 mA h. The morphology of the anode surface showed that the diameter of the pores formed due to aluminum dissolution increased with an increase in the discharge current density. Specifically, the diameter ranged from 20 to 50 nm at a current density of 0.1 mA cm^{-2} compared to a diameter of 200 to 400 nm at a current density of 1.5 mA cm^{-2}. The ionic liquid electrolyte-based Al–air battery demonstrated 70% of the predicted discharge capacity and a remarkably low corrosion current density.[183]

5.3 Polymer gel/solid electrolyte

An ethanol-based alkaline gel electrolyte was proposed by Wang *et al.*, employing polyethylene oxide (PEO) as an agent for gel formation and a KOH–ethanol mixture as the solvent. The gel was optimized at different thicknesses between 0.5 and 2 mm. With an increase in thickness, both the ohmic and polarization resistance increased. The 0.5 mm-thick gel showed a shorter discharge time than the comparatively thick gels and had the lowest capacity. In contrast, the 2 mm gel showed the maximum discharge time and the maximum capacity, reaching 2546 mA h g^{-1} at 1 mA cm^{-2}, which is 85.4% of the theoretical capacity.[184] Liu *et al.* proposed a polymer gel electrolyte using a mixture of polyvinyl alcohol (PVA) and PEO together with *N,N′*-methylene bisacrylamide (MBA). Different mass ratios in the range of 0.1–1.0 were tested, and among the compositions, PPM-0.3 showed the best performance. An optical image of the gel and its retained structure with a 100 g weight is shown in Fig. 8(a). The addition of PEO to PVA improved its physical bonding and flexibility due to the formation of hydrogen bonds. It also tended to crystallize quickly, which caused a reduction in its ionic conductivity. This was compensated by the addition of MBA, which resulted in the formation of many C–O bonds as active sites for protons. The proposed mechanism of gel formation is shown in Fig. 8(b), which eventually results in the formation of an amorphous and porous structure. Its conductivity reached 2.1 × 10^{-1} S cm^{-1} and its power density and specific capacity reached 44.5 mW cm^{-2} and 1099 mA h g^{-1}, respectively. The flexibility of the developed battery was evaluated under different bending conditions with different discharge current rates, as shown in Fig. 8(c). The insignificant change in the battery performance showed the robustness of the cell with flexibility.[185]

Ryohei Mori demonstrated a solid-state rechargeable-type Al–air battery. He mixed $AlCl_3$, urea, CMC, and glycerin in
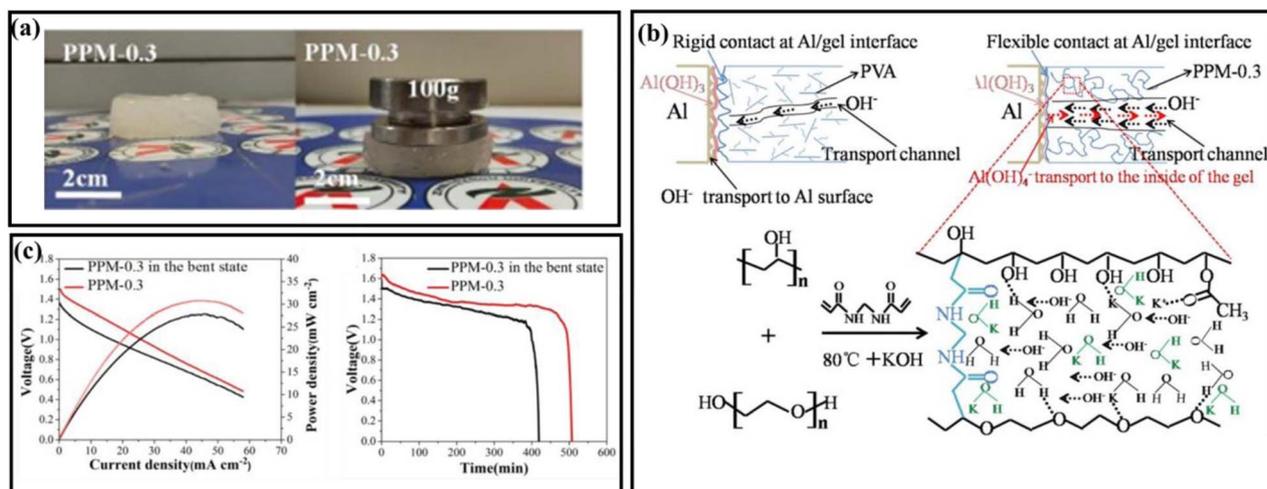
Fig. 8 (a) Optical photograph of PPM-0.3 with a weight resistance of up to 100 g. (b) Mechanical illustration of the process for the synthesis of PPM gel. (c) Electrochemical analysis with the power density and discharge curve to test the change in bent state *vs.* normal state of gel PPM-0.3.[185]

a 3 : 2 : 1 : 1 molar ratio as the electrolyte and soaked it in commercial gauze during the process of charging/discharging the solid-state Al–air battery. The applied current rate was 0.1 mA cm^{-2}, with a cutoff potential in the range of 0.2–1.5 V. The initial capacity of the cell was 35.8 mA h g^{-1}, which retained ~35.0 mA h g^{-1} after 50 charge–discharge cycles, exhibiting 97.8% capacity retention. Here, the air cathode used TiN, a suitable catalyst for promoting ORR. It is worth noting that neither Al$_2$O$_3$ nor Al(OH)$_3$ was formed as a byproduct. The other byproducts formed did not cause any hindrance in the reaction kinetics.[186] Xu and group directly demonstrated a fiber-embedded Al–air battery in a wristwatch. This demonstration showed flexibility and proposes a way to maintain it during application. The solid-state polymer electrolyte was comprised of PVA and PEO mixed in KOH aqueous solution together with ZnO and Na$_2$SnO$_3$ additives. Here, a spring-shaped anode was considered with the electrolyte, which cross-linked the anode spring *via* the freeze-thawed method. The air cathode was conjugated with Ag nanoparticles coated with CNT and covered on a Teflon plate. The flexible solid-state battery exhibited a practical energy density of about 1.17 kW h kg^{-1} and a specific capacity of 12 A h g^{-1}. However, the rechargeability was not demonstrated for this cell.[187]

5.4 Hybrid electrolyte

One of the strategies for corrosion inhibition is mixing electrolytes to balance the synergy. Using only an ionic electrolyte will not be effective in terms of cost, handling, and sustainability. If 4 M KOH is mixed with some ethanol content, the corrosion is reduced significantly, but adding more ethanol (more than 50 : 50) negatively impacts the performance. Zhang *et al.* attempted to use imidazole-based ionic liquid 1-(2-hydroxyethyl)-3-methylimidazolium chloride (HMIC) as an additive in the traditional 4 M NaOH aqueous electrolyte. It reduced the corrosion by more than 58%. Different

concentrations of HMIC in the range of 1–7 mM was examined, and a reduction in hydrogen evolution rate was observed at 0.414 mL cm^{-2} min^{-1} for 7 mM HMIC compared to 0.791 mL cm^{-2} min^{-1} without HMIC. Consequently, when the HMIC inhibitor was tested in a complete cell of the Al–air battery, the mass loss in the Al anode (here, Al 5052 alloy anode) was controlled by more than half of the initial value, which resulted in an enhanced specific capacity and energy density of 2469 mA h g^{-1} and 3313 W h kg^{-1}, respectively.[188] Huang *et al.* also showed a significant improvement in electrochemical parameters using organic additive in 4 M NaOH. They used 0.03–0.09 M L-tryptophan as the corrosion inhibitor. An increase in inhibitor concentration positively impacted the performance by minimizing the corrosion of the Al-5052 anode. The calculated rate of hydrogen evolution for the anode in 4 M NaOH electrolyte was 0.823 mL cm^{-2} min^{-1}. The rate was reduced to 0.411 mL cm^{-2} min^{-1} for the electrolyte modified with 0.09 M concentration of L-tryptophan inhibitor. Consequently, the mass loss was less in the presence of the inhibitor, and discharge potential increased from 1.33 to 1.51 V. At 20 mA cm^{-2} current density, the recorded specific capacity was 2702 mA h g^{-1}, which was ~990 mA h g^{-1} without any inhibitor.[115] These studies suggest that organic inhibitors can endow the anode with better stability by reducing its corrosion in aqueous electrolyte. However, the long-term stability of modified electrolytes must be established to understand the corrosion reduction characteristics of inhibitors.

ZnO has been researched as an additive in alkaline electrolyte.[169] Thus, it is worth checking the performance of ZnO with other inhibitors to enhance the potential of Al–air cells. Wang *et al.* developed a non-ionic surfactant branched alkyl glycoside (BAG) and ZnO-based hybrid inhibitor, and the respective inhibition mechanism is illustrated in Fig. 9(a). ZnO has a mild inhibitory effect on aluminum corrosion because of its corrosion-resistant characteristics. Further, in the case of the BAG/ZnO hybrid inhibitor, the BAG molecules attach to the Al
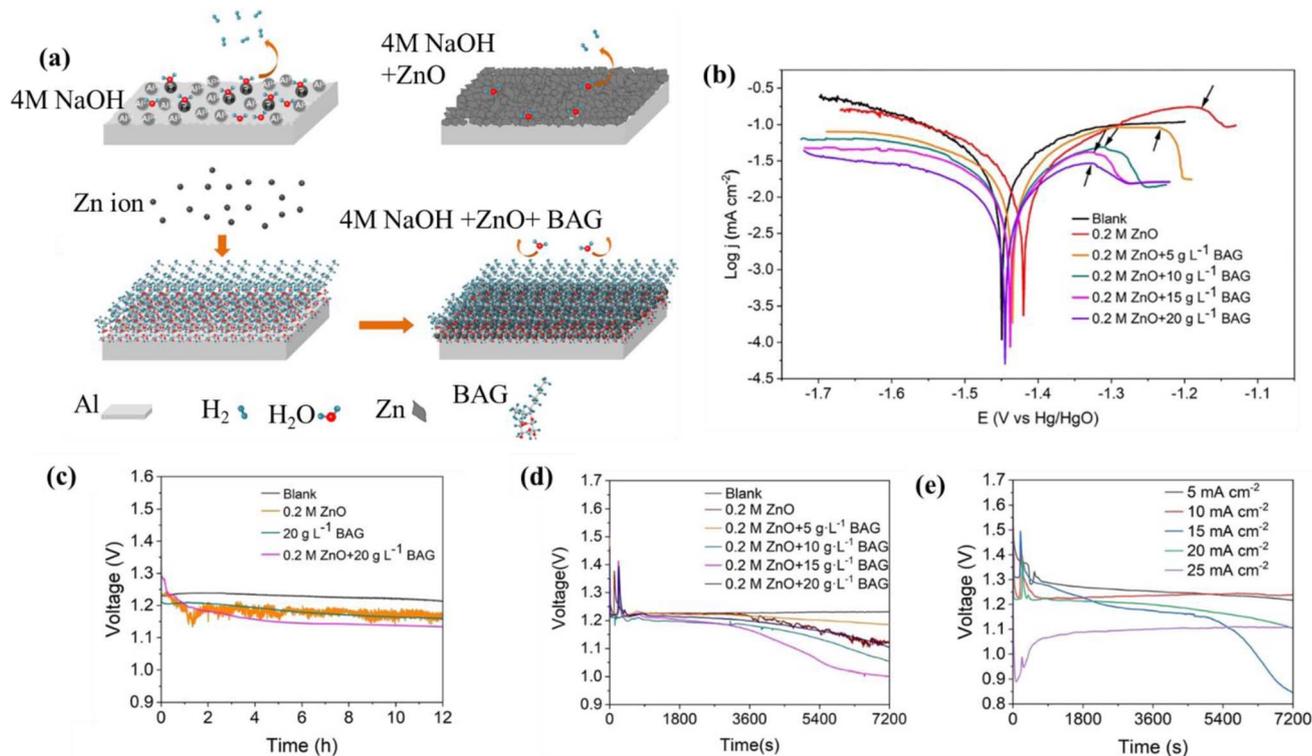
Fig. 9 (a) Schematic illustration of inhibition mechanism ZnO/BAG. (b) Polarization curves of Al in 4 M NaOH electrolytic solution with and without inhibitor. (c) Discharge curves at 20 mA cm^{-2} for 12 h. (d) Discharge curves at 20 mA cm^{-2} for 2 h using hybrid electrolytes. (e) Discharge curves at 10–25 mA cm^{-2} with the hybrid of 0.2 M ZnO and 20 g per L BAG.[189]

surface and organize themselves into structured molecular arrays, as explained schematically in Fig. 9(a). The oxygen functional groups primarily occupy the active sites for hydrogen evolution, while the hydrocarbon chains protect the Al base from the surrounding solution. The Zn^{2+} ions form a molecular network by interacting with the –OH groups on the glucoside. Simultaneously, a few Zn^{2+} ions move across the network, filling the positions between molecules. The glucoside–Zn coordination complex functions as a structural foundation for the deposition of Zn, thereby accounting for the consistent distribution of Zn nanoparticles. In addition, the presence of glucoside–Al bond anchors inside the network enhances the stability of the protective layer. This is also visible in the electrochemical performance in Fig. 9(b)–(e). According to Fig. 9(b), it can be observed that the initial passivation potentials of the hybrids exhibit a negative shift compared to the passivation potential of ZnO alone of −1.196 V. Moreover, the density shoulders observed in the hybrids exhibit a notable decrease compared to that observed in ZnO only. This indicates that BAG can expedite the deposition of Zn and enhance the density of the protective layer. The discharge curve of a complete Al–air battery for 12 h at a current density of 20 mA cm^{-2} is shown in Fig. 9(c) to test the impact of the electrolyte on the discharge performance. The voltage at which ZnO and the hybrid electrolytes operated seemed to decrease as the depth of discharge increased. The observed phenomenon can be attributed to the buildup of byproducts on the anode. The battery containing ZnO demonstrated fluctuations in battery voltage, which was attributed to

the ongoing process of Zn layer deposition and stripping. The addition of BAG with ZnO in the electrolyte solution resulted in a significant reduction in these fluctuations. Upon addition of the hybrid of 0.2 M ZnO and 20 g per L BAG, the specific capacity reached 2396 mA h g^{-1}, which was ~1253 mA h g^{-1} without any additive at the same current (Fig. 9(d)). Furthermore, a series of discharge experiments was conducted at various current densities in the range of 5–25 mA cm^{-2} to assess the viability, as presented in Fig. 9(e). This finding demonstrates that the incorporation of BAG can significantly augment the stability of the protective layer.[189]

6. Electrocatalyst

The composition of the air-cathode of the Al–air battery includes a GDL and catalytic layer anchored on the current collector. The GDL consists of a carbon substance and a hydrophobic binder, allowing only air to pass through and preventing the penetration of water. Typically, the current collectors consist of a mesh composed of nickel metal or carbon cloth, which can be connected to an external circuit to enhance the electron transfer processes.

The active layer of the catalyst is composed of the active material, acetylene black, and binder dissolved in N-methyl-2-pyrrolidone (NMP). The catalytic ink is usually applied on the current collector on the air cathode side. It serves as the site for ORR to trigger the reaction. The electrocatalyst present in the air electrode is crucial in defining the performance of the electrode

and maximizing the energy density. The effectiveness of the Al–air battery is determined by the efficiency and rate of electrochemical ORR at the cathode. These properties can be enhanced by customizing the cathode catalysts *via* nano-engineering. The limited practical application of the Al–air battery is primarily due to the sluggish ORR at the cathode. In this case, despite their high cost and limited availability, platinum and its alloys are widely recognized as the most effective electrocatalysts for ORR in alkaline aqueous solutions. Nevertheless, the successful execution of commercial applications necessitates an economically feasible and environmentally sustainable catalyst. Also, the particle shape and exposed surface are critical in determining the catalyst performance.[57] A positive correlation exists between the response rate and the extent of exposure to the catalyst surface. For the feasibility of an Al–air battery, the air cathode must incorporate an appropriate electrocatalyst to modify its ORR activity. The different types of catalysts used for Al–air batteries are discussed in the following sub-sections.

6.1 Metal-based catalysts

Catalysts composed of noble metals are widely recognized and extensively explored for oxygen electrochemistry, including water splitting, biosensors, and fuel cells. The ORR activity of Pt, Pd, Au, and its alloys is high due to their vacant d-orbitals, which enable them to absorb reactant molecules quickly, whereas they show modest OER activity. In contrast, RuO_2 and IrO_2 exhibit elevated OER activity, although they demonstrate sub-par ORR efficacy. Pt has been the subject of intense research in recent decades as a noble metal catalyst due to its exceptional catalytic activity.[190] This is why a Pt/C slurry as the catalyst ink is considered the reference for metal–air batteries and fuel cells due to its superior ORR performance. The half-wave potential of the noble catalyst (Pt/C) generally used is ~0.86 V *vs.* RHE in 0.1 M KOH solution.[78,191] The catalytic activity of Pt catalysts can be further enhanced by modifying their electronic states, given that the surface atomic arrangement and electron level state significantly influence activity. Researchers have examined the impact of the particle size and crystallographic facets of Pt on its catalytic activity. It has been found that the strength of the binding between Pt atoms and reactant species can determine the catalytic activity of ORR on different crystallographic facets, with Pt {100} showing the maximum activity followed by {110} and {111}.[192,193]

Despite the numerous hurdles associated with Pt catalysts, such as the need to regulate their facet distribution and manage their particle size, the primary issue stems from the high cost and limited availability of Pt as a finite natural resource. Hence, it is crucial to develop Pt-based catalysts that exhibit high efficiency while minimizing the Pt loading. In this case, one viable approach involves the loading of Pt on catalytic substrates with substantial surface areas. Wang *et al.* described that the catalytic efficiency of Pt alloys can surpass that of pure Pt. That occurs due to the phenomenon involving a reduction in the size of the Pt lattices and modification of its d-orbital states by the incorporation of transition metal atoms.[194] This enables the

attainment of higher catalytic activities compared to pure Pt. The catalytic activity of Pt metal catalysts is also influenced by various factors such as their particle size, structure, chemical composition, and electronic structure when combined or doped with other metals. Pt was also integrated with different transition metals to examine their impact on Pt alloys. For example, a 9 nm octahedral Pt–Ni catalyst exhibited favorable catalytic performances.[195] Also, octahedral Pt–Ni nanoparticles displayed enhanced ORR activities compared to cubic-structured Pt–Ni nanoparticles.[196] This implies that the catalytic activity is significantly influenced by the size and crystalline structure of Pt. However, despite the excellent performance, it is important to note that the catalytic activities may degrade over extended periods due to the limited durability of mixed transition metals. Thus, to mitigate this, some researchers have suggested the use of core–shell-structured catalysts, limiting the amount of Pt employed on the surface and protecting the transition metals on the catalytic surfaces.[197–201] Luo *et al.* synthesized a catalyst with Au nanoparticles with Pt loaded on MWCNT using a one-pot synthesis method. Among the different ratios of Au and Pt, the optimized slurry was a 10.2 wt% slurry of Au : Pt in the ratio of 0.67 : 1, exhibiting excellent ORR activity and durability with 20 wt% Pt/C. Further, with an increment in the amount of Au : Pt (1.68 : 1), the specific capacity and power density increased to 921 mA h g^{-1} and 1486.8 mW cm^{-2}, respectively.[103]

A nanoporous gold nanoparticle catalyst was prepared through the dealloying of gold–silver leaves by M. Wang and coworkers. They claimed that this catalyst is 55 times cheaper than Pt/C. This promising catalyst could minimize the overpotential to 56 mV dec^{-1}, which was 78 mV dec^{-1} in the case of Pt. Its stability was also comparable to that of Pt/C. However, the difference can be seen in the sample preparation using chemical and electrical dealloying together with and without surfactants. The difference in the orientation of the facets was suggested to be responsible for the change in ORR behavior. Theoretically, (100) facets are likely to be more electrochemically favorable for ORR.[104]

Among the metals, Ag also seems to be a good option for utilization as a catalyst due to its impressive conductivity and low cost compared to Pt and gold. However, Ag powder suffers from weaker oxygen adsorption, creating hindering its catalytic behavior. Hong *et al.* developed a silver catalyst on carbon fiber paper without using a binder, which was deposited *via in situ* electrodeposition. The calculated Tafel slope was around 98 mV dec^{-1}. At a current density 30 mA cm^{-2}, the silver catalyst demonstrated a very high specific capacity of more than 2780 mA h g^{-1} and an energy density of 4342.3 W h kg^{-1}. The demonstrated capacity is quite close to the theoretical capacity of the Al-anode.[202] Wang *et al.* prepared Ag–Cu alloy nanoparticles using hot-arc plasma technology.[203] The synthesis procedure is illustrated in Fig. 10, where the N-doped porous nanocarbon was mixed *via* wet grinding to enhance its conductivity. Ag and Cu both are known for their catalytic properties. Thus, alloying of both particles is expected have a synergistic effect. Further, the addition of N-doped nanocarbon tends to provide more active sites for ORR. The rapid heating and cooling process caused it to form a eutectic mixture
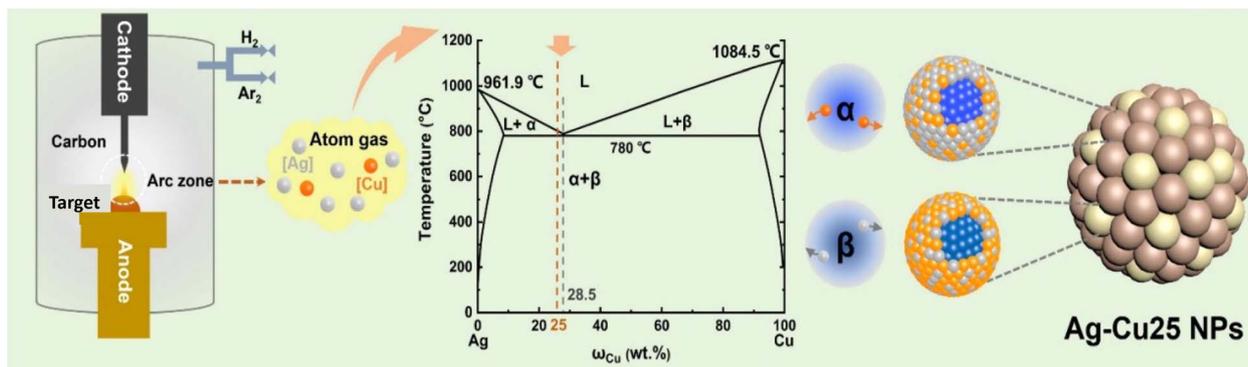
Fig. 10 Schematic illustration of the synthesis of Ag–Cu nanoparticles.[203]

of Ag–Cu, which changed its inert electronic structure. The prepared structure was a 3-D porous structure with a surface area of ~400 m^2 g^{-1} and an average pore size of 2.77 nm.

Different compositions of Ag–Cu were evaluated electrochemically, as shown in Fig. 11(a)–(e). Among the prepared catalysts, the Ag–Cu$_{25}$/NPC catalyst exhibited the maximum ORR peak voltage of 0.80 V, which was ~50 mV lower than the Pt/C peak potential of 0.84 V, as can be seen in Fig. 11(a). The peak potential of the ORR for Cu/NPC was 0.78 V, which is greater than that observed for Ag/NPC of, but the peak potential of AgCu$_{25}$/NPC was 0.77 V, falling between them. According to the LSV curve in Fig. 11(b), AgCu$_{25}$/NPC showed a half-wave potential, the second highest after Pt/C. Also, the number of electrons was 3.9, which is comparable with that of Pt/C (3.89), and H$_2$O$_2$ was suppressed by up to 7.93% (Fig. 11(c)). Similarly,

it can be inferred from the Tafel slope and plot of current density as a function of scan rate, as shown in Fig. 11(d) and (e), respectively, the AgCu$_{25}$/NPC composition is the most favorable. Subsequently, utilizing the AgCu$_{25}$/NPC catalyst, the fabricated Al–air battery demonstrated remarkable electrochemical capabilities. It achieved a power density of around 191 mW cm^{-2}, maintained a good current output, and sustained a stable high voltage for 120 h. These results highlight the significant potential of this battery to serve as a viable alternative to conventional Pt/C catalyst-based batteries.[203]

6.2 Transition metal–oxide based catalysts

Transition metal oxides can easily be synthesized and are cost effective, exhibiting considerable potential as non-noble catalysts. The conventional function of metal oxide in ORR catalysis
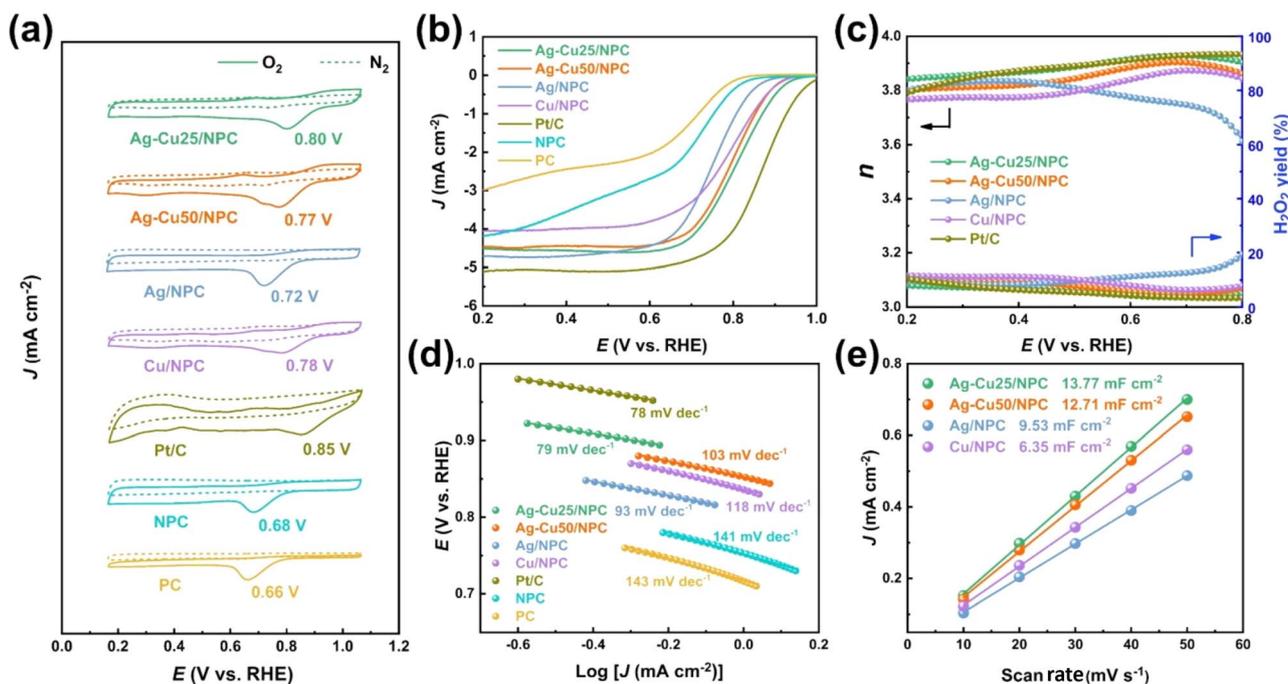

Fig. 11 Electrochemical performance of different compositions of catalysts in 0.1 M KOH O$_2$/N$_2$-saturated electrolyte using RDE. (a) Cyclic-voltammetry curves, (b) linear sweep voltammetry curves, (c) electron transfer number, n, and hydrogen peroxide yield, (d) Tafel slopes, and (e) current density as a function of scan rate at 0.4 V vs. RHE.[203]

is to facilitate the decomposition of H_2O_2 into H_2O and O_2. Recently, Ipadeola *et al.* showed the potential of porous transition metal oxides as the catalytic layer on the side of the cathode, resulting in an improved battery efficiency by enhancing the ORR and OER performances.[204] The advantages of using transition metal oxides are mainly a reduction in cost by replacing noble metal catalysts, abundantly available inexpensive precursors, and simple synthesis techniques. These materials can be tailored to achieve the desired morphology, particle size, and rich active sites, which provide high charge mobility and large surface area to improve the reaction kinetics. Li *et al.* prepared a Co/MnO Mott Schottky heterostructure using a one-pot pyrolysis method and applied it as a catalyst. The performance of these catalysts is also comparable with noble metals. Here, the number of electrons involved in the ORR mechanism is ~3.72. The Al–air battery using Co/MnO nanoparticles encapsulated in N-doped carbon achieved a power density of 139.8 mW cm^{-2}, which is comparable to the power density of the Pt/C-based Al–air battery of 136.2 mW cm^{-2} at a current density of 100 mA cm^{-2}.[205]

6.3 Perovskite-based catalysts

Vasudevan *et al.* prepared a sol–gel-derived LaCoO$_3$ (LCO) perovskite as a catalyst in an Al–air battery. This catalyst was first tested in a 3-electrode system and compared with bare GCE and Pt/C on GCE to complete the battery discharge profile. The

LCO/GCE material exhibited a cathodic reduction peak at 0.76 V (compared to the RHE) in O$_2$-saturated 0.1 M KOH electrolyte at a current density of −6.02 mA cm^{-2}. The GCE exhibited a decrease in potential of 0.8 V (compared to RHE) when subjected to a current density of 0.7 mA cm^{-2}, which was 0.72 V (*vs.* RHE) at −0.79 mA cm^{-2} for 20 wt% Pt/C. In the case of the whole battery, in which PVA–KOH gel electrolyte was employed, the OCV was obtained at 1.37 V, and the discharge characteristics of LCO were recorded at different current densities, *i.e.*, 0.5, 1, and 3 mA cm^{-2}, with specific capacity 309, 677 and 1770 mA h g^{-1}, respectively.[206] Shui *et al.* compared four perovskite-based 3-D ordered microporous structures (3DOM). The synthesis of perovskite oxides, specifically 3DOM La$_x$Sr$_{1-x}$Mn$_\delta$Co$_{1-\delta}$O$_3$, involves the inclusion of LaMnO$_3$ (3DOM LMO), La$_{0.75}$Sr$_{0.25}$MnO$_3$ (3DOM LSMO), La$_{0.75}$Sr$_{0.25}$CoO$_3$ (3DOM LSCO), and La$_{0.75}$Sr$_{0.25}$Co$_{0.5}$Mn$_{0.5}$O$_3$ (3DOM LSCMO). Among them, the 3DOM LSMO exhibited the most favorable catalytic activity for ORR and demonstrated the highest durability. Additionally, it possessed a significant specific surface area of 43.1 m^2 g^{-1}. The value of n was around 3.8, and the purity of H$_2$O$_2$ was as low as 10%. Furthermore, the use of 3DOM LSMO as the air electrode in the Al–air battery resulted in exceptional electrochemical properties. The specific capacity of the battery reached around 1084 mA h g$_{Al}^{-1}$, while the energy density reached 1493.3 mW h g$_{Al}^{-1}$. These findings substantiate that the 3DOM LSMO holds great potential as an ORR catalyst for flexible metal–air batteries.[207]
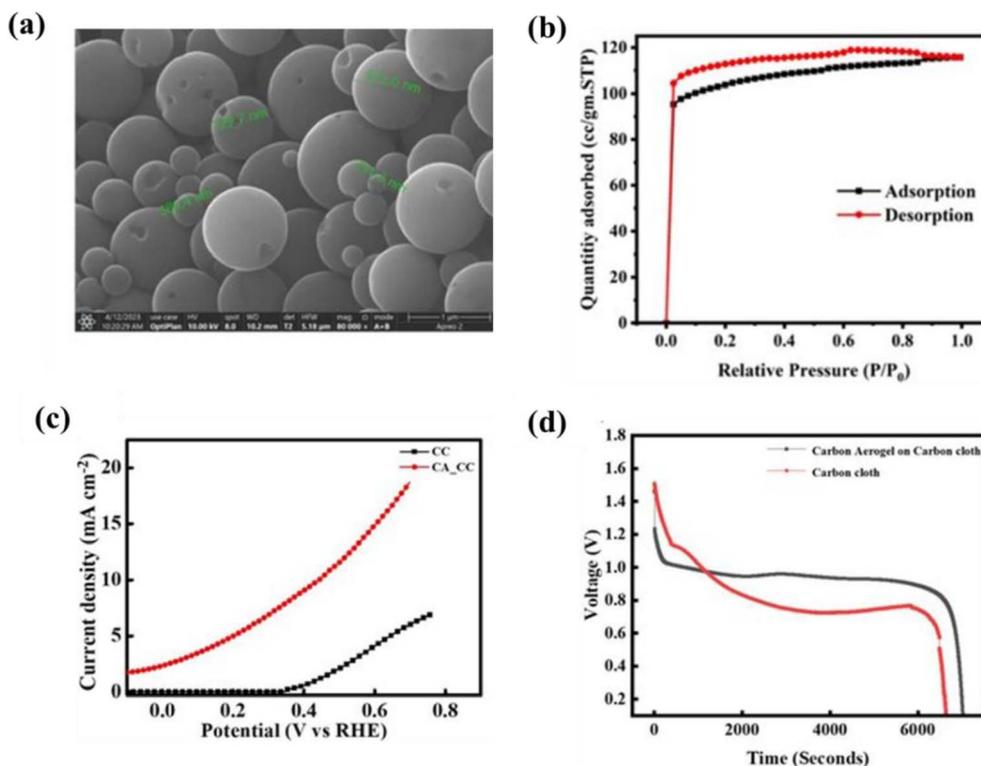

Fig. 12 (a) SEM micrograph of carbon aerogel showing its porous network of microspheres. (b) Nitrogen-adsorption isotherm to evaluate surface area. Comparison of the electrochemical activity with carbon aerogel and without carbon aerogel using (c) linear sweep voltammetry curve and (d) discharge performance at 1.275 mA cm^{-2}.[210]

Table 5 Recent catalysts employed in Al–air battery and their respective electrochemical parameters

S. N.	Catalysts	E_{onset} vs. RHE (V)	$E_{1/2}$ vs. RHE (V)	Tafel slope (mV dec^{-1})	OCP (V)	Specific capacity (mA h g^{-1})	Power density (mW cm^{-2})	At current density (mA cm^{-2})	Ref.
1	LaCoO$_3$ perovskite	1.124	0.929	83.7	1.35	1770	10	0.33	206
2	(Co,Mn)$_3$O$_4$-doped carbon nanotube composite	—	0.831	87.17	1.48	—	147	50	216
3	Fe–Cu dual-site nanoparticles	1.01	0.867	69	1.56	—	—	20	217
4	NiFe LDH A-FeSACoSA-FeCoAlloy-CNT/NC	0.93	0.86	125.5	1.49	120 mA h g^{-1} (at 1 mA cm^{-2})	145	157	218
5	Fe/Ce-NCNT	0.97	0.88	98	1.81	—	164	100	219
6	Mn-based@GO	0.91	0.77	112.62	1.5	1682 (at 30 mA cm^{-2})	57	50	214
7	Fe-N$_x$@NC/rGO	1.03	0.925	58.99	2.01	2584 (at 100 mA cm^{-2})	98	150	212
8	Ag-Cu$_{25}$/NPC	—	0.82	79	1.89	2412	193	120	203
9	Co@N/GNP	0.98	0.87	78	1.61	—	143	191.83	220
10	Ag@MnO$_2$/MWNT	—	0.87	106	1.68	1240	140	20	124
11	Fe-NG-MXene	—	0.91	77	—	—	82	50	221
12	α-MnO$_2$/Co$_3$O$_4$	0.833	0.76	89	—	185	—	50	222
13	MnS/NS-C	1.07	0.91	58	1.56	—	135	192.3	223
14	CoNi@NCNTs/CC	0.89	0.82	64	1.68	1029	151	221	224
15	FePc@HNSC	0.99	0.88	77	1.92	—	205	150	211
16	3DOM LSMO	0.89	0.87	85.3	1.44	1084	—	5	207
17	NiSAFeSA-Ni@FeNPs/CNTs-NGNS	0.92	0.87	86.7	1.61	—	184	270	225
18	NCAG/Fe-Cu	1.07	0.94	55	2.00	—	137	10	226
19	3.5ZnS/NSC-NaCl-900	1.02	0.905	98.3	1.71	936	251	50	227
20	FeCo/N–C–pistachio	0.93	0.83	—	—	—	100	10	228
21	FeCo/N–C–peanut	0.91	0.71	—	—	—	60	10	228
22	Chem-npAu	0.93 ± 0.01	0.83 ± 0.01	57	—	—	237	360	104
22	Elec-npAu			78					
23	0.8-CoNCNT	0.94	0.85	—	1.794	—	159.6	217.8	229
24	Au$_{1.68}$Pt/MWNTs	1.159	0.892	74	1.75	—	146.8	200	103
25	MnOOH@CeO$_2$	0.91	0.80	111.1	—	—	302.8	400	230
26	Co$_3$Fe$_7$–Fe$_3$C/HNC	0.78	0.64	85	—	—	210	286	231
27	reduced m-Co$_3$O$_4$/3DG	0.93	0.84	71.45	1.53	422.74	—	1	159
28	MnO/Mn$_2$O$_3$/ONCNF-3	0.903	0.805	103.8	~1.8	—	129.7	165	232
29	Fe-SA-NC@CC	0.97	0.86	—	1.53	—	3.94	1	233
30	FeNi-NP/NC	—	—	89	~1.6	—	24.9	1	234

6.4 Carbon composite catalysts

Carbon materials such as CNT and carbon black are used most in batteries as a conductive agent added in the slurry. The carbon composites provide more active sites for oxygen and promote the efficiency of the battery. A lightweight carbon material, *e.g.*, carbon aerogel, is well known for its porous network sites.[208,209] The A-MAD research group used a carbon aerogel in catalytic ink for an Al–air battery. The carbon aerogel was prepared *via* the sol–gel polymerization of resorcinol-formaldehyde precursors, followed by carbonization after the acetonic exchange of the gel. Fig. 12(a) shows the SEM image of the aerogel, which possessed a porous network of microspheres. The BET results, as shown in Fig. 12(b), exhibited its surface area of $\sim$472 $m^2\,g^{-1}$ and pore volume of 0.17 cc g^{-1}. As shown by the electrochemical performance in Fig. 12(c) and (d), it was predicted that implementing the carbon aerogel enhanced the reaction kinetics and performance of the whole assembled battery by around twice that of the blank one.[210] Another work by Luo *et al.* proposed a core–shell structure of iron phthalocyanine (FePc) induced by securing it on heteroatom-doped carbon spheres (HNSC) through Π–Π stacking. The optimal kinetics of FePc@HNSC in the ORR process was confirmed by its lower Tafel slope of 77 mV dec^{-1} compared to that of Pt/C, *i.e.*, 79 mV dec^{-1}, whereas FePc showed a value of 133 mV dec^{-1} and HNSC showed 108 mV dec^{-1}. Furthermore, FePc@HNSC demonstrated an exceptional $E_{1/2}$ and displayed a significantly greater kinetic current ($J_k = 54.9$ mA cm^{-2} at 0.8 V) than Pt/C and the reference catalysts. The estimated specific capacity of the battery anchored with FePc@HNSC was 1320 mA h g^{-1} at a current rate of 100 mA cm^{-2}, considering the mass of aluminum consumed during the galvanostatic discharge process. This value surpasses that of the Pt/C battery, which has a specific capacity of 1252 mA h g^{-1}.[211] Meng *et al.* prepared Fe_3C nanoparticles *via* pyrolysis to promote the active sites to Fe–N_x–C. Ultimately, the precursors were subjected to pyrolysis, resulting in the formation of carbon nanofibers with a single dimension. The nanofibers contained a significant number of Fe–N_xC sites and Fe_3C nanoparticles, which enhanced the catalytic activity of the Fe–N_x–C sites. During the pyrolysis process, the graphene oxide undergoes reduction to become graphene, resulting in enhanced graphitization and increased electrical conductivity in the catalyst. The power density of the Al–air battery with an Fe–N_x@NC/rGO air cathode was observed to be around 97.66 mW cm^{-2} at the current density of 150 mA cm^{-2}. This value is notably greater than the power density of the battery with a Pt/C air cathode, which was approximately 62 mW cm^{-2} at a current density of 78 mA cm^{-2}.[212] Hu presented a mesoporous carbon framework of MnS particles. Firstly, Mn_2O_3 was prepared *via* the hydrothermal technique. The Mn_2O_3 substrate was subjected to sulfurization to MnS with the application of 2-aminothiophenol vapor during pyrolysis. This resulted in the formation of N,S-co-doped carbon-covered MnS particles, referred to as NS-C@MnS. This carbon framework exhibited a discharge time of around 35 h at a constant voltage plateau of 1.28 V and current rate of 1 mA cm^{-2} in an Al–air battery. At a voltage of 0.69 V and current

density of 192.3 mA cm^{-2}, the peak power density was measured to be 134.6 mW cm^{-2}. Given that the fabricated battery was flexible in nature, it was tested at various angles at which its performance was not altered.[213]

Liu *et al.* added graphene oxide in an Mn-based catalyst to improve the catalyst response and compared the Mn-catalyst with the composite of graphene oxide-added manganese catalyst (Mn-based @GO) and commercial 20% Pt/C. The discharge voltage of the Al–air battery utilizing the Mn-based catalyst as the catalyst initially dropped rapidly and reached a stable level after 1.5 h, reaching approximately 0.85 V. The Al–air battery, when using the Mn-based@GO catalyst as the air-cathode rapidly reached a stable discharge voltage of approximately 1.26 V. This value closely matched the voltage of the commercial 20% Pt/C cathode, which was 1.28 V. When comparing the Mn-based catalyst to the Mn-based@GO catalyst, the latter enhanced the discharge voltage of the Al–air battery by 0.41 V at a current density of 30 mA cm^{-2}. Additionally, the stability of the Mn-based@GO catalyst was superior. The distinctive form of the Mn-based@GO, which was synthesized using a hydrothermal method using 20% GO, can be attributed to the combined influence of α-MnO_2, MnO(OH), and GO. The incorporation of GO resulted in the generation of MnO(OH) nanorods, leading to the synthesis of a new nanocomposite consisting of MnO_2/MnO(OH)@GO. The addition of GO in Mn successfully reduced the consumption of aluminum, and the mass-energy density increased from 1485 to 2119 W h kg_{Al}^{-1}. Furthermore, the incorporation of GO significantly enhanced the surface defects in the nanocomposite material, hence facilitating the enhancement of its electrochemical characteristics. In addition, the electrochemical test demonstrated that the incorporation of GO substantially improved the performance of the manganese-based catalyst.[214] It has been perceived that adding a graphene oxide-like carbon material may also be useful for other metal and metal oxide-based catalysts. Similarly, Qin *et al.* added 20% graphene oxide to Mn-doped $SrCoO_3$ (G-$SrCo_{0.5}Mn_{0.5}O_3$), exhibiting better electrochemical activity and discharge performance. The discharge power density for $SrCoO_3$ was recorded at 13.26 mW h cm^{-2}, which decreased after adding manganese ($SrCo_{0.5}Mn_{0.5}O_3$) to 12.75 mW h cm^{-2} and increased after loading graphene to 13.85 mW h cm^{-2}, at a current rate of 10 mA cm^{-2}.[215]

Directing the catalytic activity of any material depends on it electrochemical selectivity. Some recent works and their results are summarized in Table 5, highlighting electrochemical parameters, including E_{onset}, $E_{1/2}$, Tafel slope, OCP, and performance.

7. Design issues with Al–air cell

The design of a battery plays a crucial role its efficiency. In this case, the air battery design is more critical given that it has to be selective and breathable to support the air cathode. Many researchers have devoted their efforts to efficiently designing Al–air batteries from aqueous to gel-based, coin cell to cassettes, and wearable to miniature ones. Furthermore, constant efforts are being devoted to overcoming the associated difficulties.

Table 6 Advantages and disadvantages of different types of electrolytes with the corresponding proposed Al–air cell design

Type of electrolyte	Advantages	Disadvantages	Suitable design
Aqueous electrolyte	• High ionic conductivity • High discharge performance • High water content reduces the cost	• Limited voltage stability • Water management/leakage issues • Disposal of corrosive products	• System with circulatory pump • Separator soaked with electrolyte
Ionic electrolyte	• Wide electrochemical stability window • Minimizing side reactions • Low volatility	• Limited conductivity • High viscosity • Heavy weight	• Separator soaked with electrolyte • Polymer-based assembly
Solid/gel electrolyte	• Enhanced safety due to no leakage • Wide temperature range • High durability and light in weight	• Limited ionic conductivity • Processing complexity • Instability due to shrinkage over time	• Flexible assembly • Thin batteries as 3-D printed/paper-based

Here, we also discuss some of the designs in the literature to draw attention to the importance of the battery design in achieving efficiency. The central role in creating a suitable design depends on the type of electrolyte. Here, some of the advantages and disadvantages are tabulated in Table 6 for different electrolytes and the corresponding proposed Al–air cell designs, which may help in creating an efficient practical design for bigger battery packs for large-scale applications.

The coin-cell-based assembly is the conventional cell used to check initial results on the lab scale and is suitable for all types of electrolytes. The A-MAD research group used the traditional 2032 coin-cell assembly by puncturing its upper case to make holes for the passage of air.[142] A schematic of the assembly is shown in Fig. 13(a). Atencio et al. comprehensively studied aqueous-to-gel electrolytes, additives, and alloys using the design of a polymer-based 3-D printed pattern composed of ABS polymer.[110,235] Some researchers use acrylic sheets, as shown by the A-MAD research group, in a similar type of assembly made up of acrylic polymers given that they are not affected by alkaline medium and will run for a longer duration.[55] There are some structural differences between the aqueous and gel electrolyte, showing that the assembly in series can withstand a higher voltage load. However, these batteries are often overlooked due to the heavy weight of metals and polymers, which limits their practical applications. Thus, to address the challenges associated with weight, researchers have explored the use of 3-D-printed batteries with ultrathin dimensions to achieve a more compact design.[236–239] Wang et al. demonstrated exceptional flexibility in their Al–air battery design, allowing for various use cases and physical bending without performance degradation. They developed a cellulose-paper-based Al–air battery. An Al foil anode was used inside the cellulose substrate, while the air-cathode was applied on its surface using catalyst ink to realize the complete Al–air cell. A detailed schematic is presented in Fig. 13(b). With its uncomplicated design and affordability, the Al–air battery exhibited a commendable power density of 19 mW cm^{-2} in alkaline electrolyte, but its operational time was just 48 min. Furthermore, a test was conducted with saline electrolyte, showing an operational longevity of up to 58 h at 1 mA cm^{-2}, and only 25 mg of aluminum could be recovered. The specific capacity of aluminum is reported to be 2338 mA h g^{-1}. This battery demonstrated exceptional flexibility

when subjected to various bending angles and repeated bending cycles exceeding 1000 cycles.[237] Another study utilizing the jet printing technique to reduce the thickness involved the preparation of an ultrathin electrolyte using aerosol printing. PVA was utilized as the gelling agent, while 1.8 M NaCl was employed as the salt supply. A flexible Al–air battery was constructed using an ultrathin electrolyte, with carbon cloth as the air cathode and aluminum foil as the anode. The cell pack weighed approximately 115 g and was less than 1.3 mm thick. A schematic of the battery is presented in Fig. 13(c), which could be fastened to the skin or clothing surface based on specific requirements. The cell pack employed in this study utilized a flexible ultrathin-neutral electrolyte, mitigating the chances of electrolyte leakage. The cellular arrangement was affixed to a muscle sticker, and the aluminum anode was not in immediate proximity to the skin, ensuring safety concerns. The discharge performance was tested at different electrolyte thicknesses with a combination of varying current densities from 0.1 to 1 mA cm^{-2}. The best discharge capacity of about 2011 mA h g^{-1} was observed at 1 mA cm^{-2} with a thickness of 74.5 µm. When checking the discharge performance at intervals of 30 min, the specific capacity was ~1506 mA h g^{-1} at 0.5 mA cm^{-2} for the electrolyte thickness of 37.8 µm. These studies show the perfect use of these thin and flexible batteries in various portable, wearable, and point-of-care applications. However, the removal of the Al$_2$O$_3$ oxide layer on the surface of the Al anode is challenging when using neutral electrolyte. The concentration of Cl$^-$ ions is restricted in a thinner electrolyte. During the electrochemical reaction, the Al anode will dislodge the Al$_2$O$_3$ shell, which will accumulate at the interface between the electrode and the electrolyte. This accumulation will increase the internal resistance of the battery and hamper the movement of ions. Furthermore, the presence of Cl$^-$ ions in the denser electrolyte is adequate for their penetration in the surface of the Al anode, enabling their active involvement in the electrochemical reaction.[240]

Pan et al. created a cotton-based Al–air battery using a low-cost industrial-grade Al plate as the anode. The selection of cotton as the substrate was based on its superior electrolyte storage capacity and reduced resistance to ion diffusion. Furthermore, a precise quantity of solid alkaline was pre-applied within the cotton material to regulate the ability of
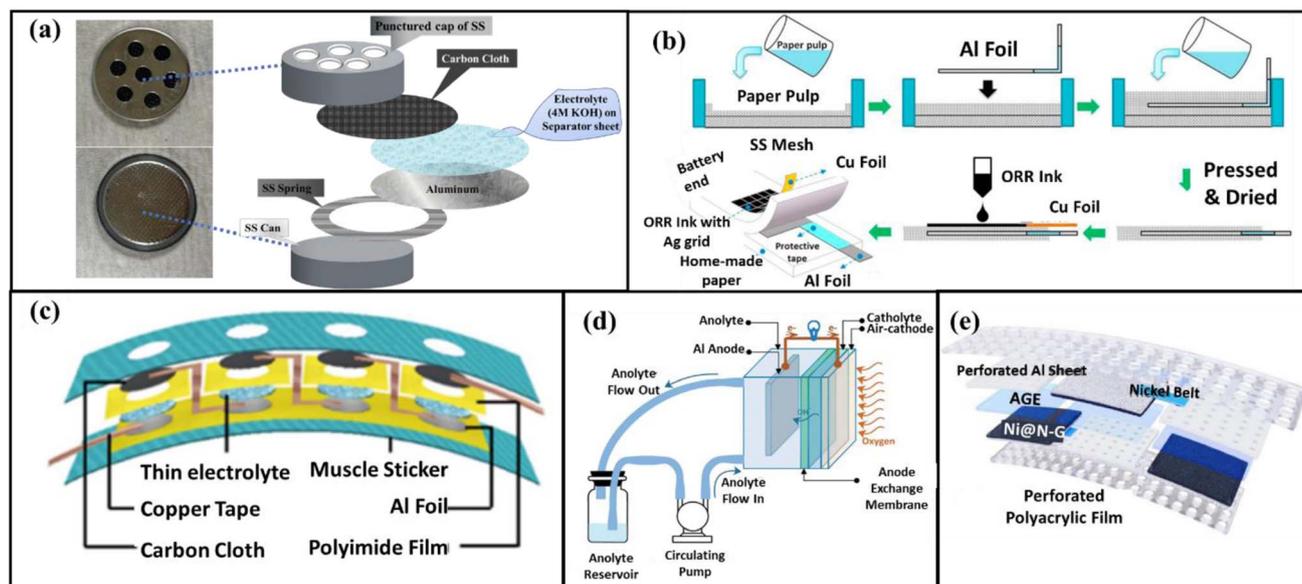
Fig. 13 (a) Coin-cell 2032-based assembly with battery components of Al–air battery.[142] (b) Process for the fabrication of 3-D printed paper-based Al–air battery.[237] (c) Schematic illustration of 4 cell pack ultrathin Al–air battery made up of solid-electrolyte using aerosol jet printer.[240] (d) Schematic image of the dual-electrolyte system consisting of liquid anolyte and gel catholyte.[242] (e) Schematic illustration of AGE-based flexible wearable Al–air battery.[243]

the battery to release energy and improve user safety. Besides, a passive water reservoir was utilized to maintain the required level of wettability. A 'passive water reservoir' is a reservoir that maintains the required level of wettability without active pumping. Additionally, pre-storing solid alkaline electrolytes in cotton enables secure operation and precise regulation of the discharge capacity. Consequently, this results in the development of a very practical power source suitable for applications that do not require much power. Furthermore, self-corrosion is effectively suppressed due to the impediment of OH^- dispersion within cotton. The cotton-based Al–air battery system demonstrated a significantly elevated peak power density of 73 mW cm^{-2}. In addition, a notable specific capacity of 940 mA h g^{-1} and substantial specific energy of 930 mW h g^{-1} were achieved at a current density of 10 mA cm^{-2}. Its voltage output may be effectively enhanced by developing a multi-cell battery pack. The affordability and sustainability of this battery technology make it particularly well-suited for recharging a range of mini-electronic devices in outdoor settings, where access to the electrical grid is limited and energy density is a critical factor.[241]

Phusittananan *et al.* demonstrated a dual electrolyte system-based Al–air battery, as illustrated in Fig. 13(d). In the case of dual electrolytes, it is necessary to store one a separate system. The substances used as anolytes in this study consisted of ethylene glycol/ethanol solutions (0, 5%, 10%, 20%, and 30% v/v), which were combined with 3 M potassium hydroxide (KOH). The catholyte utilized in this study is a polymer gel electrolyte known as Carbopol® 940. Given that one electrolyte is aqueous and the other is a gel, a circulatory pump is attached to the aqueous anolyte to minimize Al corrosion, triggered by HER. These findings indicate that utilizing the dual-electrolyte Al–air

flow battery can effectively mitigate anodic corrosion and passivation, contributing to an improved battery performance and longevity. However, the sluggish reaction kinetics could not be completely resolved.[242]

The management and utilization of liquid alkaline electrolytes pose significant challenges in the context of wearable power supplies. Al–air batteries with a semi-open layout can cause battery degradation and severe burns to the human skin due to the leakage of the electrolytes and alkali escape. Thus, the outdoor use of these battery assemblies is contingent on the resolution of this complex matter. To show the battery application in wearable and portable devices, Sun *et al.* developed a flexible battery. A high-strength agarose gel electrolyte (AGE) was developed to create a wearable battery with excellent energy density, safety, and significantly reduced self-corrosion. This AGE has a combination of outstanding strength and remarkable capacity to withstand alkaline solutions. The high-toughness AGE exhibited exceptional resistance to deformation under high pressure, preventing any electrolyte leakage (Fig. 13(e)). It ensured a stable interface between Al and AGE, facilitating the attachment of the passive layer to the Al anode surface and effectively preventing self-corrosion. The use of AGE reduced the self-corrosion rate of Al by up to 402% compared to solution-based alternatives. Significantly, the soft-package Al–air battery with a surface area of 10 cm^2 exhibited a discharge endurance of 20.1 h and a remarkable specific capacity of 2148.5 mA h g^{-1}. A wearable Al–air battery pack with practical utility was additionally equipped to power an LED array and a smartphone for practical applications.[243]

The aqueous electrolyte is mandatory for a higher operating voltage in Al–air batteries. However, it is restricted given that the anode continues to corrode when the battery is not in use
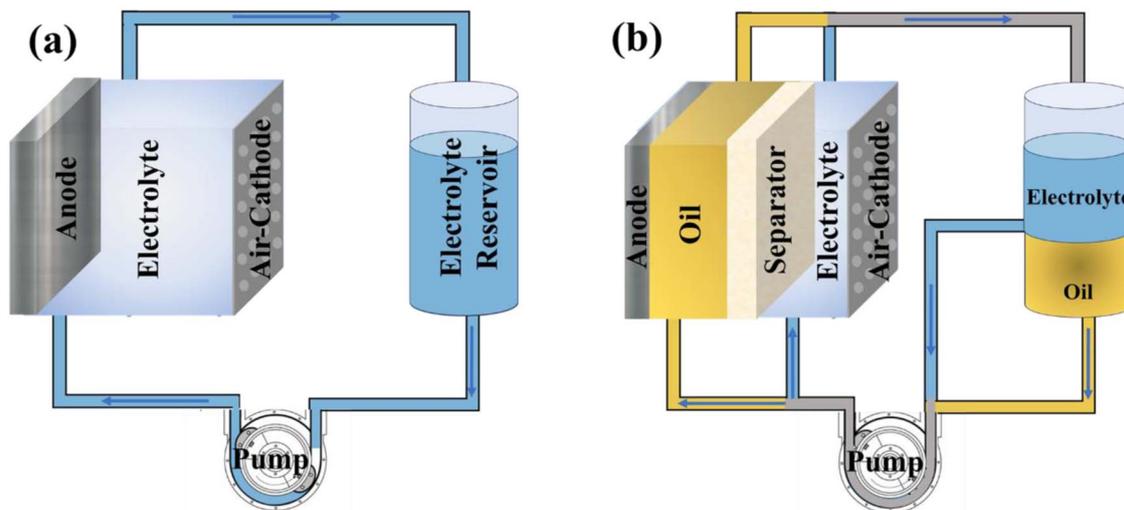
Fig. 14 (a) Schematic of conventional electrolyte with circulatory pump. (b) Oil displacement method during on/off state connected with circulatory pump.[244]

because of the continuous contact of the anode with the electrolyte. A schematic of the conventional aqueous electrolyte with a circulatory pump is shown in Fig. 14(a). Considering this issue, especially with aqueous electrolytes, Hopkins *et al.* provided a solution.[244] The mitigation of open-circuit corrosion was achieved by replacing the electrolyte on the electrode surface with a nonconducting oil during the off-battery phase. Oil displacement with electrolyte facilitated the battery discharge, resulting in an enhanced power and energy density. The ability of the proposed cell surfaces to exhibit underwater-oleophobic wetting characteristics enabled the reversible displacement of oil (see Fig. 14(b)). For this purpose, they measured the advancing and receding underwater contact angles of silicone oil and PFPE oil on the Celgard separator and the Al electrode. When exposed to water on the Al electrode, both silicone and PFPE oil exhibited oleophilic properties. However, the silicone oil caused the Celgard to wet, whereas the PFPE oil formed beads on the hydrophilic PTFE separator. During the on–off cycles, the current rate was 150 mA cm^{-2} for 25 min, with a 1 h interval during the rest state. Following the injection of silicone oil, the successive expulsion voltages exhibited a negative value, showing that the silicone oil caused fouling in the Celgard separator. The silicone-Celgard combination resulted in a total energy density of 0.66 ± 0.08 W h g$_{Al}^{-1}$. In contrast, the PFPE–PTFE combination resulted in a total energy density of 3.55 ± 0.08 W h g$_{Al}^{-1}$, similar to that obtained from charging the battery without any interruptions and without the addition of oil. Thus, the combination of PFPE–PTFE may be helpful in practical applications with the successive mitigation of Al corrosion, achieving high utilization efficiency.[244]

8. Rechargeability

The rechargeable nature of an Al–air battery is not possible in aqueous electrolyte, as inferred from the Pourbaix diagram.

However, it seems possible in some hybrid systems, as discussed in Sub-sections 5.2 and 5.3. Ryohei Mori showed the rechargeability od Al–air batteries with aluminum terephthalate as a metal–organic framework (MOF) for the air cathode and ethyl-3-methylimidazolium chloride [EMIM]Cl as an ionic liquid electrolyte. The open circuit potential of this battery was 0.7 V. However, this capacity seems relatively low, and the signature cathodic peaks disappeared after only 25 cycles. The observed disappearance may likely be attributed to the electrochemical reaction during the initial phase, facilitated by utilizing the MOF and conductive carbon components. The carbon materials underwent combustion, and their impact dissipated over multiple cell cycles. Also, [EMIM]Cl is hydrophilic and can absorb moisture from the surroundings. Notably, an AlCl$_3$–urea-based ionic liquid electrolyte was employed in conjunction with Co–MnO$_2$/C catalysts as air-cathodes, highlighting a novel approach to enhance the battery performance. By varying the mole ratio of Co in the range of 10–50%, they achieved the best catalytic activity with ~40%. The limited capacity of ~375 mA h g^{-1} was observed, and results were shown for a few cycles. Here, the discharge voltage also gradually decreased due to the decomposition of the ionic liquid electrolyte.[245]

Most of the reported studies on aluminum rechargeable batteries used non-aqueous electrolytes, which may be eco-toxic and show unstable cyclability. Also, the energy density of these cells is very poor. Furthermore, the use of organic electrolytes poses certain issues related to recycling, sustainability, and large-scale production. Although the water on anodes in metal–air batteries can have adverse effects, it is advantageous and essential for cathodes due to its facilitation of efficient oxygen cathodic reactions. These reactions occur during both the release of oxygen and the charging process. Additionally, water aids in the effective diffusion of ions towards the catalytic sites. A dual electrolyte system made up of alkaline and acidic electrolytes was also used to demonstrate rechargeability.[246]

Concerning all these facts, Gaele *et al.* demonstrated the viability of recharging Al–air cells using a dual electrolyte system based on water–gel electrolytes using polymers PVA and xanthan-gum without any separator. PVA–HCl was used as the anolyte, whereas Xa–KCl was used as the catholyte. In the configuration of dual-electrolyte, the water content was lower for the anolyte and higher for the catholyte. The electrochemical characterizations were separately performed in three-electrode systems for the anode and cathode. The results indicated that the anodic potential remained constant for the initial four cycles of charging. Moreover, the variations in anode potentials during charge–discharge were minimal with a difference of 50 mV. The charging potential exhibited an upward trend towards negative values, which indicated a diminished efficiency, while the deposition of aluminum. The discharge potentials stabilized at a constant value and maintained a steady discharge performance. The cathode discharge potentials exhibited a symmetric pattern for the initial six cycles. Besides, there was a notable increase in the variability in charge–discharge potentials of the cathode. The observed trend of the cathode charge shifted the voltage towards the positive

direction similar to the behavior of the anode potential. This phenomenon is likely linked to the re-deposition of aluminum.[109] However, although rechargeability was shown in these systems made up of dual-electrolytes, to achieve better cyclability and stability, other combinations of catholytes and anolytes need to be explored.

Similarly, a tri-electrolytic system with the integration of polymer ion-exchange membranes, organic electrolytes with alkaline anolyte, and acidic catholyte, reaching an excellent OCV of 2.2 V was reported by Wang *et al.* By appropriately arranging two ion-selective membranes, the occurrence of acid–base neutralization was effectively prevented, ensuring a consistent battery performance. A schematic representation of the complete system and camera image is shown are Fig. 15(a) and (b), respectively. The anode utilized in this study was standard kitchen aluminum foil. The three chambers of the cell, containing the $NaOH/CH_3OH$ anolyte, $NaCl/H_2O$ as the bridge electrolyte, and HCl/H_2O catholyte, were segregated through the implementation of a robust alkali Cl^- exchange membrane and a strong acid Na^+ exchange membrane. The air-breathing cathode employed was a GDE with Pt/C catalyst. By utilizing
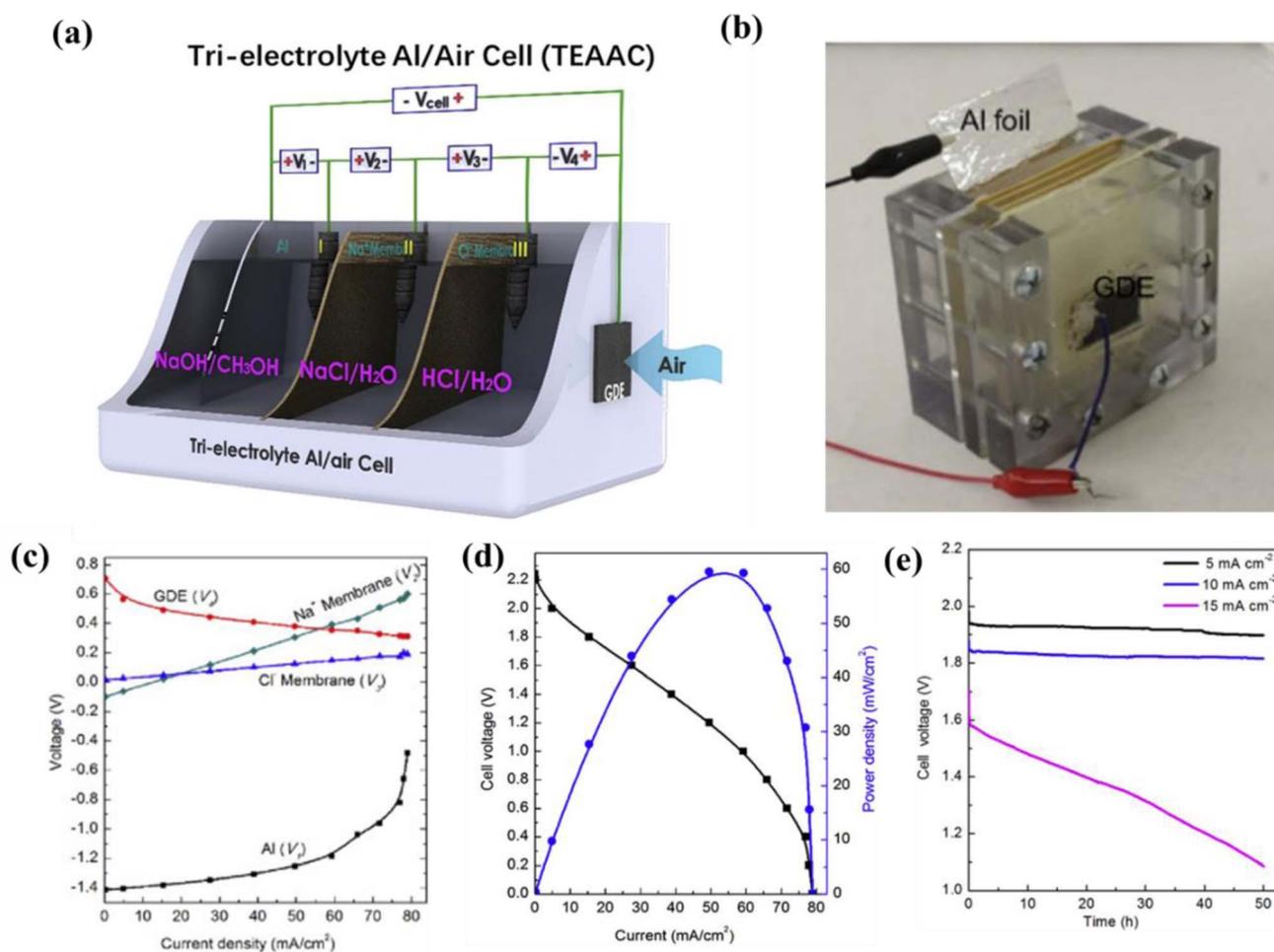

Fig. 15 (a) Schematic setup of the tri-electrolyte system of Al–air battery. (b) Camera image of the assembled Al–air cell. (c) Single-cell electrode polarization of Al, Na^+ membrane, Cl^- membrane, and GDE. (d) Power density curve of the Al–air cell. (e) Discharge curve of Al–air cell at a current density in the range of 5–15 mA cm^{-2}.[247]

organic anolyte in a targeted manner, the parasitic hydrolysis reaction linked to the oxidation of aluminum was nearly eradicated. The substitution of the alkaline catholyte with acidic catholyte resulted in a 0.83 V increase in the potential for ORR. As shown in Fig. 15(c), the polarization of each component of the cell was investigated. Anodic polarization usually causes the observed difference between OCP and theoretical cell voltage. Here, it was also verified from the polarization of Al that its change in voltage is ~0.9 V, which implies that nearly half of the voltage drop is because of the anode itself. That can be attributed to the consumption of hydroxide ions in the electrolyte during the formation and limited mass transport. The cathodic polarization predicts the GDE drop, which seems to be caused by sluggish ORR kinetics. It can be expected that the polarisation across both membranes exhibits a predominantly linear pattern. The potential across the Na^+ exchange membrane was in the range of 0.1 to 0.6 V, while the potential across the Cl^- exchange membrane demonstrated a minor variation from 0 to 0.2 V. Therefore, the potential reduction of 0.7 V and 0.2 V was attributed to the overpotential across both membranes. The conventional Al–air battery with alkaline electrolyte demonstrated a linear polarisation curve characterized by a voltage of 1.5 V and a short-circuit current density (J_{SC}) of 340 mA cm^{-2}. The tri-electrolyte system demonstrated a significantly greater V_{OC} of 2.2 V, while exhibiting a lower J_{SC} of 80 mA cm^{-2}. According to the polarization curve shown in Fig. 15(d), a maximum power density of 60 mW cm^{-2} was achieved at a current rate of 55 mA cm^{-2}. Also, the hydrogen evolution observed in the conventional aqueous solution was significantly mitigated. The use of an acidic catholyte enhanced the battery voltage to 2.2 V, while resolving the carbonation problems associated with traditional air cathodes. However, after considering the discharge curves in Fig. 15(e), it worked well up to a current rate of 10 mA cm^{-2}, whereas for 15 mA cm^{-2}, the battery performance showed a linear decay.[247] Thus, by appropriately arranging the anion and cation membranes, the occurrence of acid–base neutralization was prevented, enabling the achievement of a steady performance, which can be useful for practical applications.

9. Applications

Al–air batteries are targeted for various practical applications due to their high energy density, lightweight design, and potential cost-effectiveness. The reaction between aluminum and oxygen from the air, as well as water in the electrolyte, occurs within the battery, generating power for the targeted application. The outcome of the release process is formed as a hydrogel, $Al(OH)_3$. The substance is subjected to heat and undergoes decomposition into Al_2O_3. Electrolysis is used to regenerate Al_2O_3 into aluminum metal. The fuel energy cycle efficiency for the Al–air cell is shown in Fig. 16. Here, the base of 1 M aluminum is considered, assuming a complete battery energy depletion of 80%, with a possibility of unused 20% aluminum.

The fuel cycle energy balance consists of four components. These factors include the useful energy stored in the aluminum
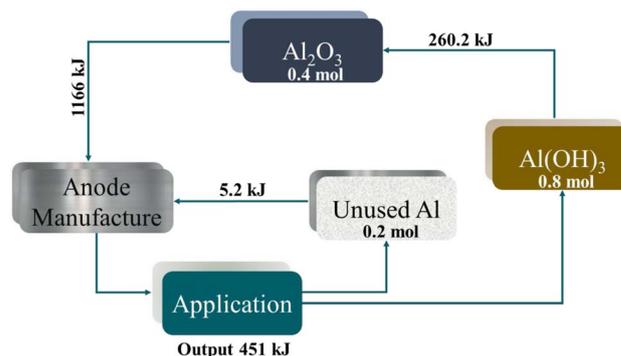

Fig. 16 Fuel energy cycle for Al–air battery applications.[248]

anodes, the thermal energy generated during the conversion of $Al(OH)_3$ to Al_2O_3 and Al_2O_3 to Al; and the unused aluminum that is transformed into the anode plates. The energy density of used aluminum is calculated to be 564 kJ mol^{-1}, which is 72% of its theoretical value of 783 kJ mol^{-1}. Therefore, the useable energy of 0.8 moles of aluminum is 451 kJ.[248] Some of the potential practical applications of Al–air batteries are discussed in the following sub-sections.

9.1 Electric/hybrid-electric vehicles

The targeted plan for applying Al–air batteries in EVs has been a point of research since the 1980s.[249] The associated challenges and research gaps discussed above are the main reasons why these batteries are still constrained to the laboratory. However, their appealing energy density compels us to devote continuous efforts to their application. Al–air batteries possesses the capacity to generate electrical energy to power automobiles and other modes of transportation. The significance of these batteries may be noteworthy in the context of the ongoing global shift from conventional gasoline-powered vehicles to hydrogen fuel cell cars. Al–air battery technology can provide sufficient energy and power to achieve driving ranges and acceleration comparable to that of conventional gasoline-powered vehicles. The utilization of aluminum as an anode can yield a cost as low as US$ 1.9 kg^{-1}, provided that the resulting reaction product is recycled. The expected energy density is 2000 W h kg^{-1}, which is suitable for mobility applications.[248–250]

The prototype of an electric car driven by an Al–air battery was built and successfully demonstrated by the 'Phinergy' company in 2013, showcasing the feasibility and potential of this technology for automotive applications.[251] Here, each Al plate possesses sufficient energy to transport an EV for an estimated distance of 20 miles. Furthermore, their current system can accommodate 50 plates simultaneously, resulting in a cumulative charge capacity of 1000 miles.[252] It is worth noting that this system required water refilling after every 200 miles. In addition, they also developed an EV that uses a combined pack of Al–air and Li-ion batteries. The Al–air battery enhanced the range of the Li-ion batteries by almost six-times. Phinergy also proposed Al–air batteries for short-range aircraft. Thus, Al–air-based energy-storage systems will be beneficial in terms of

both weight and expense without compromising the mobility ranges. Recently, Hindalco Industries Limited signed a memorandum of understanding (MoU) with Phinergy to develop and pilot the production of Al batteries.[253,254] Here, battery swapping stations, similar to current petrol pumps, are proposed to replace the anode and fill electrolytes. Further, the integration of Al–air batteries into remote sensor networks and surveillance systems may also be realized for longer durations, especially in strategic areas.

9.2   Military and underwater applications

The primary constraint in the widespread adoption of portable gadgets, encompassing various applications in military operations such as communications, health tracking, chemical-biological-radiological (CBR) sensors, helmet-mounted displays of real-time maps and data from other war fighters, headquarters, UAVs, satellites, and administered hovering channels, is the limited availability of power sources, *i.e.*, energy storage systems. The batteries must be lightweight, durable, rapid, rechargeable in the field, durable, and safety, which are critical to achieve successful missions for the army. Also,

military activities have distinct demands that diverge from those often associated with automobiles and commercial motor vehicles. Military land vehicles require batteries with substantial energy capacity to operate silently and the ability to generate high power for engine initiation and load leveling. In addition, these systems must possess the ability to endure challenging military environmental conditions and provide adequate overhead capacity to support anticipated increases in the electrical power demands of vehicles. In an average 72 h deployment, soldiers are expected to carry around twenty pounds of batteries in addition to their massive combat gear. Furthermore, future sophisticated equipment will necessitate a substantially greater amount of energy and power.[255–257]

Therefore, Al–air batteries appear advantageous due to their lightweight nature and capacity to function under challenging conditions without the risk of flammability, unlike traditional commercial batteries. According to the modern military system, a soldier carries around 70 batteries weighing 7 kg on a mission, as shown schematically in Fig. 17.[256,257] The saltwater battery is most suitable for applications with moderate power requirements and where multiple uses are desired, necessitating the
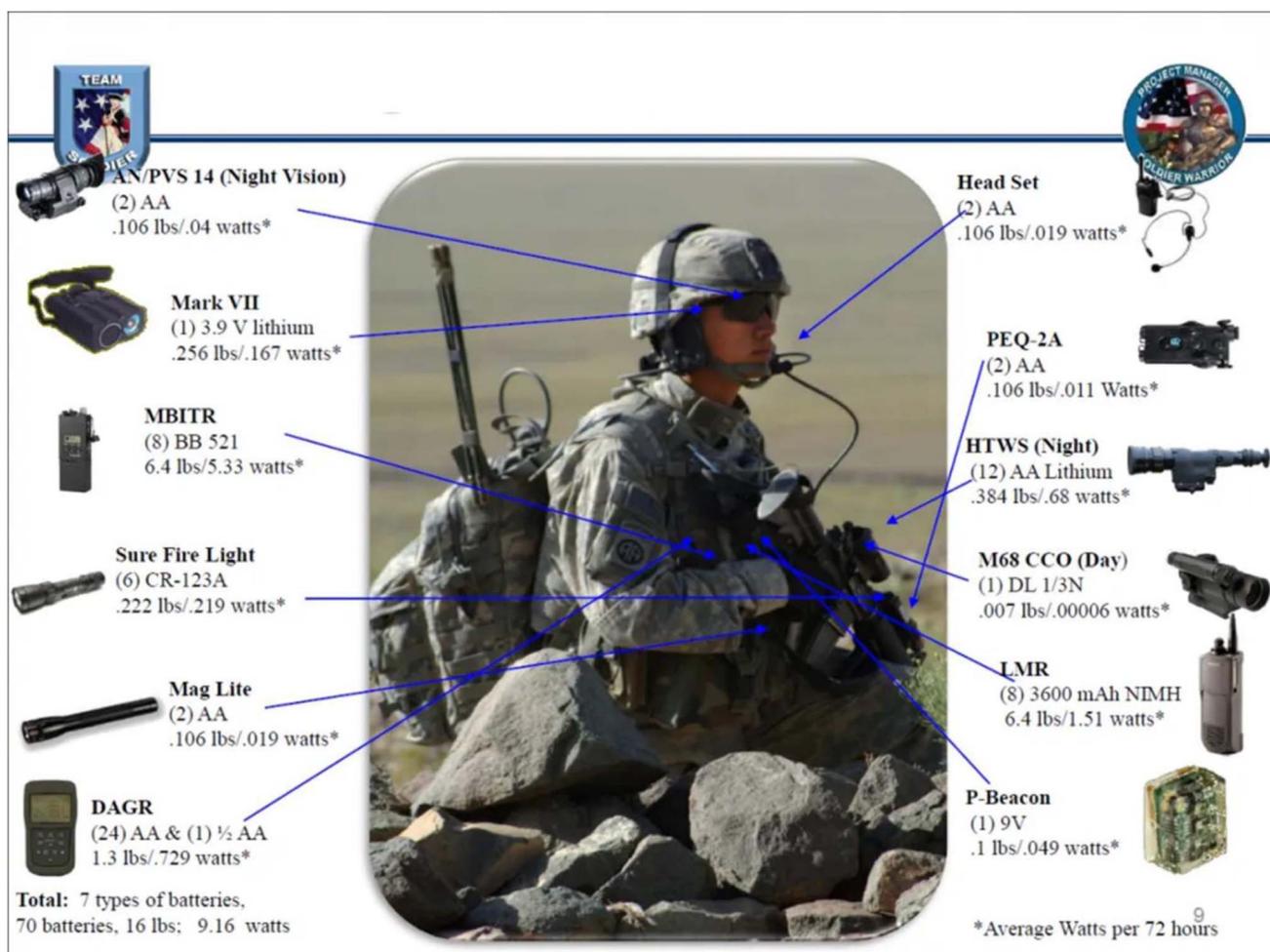

Fig. 17 Equipment carried by a soldier on a mission, with types of batteries used together with their corresponding weight and power ratings.[256,257]

emptying and cleaning of the battery between each use. An alkaline electrolyte can be utilized to construct a self-contained, portable battery for satellite communication, offering advantages such as stable performance and extended operational lifespan. The operational specifications necessitated a rapid cold start-up at -40 °C within half-hour, a power output ranging from 6 to 400 W, and an energy density of 435 W h kg^{-1}. The process of battery activation involves the removal of the electrolyte from the reservoirs located at the uppermost part of the cells.[120,258]

Al–air batteries are also targeted for propulsion in submarines and underwater vehicles, providing electrical power for propulsion motors and onboard systems. The high energy density of Al–air batteries allows underwater vehicles to operate submerged for extended periods without frequent recharging or refueling. The utilization of neutral electrolytes in marine and consumer applications shows excellent potential. Seawater naturally possesses inherent capability to serve as a neutral electrolyte due to its composition of around 3.5 wt% NaCl, conferring a natural advantage to Al–air batteries in underwater applications. Thus, Al–air batteries can be utilized offshore as well using simply Al plates and air cathodes. The electrolyte can be sourced directly from the ocean, resulting in non-toxic by-products and can be immediately released into the sea. Thus, the primary benefit of utilizing neutral Al–air batteries in underwater consumption arises from their exceptional safety features.[120]

9.3 Portable systems and strategic applications

The demonstrations of various portable systems such as mobile-phone charging and sensors are shown at the lab-scale, some of which were already discussed in the previous sections. For portable purposes, gel-based electrolytes seem to be efficient due to their flexibility. This system also shows promise for applications in power backup and point-of-care (POC) devices, addressing critical needs in remote regions and disaster relief efforts. Conventional waste disposal services are frequently unavailable when medical care is delivered in remote regions or during disaster relief circumstances. Therefore, POC devices

must be provided with lightweight and disposable batteries that do not contribute to the pollution of the local soil and aquatic environment upon disposal. In the literature, a cable-shaped Al–air battery was targeted to maintain a low assay cost, while the disposal of POC devices necessitates inexpensive components. Fotouhi *et al.* introduced a cable-shaped Al–air battery designed for on-demand activation by utilizing biological fluids. The procedure involved enveloping an Al wire within a nano-material paper matrix consisting of CNT coupled to cellulose fibers. A silver-plated copper wire was used as a current collector, wrapping around the Al wire with the nanomaterial paper matrix. The layered cable-shaped architecture enabled the activation of biological fluids on demand. The functioning of the battery was assessed by the utilization of electrolytes, which included possible reagents and samples of biological and physiological fluids. The cable-shaped battery was highly flexible and could be quickly flexed and severed for shape-adaptive applications. Also, it could be seamlessly incorporated into the circuitry to achieve the desired voltage and current levels.[259]

An Al–air battery, which was shaped-like fibers, could be easily manipulated into different forms and flexed at different angles without causing any noticeable structural damage. Ensuring consistent release of fluid during bending and stretching is crucial for practical applications, given that inconsistent release may lead to operational inefficiencies or discomfort, especially considering the dynamic motion of the human body. Thus, the fiber-shaped battery is well-suited for integration into fabrics. To illustrate its application, two Al–air batteries with fiber-like structures were enclosed in a permeable tube and linked in a series configuration to increase the output voltage and power. Subsequently, these batteries were integrated into a flexible textile to power a light-emitting-diode (LED) watch worn on a human wrist, as shown in Fig. 18(a) and (b).[187]

Aqueous electrolyte-based Al–air batteries are appropriate options for stationary purposes given that their ionic conductivity and practical discharge plateau are high. The demonstration using an aqueous rechargeable battery with the LED
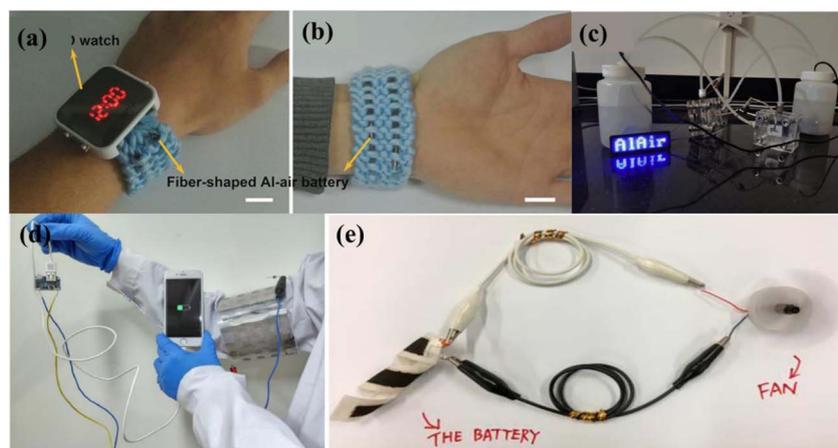

Fig. 18 Demonstration pictures of commercial LED watch operated by cabled-Al–air batteries woven into fabric from (a) front and (b) back side.[187] (c) Use of aqueous Al–air battery with circulating electrolyte.[260] (d) AGE-based flexible wearable Al–air battery showing the potential to charge a mobile phone.[243] (e) Ultrathin paper-based battery for powering a fan.[237]

showing 'Al–air' is shown in Fig. 18(c). 3-D printed ultrathin batteries can also be useful for portable purposes, as discussed in Section 7.[236–239] The charging of mobile phones and working of a small fan were also demonstrated using polymer-based flexible batteries (see Fig. 18(d) and (e)).[237,243] These applications demonstrate the versatility and potential of Al–air battery systems for a wide range of portable and strategic applications, including flexible platforms.

10.   Challenges and future prospects

Al–air batteries exhibit significant promise as energy storage systems with high energy density. By looking at the available literature, their practical application is impeded by a range of scientific and engineering obstacles. Thus, to effectively tackle these issues, it is imperative to undertake comprehensive research endeavors that encompass several fields such as materials science, electrochemistry, design, and sustainability. The basic challenges associated with Al–air batteries and corresponding prospects are summarized in Fig. 19. These challenges begin with aluminum corrosion and passivation, necessitating effective strategies to mitigate corrosion and improve the durability of aluminum anodes. This involves exploring novel materials, coatings, and surface treatments to protect the aluminum anodes from corrosion while maintaining electrochemical activity.

The maintenance of electrolyte stability is crucial for ensuring the optimal functioning of Al–air batteries. However, the process of battery discharging can lead to electrolyte dissolution, evaporation, and side reactions, potentially impacting the performance and safety. Resolving these concerns requires advancements in stable formulations and additives for electrolyte systems. Additionally, understanding the electrolyte degradation mechanisms and developing electrolytes with enhanced stability, conductivity, and compatibility with aluminum anodes are essential research areas. For example, stopping the reaction when required, given that in the non-operating stage it continues to corrode the anode. Al–air batteries depend on uninterrupted oxygen provision from the surrounding atmosphere to maintain their ORR activity. However, controlling the oxygen diffusion and airflow poses significant challenges, particularly in sealed systems. The ingress of CO_2 from the atmosphere can deteriorate the battery activity, leading to the formation of insoluble carbonates in alkaline electrolyte, hindering the ionic conductivity and decreasing the power efficiency. Purging of pure oxygen in the battery can mitigate this issue by integrating the suitable design; however, it may increase the battery weight and may require a complicated battery management system. Further, incorporating neutral pH electrolytic media can be beneficial, reducing the likelihood of carbonate formation. Thus, research efforts should be aimed at enhancing the oxygen utilization
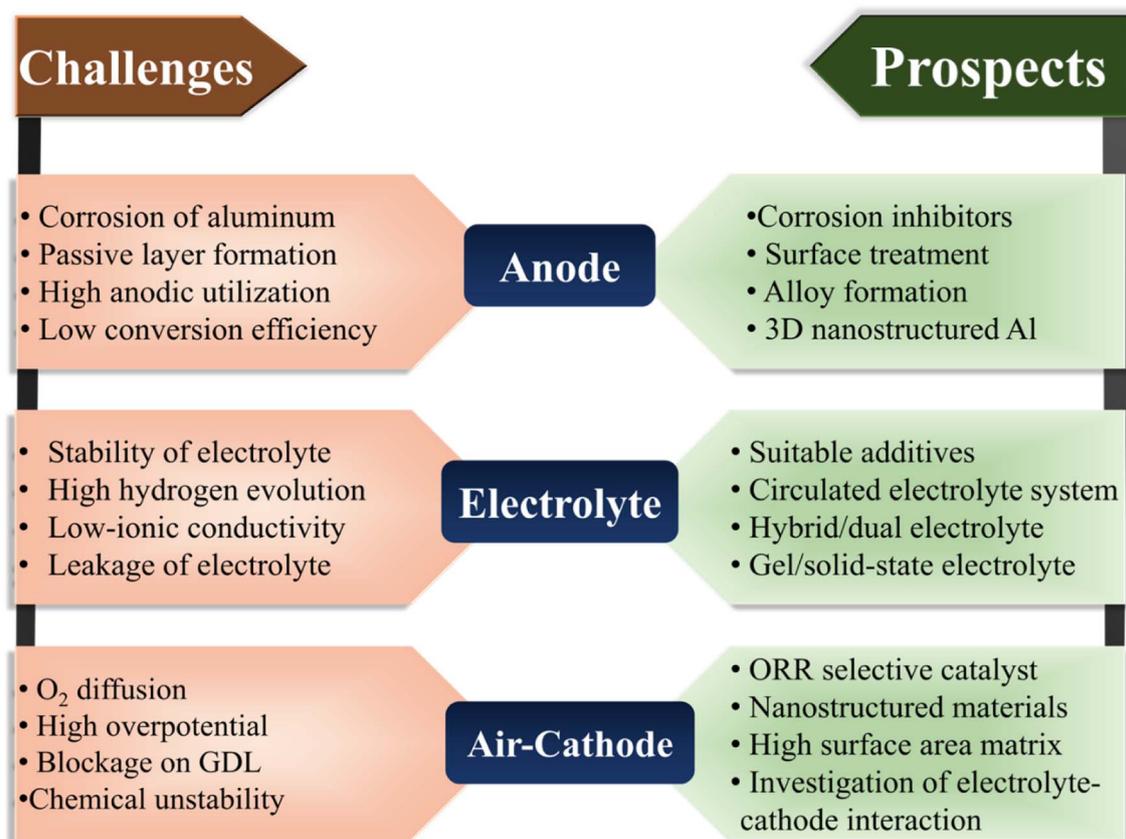

Fig. 19   Challenges and prospects related to Al–air battery.

efficiency and preventing impurities and CO_2 dissolution, which is crucial for optimizing the Al–air battery performance. This entails the development of novel air-breathing structures and diffusion layers, and the investigation of sophisticated ventilation methodologies. Achieving optimal efficiency and stability in both anode and cathode materials is essential for the overall Al–air battery performance. Significant challenges persist in developing appropriate catalysts and electrode designs, particularly in the creation of sophisticated air-cathode materials with improved electrochemical characteristics and stability. Research efforts are required to investigate novel catalyst materials, develop nanostructured electrode structures, and understand the kinetics involved in electrode reactions.

To better understand the electrochemical reactions, conventional pre- and post-discharge analysis is performed to understand the reaction mechanism. However, these measurements only provide indirect information, which will not assist in the comprehensive understanding of the changes occurring during the discharge processes. The characteristics of the catalysts are complex and can vary under real electrochemical conditions. In this case, *in situ* measurements can be helpful. There are some reports in the literature based on lithium– and zinc–air batteries related to *in situ* operation such as *in situ* XRD, *in situ* Raman, and XPS, providing a better understanding of the reaction mechanism and microscopic changes in different charge/discharge states.[261,262] Operando XRD can highlight the activity of the metal–air battery by monitoring the ORR process by the detection of the adsorption of oxygen intermediates, resulting in different Al-crystallographic phases.[263] Similarly, *in situ* Raman measurements will also be beneficial with less limitations to check the structural changes and provide details of the interfaces during the discharge/charge process, especially to check the formation of carbonates and any anode surface degradation while interacting with the electrolyte.[264] The same strategies of *in situ* measurements can also be applied to Al–air batteries to overcome the limitations and to control the reaction parameters for both primary (non-rechargeable) and secondary (rechargeable) Al–air batteries.

The goal of sustainability in Al–air batteries necessitates the resolution of obstacles pertaining to the recycling and ecological implications associated with aluminum anodes and electrolyte components. Thus, further investigation is required to establish effective recycling methodologies for the retrieval of aluminum and the regeneration of the electrolyte. Furthermore, it is crucial to evaluate the ecological consequences of Al–air batteries and devise approaches for their sustainable disposal at the end of their lifespan, consequently avoiding new environmental problems, while solving the existing ones.

11. Conclusions

The fast depletion of fossil fuels and increasing demand for energy make it necessary to look for green energy solutions. The developed solution, in terms of an energy storage system, LIB, is also not abundant and easily recyclable. In contrast to LIB, the Al–air battery shows potential among the metal–air batteries and worth exploring due to its availability, mining, and

recycling processes. The global market revenue crossed more than 272 million US$ in 2022.[265–267] Continuous efforts are required to resolve the existing problems, such as aluminum corrosion. The use of a polymer gel-like electrolyte has the potential to provide excellent conductivity, which can reach as high as that of aqueous electrolytes, and simultaneously avoid leakage issues. The liquid-based electrolyte systems are suitable for smart grid systems, providing excellent capacity. Different catalysts are employed to increase the ORR activity, and it is essential to look for catalysts with a high half-wave potential. Currently, only MnO_2 has shown promising catalytic activity and the potential to replace noble-metal electrocatalysts. Further, the active sites can be increased by combining them with carbonaceous materials. For its proper commercialization, more understanding of its kinetics is required. Besides, the structural design of the Al–air cell also requires work because its performance does not increase linearly with scaling the battery geometries. An appropriate design is essential to achieve the maximum performance of the Al–air battery, together with mitigating the associated challenges. Thus, the work has different scopes, including materials science, electrochemistry, and innovative designs. This article provided the current status of Al–air cells with microscopic details about their probable electrochemical process for a better understanding and will pave the way for further developments.

Conflicts of interest

There are no conflicts to declare.

Acknowledgements

References

1 H. Chen, T. N. Cong, W. Yang, C. Tan, Y. Li and Y. Ding, *Prog. Nat. Sci.*, 2009, **19**, 291–312.

2 T. M. Gür, *Energy Environ. Sci.*, 2018, **11**, 2696–2767.

3 D. Larcher and J.-M. Tarascon, *Nat. Chem.*, 2015, **7**, 19–29.

4 Q. Li, Y. Liu, S. Guo and H. Zhou, *Nano Today*, 2017, **16**, 46–60.

5 T. S. Mathis, N. Kurra, X. Wang, D. Pinto, P. Simon and Y. Gogotsi, *Adv. Energy Mater.*, 2019, **9**(39), 1902007.

6 C. Liu, F. Li, L. Ma and H. Cheng, *Adv. Mater.*, 2010, **22**(8), E28–E62.

7 T. A. Faunce, J. Prest, D. Su, S. J. Hearne and F. Iacopi, *MRS Energy Sustain.*, 2018, **5**, 10.

8 H. S. Das, M. M. Rahman, S. Li and C. W. Tan, *Renewable Sustainable Energy Rev.*, 2020, **120**, 109618.

9 A. Dixit, *Soc. Mater. Chem.*, 2020, **10**, 151–166.

10 J. K. Yadav, B. Rani, A. Tiwari and A. Dixit, *J. Renewable Sustainable Energy*, 2024, **16**(1), 014101.

11 P. Saini, B. Rani, J. K. Yadav, P. Choudhary, P. Sahoo and A. Dixit, *Advances in Sustainability Science and Technology*, Springer, Singapore, 2024, vol. 1, pp. 125–136.

12 S. Shaheen Shah, S. M. Abu Nayem, N. Sultana, A. J. Saleh Ahammad and Md. Abdul Aziz, *ChemSusChem*, 2022, **15**(1), e202101282.

13 J. K. Yadav, B. Rani and A. Dixit, *Ionics*, 2023, **29**, 1497–1506.

14 R. Sharma, H. Kumar, G. Kumar, S. Sharma, R. Aneja, A. K. Sharma, R. Kumar and P. Kumar, *Chem. Eng. J.*, 2023, **468**, 143706.

15 N. Nakamura, S. Ahn, T. Momma and T. Osaka, *SSRN Electron. J.*, 2023, **558**, 232566.

16 J. K. Yadav, B. Tiwari and A. Dixit, *Advances in Sustainability Science and Technology*, Springer, Singapore, 2024, 1, pp. 35–47.

17 Y. Liang, H. Dong, D. Aurbach and Y. Yao, *Nat. Energy*, 2020, **5**, 646–656.

18 J. Xie and Q. Zhang, *Small*, 2019, **15**(15), 1805061.

19 T. He, X. Kang, F. Wang, J. Zhang, T. Zhang and F. Ran, *Materials Science and Engineering R*, 2023, **154**, 100737.

20 J. K. Yadav, B. Rani and A. Dixit, *Advances in Sustainability Science and Technology*, Springer, Singapore, 2024, 1, pp. 103–113.

21 J. B. Goodenough, *J. Solid State Electrochem.*, 2012, **16**, 2019–2029.

22 P. Li, S. Luo, L. Zhang, Q. Liu, Y. Wang, Y. Lin, C. Xu, J. Guo, P. Cheali and X. Xia, *J. Energy Chem.*, 2024, **89**, 144–171.

23 J. K. Yadav, B. Rani and A. Dixit, *J. Power Sources*, 2023, **567**, 232943.

24 Y. Sun, *Highl. Sci. Eng. Technol.*, 2023, **58**, 365–370.

25 S. Rana, R. Kumar and R. S. Bharj, *Chem. Eng. J.*, 2023, **463**, 142336.

26 D. Zhang, H. Zhao, F. Liang, W. Ma and Y. Lei, *J. Power Sources*, 2021, **493**, 229722.

27 J. Deng, S. Fang, Y. Fang, Q. Hao, L. Wang and Y. H. Hu, *Catal. Today*, 2023, **409**, 2–22.

28 T. Li, M. Huang, X. Bai and Y.-X. Wang, *Prog. Nat. Sci.: Mater. Int.*, 2023, **33**, 151–171.

29 Q. Liu, Z. Pan, E. Wang, L. An and G. Sun, *Energy Storage Mater.*, 2020, **27**, 478–505.

30 F. Wu, C. Wang, K. Liao and Z. Shao, *Energy Fuels*, 2023, **37**, 8902–8918.

31 Y. Chen, J. Xu, P. He, Y. Qiao, S. Guo, H. Yang and H. Zhou, *Sci. Bull.*, 2022, **67**, 2449–2486.

32 W. Shao, R. Yan, M. Zhou, L. Ma, C. Roth, T. Ma, S. Cao, C. Cheng, B. Yin and S. Li, *Electrochem. Energy Rev.*, 2023, **6**, 11.

33 D. Zindani, G. Das, V. Bhagwat and G. Singh, *Mater. Today: Proc.*, 2023, **72**, 2315–2321.

34 G. Girishkumar, B. McCloskey, A. C. Luntz, S. Swanson and W. Wilcke, *J. Phys. Chem. Lett.*, 2010, **1**, 2193–2203.

35 Y. Ding, Y. Li and Z. Wu, *Battery Energy*, 2023, **2**(2), 20220014.

36 T. Bai, D. Li, S. Xiao, F. Ji, S. Zhang, C. Wang, J. Lu, Q. Gao and L. Ci, *Energy Environ. Sci.*, 2023, **16**, 1431–1465.

37 T. Liu, S. Zhao, Q. Xiong, J. Yu, J. Wang, G. Huang, M. Ni and X. Zhang, *Adv. Mater.*, 2023, **35**(20), 2208925.

38 A. Kondori, M. Esmaeilirad, A. M. Harzandi, R. Amine, M. T. Saray, L. Yu, T. Liu, J. Wen, N. Shan, H.-H. Wang, A. T. Ngo, P. C. Redfern, C. S. Johnson, K. Amine, R. Shahbazian-Yassar, L. A. Curtiss and M. Asadi, *Science*, 2023, **379**, 499–505.

39 B. Huang, W. Zhang, J. Chen, Y. Cui, C. Zhu and S. Yan, *J. Electrochem. Soc.*, 2023, **170**, 020506.

40 Z. Gao, I. Temprano, J. Lei, L. Tang, J. Li, C. P. Grey and T. Liu, *Adv. Mater.*, 2023, **35**(1), 2201384.

41 K. Chen, D.-Y. Yang, G. Huang and X.-B. Zhang, *Acc. Chem. Res.*, 2021, **54**, 632–641.

42 K. W. Leong, Y. Wang, M. Ni, W. Pan, S. Luo and D. Y. C. Leung, *Renewable Sustainable Energy Rev.*, 2022, **154**, 111771.

43 Z. Zhu, T. Jiang, M. Ali, Y. Meng, Y. Jin, Y. Cui and W. Chen, *Chem. Rev.*, 2022, **122**, 16610–16751.

44 N.-Q. Meng, Y.-X. Fan and J.-S. Cai, *Tungsten*, 2024, **6**, 164–173.

45 A. Kundu, T. Kuila, N. C. Murmu, P. Samanta and S. Das, *Mater. Horiz.*, 2023, **10**, 745–787.

46 A. Iqbal, O. M. El-Kadri and N. M. Hamdan, *J. Energy Storage*, 2023, **62**, 106926.

47 W. Li, L. Cheng, X. Chen, Y. Liu, Y. Liu, Q. Liu and Y. Huang, *Nano Energy*, 2023, **106**, 108039.

48 R. D. McKerracher, C. Ponce de Leon, R. G. A. Wills, A. A. Shah and F. C. Walsh, *ChemPlusChem*, 2015, **80**, 323–335.

49 N. Chawla, *Mater. Today Chem.*, 2019, **12**, 324–331.

50 G. Mirmoghtadaei, M. Mehrpooya, M. Mahmoudi and M. R. Ganjali, *Energy Convers. Manage.*, 2023, **290**, 117213.

51 J. Tu, W.-L. Song, H. Lei, Z. Yu, L.-L. Chen, M. Wang and S. Jiao, *Chem. Rev.*, 2021, **121**, 4903–4961.

52 T. Wang, H. Cheng, Z. Li, Y. Lu, Y. Li, Z. Wang and Z. Tian, *J. Power Sources*, 2023, **579**, 233294.

53 R. Zhu, G. Xu, G. Shao and Z. Wang, *ACS Appl. Energy Mater.*, 2024, 7(6), 2120–2128.

54 C. Lv, Y. Li, Y. Zhu, Y. Zhang, J. Kuang, D. Huang, Y. Tang and H. Wang, *Chem. Eng. J.*, 2023, **462**, 142182.

55 B. Rani, J. K. Yadav and A. Dixit, *Advances in Sustainability Science and Technology*, Springer, Singapore, 2024, 1, pp. 91–101.

56 C. Xu, X. Liu, O. Suminska-Ebersoldt and S. Passerini, *Batteries Supercaps*, 2024, DOI: **10.1002/batt.202300590.**

57 S. Islam, S. M. A. Nayem, A. Anjum, S. Shaheen Shah, A. J. S. Ahammad and M. A. Aziz, *Chem. Rec.*, 2024, **24**(1), e202300017.

58 G. A. Elia, K. V. Kravchyk, M. V. Kovalenko, J. Chacón, A. Holland and R. G. A. Wills, *J. Power Sources*, 2021, **481**, 228870.

59 A. Jaradat, C. Zhang, S. K. Singh, J. Ahmed, A. Ahmadiparidari, L. Majidi, S. Rastegar, Z. Hemmat, S. Wang, A. T. Ngo, L. A. Curtiss, M. Daly, A. Subramanian and A. Salehi-khojin, *Small*, 2021, **17**(42), 2102072.

60 P. Mao, H. Arandiyan, S. S. Mofarah, P. Koshy, C. Pozo-Gonzalo, R. Zheng, Z. Wang, Y. Wang, S. K. Bhargava, H. Sun, Z. Shao and Y. Liu, *Energy Adv.*, 2023, **2**, 465–502.

61 D. Zhong, K. Wang, Y. Zuo, M. Wei, J. Xiong, H. Wang, P. Zhang, N. Shang, Z. Chen and P. Pei, *J. Mater. Chem. A*, 2023, **11**, 25115–25135.

62 P. Katsoufis, V. Mylona, C. Politis, G. Avgouropoulos and P. Lianos, *J. Power Sources*, 2020, **450**, 227624.

63 A. I. Ikeuba, P. C. Iwuji, I.-I. E. Nabuk, O. E. Obono, D. Charlie, A. A. Etim, B. I. Nwabueze and J. Amajama, *J. Solid State Electrochem.*, 2024, DOI: 10.1007/s10008-024-05866-x.

64 X. Zhao, J. Chen, Z. Bi, S. Chen, L. Feng, X. Zhou, H. Zhang, Y. Zhou, T. Wågberg and G. Hu, *Adv. Sci.*, 2023, **10**(8), 2205889.

65 Z. He, F. Xiong, S. Tan, X. Yao, C. Zhang and Q. An, *Mater. Today Adv.*, 2021, **11**, 100156.

66 S. Zaromb, *J. Electrochem. Soc.*, 1962, **109**, 1125.

67 F. Ambroz, T. J. Macdonald and T. Nann, *Adv. Energy Mater.*, 2017, **7**(15), 1602093.

68 F. Wu, H. Yang, Y. Bai and C. Wu, *Adv. Mater.*, 2019, **21**(16), 1806510.

69 E. Zhang, W. Cao, B. Wang, X. Yu, L. Wang, Z. Xu and B. Lu, *Energy Storage Mater.*, 2018, **11**, 91–99.

70 https://phinergy.com.

71 https://www.alcoa.com.

72 M. Jiang, C. Fu, P. Meng, J. Ren, J. Wang, J. Bu, A. Dong, J. Zhang, W. Xiao and B. Sun, *Adv. Mater.*, 2022, **34**(26), 2204460.

73 T. Leisegang, F. Meutzner, M. Zschornak, W. Münchgesang, R. Schmid, T. Nestler, R. A. Eremin, A. A. Kabanov, V. A. Blatov and D. C. Meyer, *Front. Chem.*, 2019, **7**, 268.

74 S. M. A. Nayem, S. Islam, M. Mohamed, S. Shaheen Shah, A. J. S. Ahammad and M. A. Aziz, *Chem. Rec.*, 2024, **24**(1), e202300005.

75 https://www.webofscience.com.

76 L. Bockstie, D. Trevethan and S. Zaromb, *J. Electrochem. Soc.*, 1963, **110**, 267.

77 M. C. Reboul, P. Gimenez and J. J. Rameau, *CORROSION*, 1984, **40**, 366–371.

78 N. M. Marković, H. A. Gasteiger and P. N. Ross, *J. Phys. Chem.*, 1996, **100**, 6715–6721.

79 J. Bernard, M. Chatenet and F. Dalard, *Electrochim. Acta*, 2006, **52**, 86–93.

80 E. Tan, P. G. Mather, A. C. Perrella, J. C. Read and R. A. Buhrman, *Phys. Rev. B: Condens. Matter Mater. Phys.*, 2005, **71**, 161401.

81 L. Zhang, L. Chen, H. Luo, X. Zhou and Z. Liu, *Adv. Energy Mater.*, 2017, **7**(15), 1700034.

82 X. Zhao, X. Niu, J. Wang, D. Yin and C. Yao, *ECS J. Solid State Sci. Technol.*, 2017, **6**, P618–P625.

83 S. Wang, S. Jiao, W.-L. Song, H.-S. Chen, J. Tu, D. Tian, H. Jiao, C. Fu and D.-N. Fang, *Energy Storage Mater.*, 2018, **12**, 119–127.

84 Y. Zhang, S. Liu, Y. Ji, J. Ma and H. Yu, *Adv. Mater.*, 2018, **30**(38), 1706310.

85 A. Kumar Sharma, R. Bhandari, A. Aherwar, R. Rimašauskienė and C. Pinca-Bretotean, *Mater. Today: Proc.*, 2020, **26**, 2419–2424.

86 K. Zhang, K. O. Kirlikovali, J. M. Suh, J.-W. Choi, H. W. Jang, R. S. Varma, O. K. Farha and M. Shokouhimehr, *ACS Appl. Energy Mater.*, 2020, **3**, 6019–6035.

87 C. Vargel, in *Corrosion of Aluminium*, Elsevier, 2020, pp. 3–6.

88 Y.-S. Lee and M. Yoshio, *Electrochem. Solid-State Lett.*, 2001, **4**, A85.

89 D. Ye, B. Luo, G. M. Lu and L. Wang, *Sci. Bull.*, 2015, **60**, 1042–1044.

90 C. Lv, Y. Li, Y. Zhu, Y. Zhang, J. Kuang, Q. Zhao, Y. Tang and H. Wang, *Adv. Sci.*, 2023, **10**(29), 2304214.

91 R. Buckingham, T. Asset and P. Atanassov, *J. Power Sources*, 2021, **498**, 229762.

92 D. Ma, D. Yuan, C. Ponce de León, Z. Jiang, X. Xia and J. Pan, *Energy Environ. Mater.*, 2023, **6**(1), e12301.

93 S. Vincent, D. R. Peshwe, B. S. Murty and J. Bhatt, *J. Non-Cryst. Solids*, 2011, **357**, 3495–3499.

94 Y. Liu, Q. Sun, W. Li, K. R. Adair, J. Li and X. Sun, *Green Energy Environ.*, 2017, **2**, 246–277.

95 J. Zhu, S. Xu, J. Wu, Y. Yin, S. Cheng, C. Zhang, Y. Qiang and W. Wang, *J. Power Sources*, 2024, **593**, 233957.

96 A. A. Vostrikov, O. N. Fedyaeva, I. I. Fadeeva and M. Y. Sokol, *Russ. J. Phys. Chem. B*, 2010, **4**, 1051–1060.

97 T. Srinivasulu, K. Saritha and K. T. R. Reddy, *Mod. Electron. Mater.*, 2017, **3**, 76–85.

98 Y. Yang, A. Kushima, W. Han, H. Xin and J. Li, *Nano Lett.*, 2018, **18**, 2492–2497.

99 J. Ma, J. Wen, Q. Li and Q. Zhang, *Int. J. Hydrogen Energy*, 2013, **38**, 14896–14902.

100 A. S. Ivanova, *Kinet. Catal.*, 2012, **53**, 425–439.

101 R. K. Gupta, *Metal–Air Batteries*, CRC Press, Boca Raton, 2023.

102 F. Cheng and J. Chen, *Chem. Soc. Rev.*, 2012, **41**, 2172.

103 Z. Luo, L. Yin, L. Xiang, T. X. Liu, Z. Song, Y. Li, L. Zhou, K. Luo, K. Wu and J. Jiang, *Appl. Surf. Sci.*, 2021, **564**, 150474.

104 M. Wang, A. C. Meng, J. Fu, A. C. Foucher, R. Serra-Maia, E. A. Stach, E. Detsi and J. H. Pikul, *ACS Appl. Mater. Interfaces*, 2021, **13**, 13097–13105.

105 E. S. Davydova, I. N. Atamanyuk, A. S. Ilyukhin, E. I. Shkolnikov and A. Z. Zhuk, *J. Power Sources*, 2016, **306**, 329–336.

106 Z. Zhang, L. Xiong, S. Wang, Y. Xie, W. You and X. Du, *J. Power Sources*, 2023, **580**, 233375.

107 Y. Liu, F. Zhan, B. Wang, B. Xie, Q. Sun, H. Jiang, J. Li and X. Sun, *ACS Appl. Mater. Interfaces*, 2019, **11**, 21526–21535.

108 X. Gao and X. Qin, *Fullerenes, Nanotubes Carbon Nanostruct.*, 2018, **26**, 111–115.

109 M. F. Gaele and T. M. Di Palma, *Energy Fuels*, 2022, **36**, 12875–12895.

110 A. P. Atencio, J. R. Aviles, M. L. Montero, D. González-Flores and P. Ocón, *Energy Fuels*, 2022, **36**, 2851–2860.

111 J. Zhang, M. Klasky and B. C. Letellier, *J. Nucl. Mater.*, 2009, **384**, 175–189.

112 S. Wu, Q. Zhang, D. Sun, J. Luan, H. Shi, S. Hu, Y. Tang and H. Wang, *Chem. Eng. J.*, 2020, **383**, 123162.

113 B. J. Hopkins and D. R. Rolison, *Energy Fuels*, 2021, **2**, 1595–1599.

114 A. A. Mohamad, *Corros. Sci.*, 2008, **50**, 3475–3479.

115 Y. Huang, W. Shi, L. Guo, Q. Zhang, K. Wang, X. Zheng, C. Verma and Y. Qiang, *J. Power Sources*, 2023, **564**, 232866.

116 W. Yu, W. Shang, P. Tan, B. Chen, Z. Wu, H. Xu, Z. Shao, M. Liu and M. Ni, *J. Mater. Chem. A*, 2019, **7**, 26744–26768.

117 Z. Huang, J. Wang, Y. Peng, C. Jung, A. Fisher and X. Wang, *Adv. Energy Mater.*, 2017, **7**(23), 1700544.

118 T. Vo, J. Gao and Y. Liu, *Adv. Funct. Mater.*, 2024, DOI: **10.1002/adfm.202314282**.

119 C. Alegre, C. Busacca, A. Di Blasi, O. Di Blasi, A. S. Aricò, V. Antonucci and V. Baglio, *Mater. Today Energy*, 2020, **18**, 100508.

120 Q. Zhao, H. Yu, L. Fu, P. Wu, Y. Li, Y. Li, D. Sun, H. Wang and Y. Tang, *Sustainable Energy Fuels*, 2023, **7**, 1353–1370.

121 A. K. U, A. Sethi, R. M. Lawrence and V. M. Dhavale, *Int. J. Hydrogen Energy*, 2021, **46**, 34701–34712.

122 H. Liu, Y. Cao, F. Wang and Y. Huang, *ACS Appl. Mater. Interfaces*, 2014, **6**, 819–825.

123 J. Masa, C. Batchelor-McAuley, W. Schuhmann and R. G. Compton, *Nano Res.*, 2014, **7**, 71–78.

124 Y. Zhang, L. Yin, Z. Luo, X. Zhuge, P. Wei, Z. Song and K. Luo, *Sustainable Energy Fuels*, 2023, **7**, 3276–3283.

125 S. Zhang, Y. Zhang, W. Jiang, X. Liu, S. Xu, R. Huo, F. Zhang and J.-S. Hu, *Carbon*, 2016, **107**, 162–170.

126 H. Yuan, J. Li, W. Yang, Z. Zhuang, Y. Zhao, L. He, L. Xu, X. Liao, R. Zhu and L. Mai, *ACS Appl. Mater. Interfaces*, 2018, **10**, 16410–16417.

127 Y. Jiao, Y. Zheng, M. Jaroniec and S. Z. Qiao, *J. Am. Chem. Soc.*, 2014, **136**, 4394–4403.

128 C. Prakash, P. Sahoo, R. Yadav, A. Pandey, V. K. Singh and A. Dixit, *Int. J. Hydrogen Energy*, 2023, **48**, 21969–21980.

129 Z. Xia, Y. Zhu, W. Zhang, T. Hu, T. Chen, J. Zhang, Y. Liu, H. Ma, H. Fang and L. Li, *J. Alloys Compd.*, 2020, **824**, 153950.

130 M. Sharma, Y. Yadav, C. Prakash, V. K. Singh and A. Dixit, *Advances in Sustainability Science and Technology*, Springer, Singapore, 2024, 1, pp. 275–285.

131 V. K. Singh, U. T. Nakate, P. Bhuyan, J. Chen, D. T. Tran and S. Park, *J. Mater. Chem. A*, 2022, **10**, 9067–9079.

132 R. N. Mutlu and B. Yazıcı, *J. Solid State Electrochem.*, 2019, **23**, 529–541.

133 A. V. Ilyukhina, A. Z. Zhuk, B. V. Kleymenov, A. S. Ilyukhin and M. Nagayama, *Fuel Cells*, 2016, **16**, 384–394.

134 A. P. Sinha, T. S. Thomas and D. Mandal, *Energy Storage Mater.*, 2023, **63**, 102988.

135 Z. Moghadam, M. Shabani-Nooshabadi and M. Behpour, *J. Mol. Liq.*, 2017, **242**, 971–978.

136 Q. Zhao, C. Guo, K. Niu, J. Zhao, Y. Huang and X. Li, *J. Mater. Res. Technol.*, 2021, **12**, 1350–1359.

137 Y. Liu, Z. Wang and W. Ke, *Corros. Sci.*, 2014, **80**, 169–176.

138 S. Linjee, S. Moonngam, P. Klomjit, N. S. Pålsson and C. Banjongprasert, *Energy Rep.*, 2022, **8**, 5117–5128.

139 J. Ren, C. Fu, Q. Dong, M. Jiang, A. Dong, G. Zhu, J. Zhang and B. Sun, *ACS Sustain. Chem. Eng.*, 2021, **9**, 2300–2308.

140 **https://cdn.standards.iteh.ai/samples/98782/ f18b88e4ddba40688b024652c808b257/ASTM-G1-03-2017**.

141 **https://www.academia.edu/download/59140879/ ASTM_G1_Standard_Practice20190506-21457-11wqwjt.pdf**.

142 B. Rani, J. K. Yadav, P. Saini, A. P. Pandey and A. Dixit, *Energy Storage*, 2024, **6**(1), e586.

143 M. Pino, C. Cuadrado, J. Chacón, P. Rodríguez, E. Fatás and P. Ocón, *J. Appl. Electrochem.*, 2014, **44**, 1371–1380.

144 M. Pino, J. Chacón, E. Fatás and P. Ocón, *J. Power Sources*, 2015, **299**, 195–201.

145 S. Palanisamy, N. Rajendhran, S. Srinivasan, A. P. Shyma, V. Murugan, B. Parasuraman and S. Kheawhom, *J. Appl. Electrochem.*, 2021, **51**, 345–356.

146 W. Zhang, T. Hu, T. Chen, X. Yang, Y. Zhu, T. Yang and L. Li, *Processes*, 2022, **10**(2), 420.

147 H. Chen, H. Xu, B. Zheng, S. Wang, T. Huang, F. Guo, W. Gao and C. Gao, *ACS Appl. Mater. Interfaces*, 2017, **9**, 22628–22634.

148 P. Wu, S. Wu, D. Sun, Y. Tang and H. Wang, *Acta Metall. Sin. (Engl. Lett.)*, 2021, **34**, 309–320.

149 Z. Sun, H. Lu, L. Fan, Q. Hong, J. Leng and C. Chen, *J. Electrochem. Soc.*, 2015, **162**, A2116–A2122.

150 Z. Wu, H. Zhang, S. Tang, J. Zou, D. Yang, Y. Wang, K. Qin, C. Ban, J. Cui and H. Nagaumi, *Electrochim. Acta*, 2021, **370**, 137833.

151 X. Liu, P. Zhang, J. Xue, C. Zhu, X. Li and Z. Wang, *Chem. Eng. J.*, 2021, **417**, 128006.

152 M. Jingling, W. Jiuba, Z. Hongxi and L. Quanan, *J. Power Sources*, 2015, **293**, 592–598.

153 L. Fan, H. Lu, J. Leng, Z. Sun and C. Chen, *J. Electrochem. Soc.*, 2016, **163**, A8–A12.

154 Z. Wu, H. Zhang, K. Qin, J. Zou, K. Qin, C. Ban, J. Cui and H. Nagaumi, *J. Mater. Sci.*, 2020, **55**, 11545–11560.

155 J. Ren, J. Ma, J. Zhang, C. Fu and B. Sun, *J. Alloys Compd.*, 2019, **808**, 151708.

156 L. D. Chen, J. K. Nørskov and A. C. Luntz, *J. Phys. Chem. Lett.*, 2015, **6**, 175–179.

157 T. J. O'Keeke, in *Encyclopedia of Materials: Science and Technology*, Elsevier, 2001, pp. 7774–7781.

158 A. Eftekhari and P. Corrochano, *Sustainable Energy Fuels*, 2017, **1**, 1246–1264.

159 Y. Liu, F. Zhan, N. Zhao, Q. Pan, Z. Li, Y. Du and Y. Yang, *J. Mater. Sci.*, 2021, **56**, 3861–3873.

160 M. Jiang, C. Fu, J. Yang, Q. Liu, J. Zhang and B. Sun, *Energy Storage Mater.*, 2019, **18**, 34–42.

161 R. K. Gupta and T. A. Nguyen, *Energy from Waste*, CRC Press, Boca Raton, 2022.

162 L. Yang, Y. Wu, S. Chen, Y. Xiao, S. Chen, P. Zheng, J. Wang and J.-E. Qu, *Mater. Chem. Phys.*, 2021, **257**, 123787.

163 N. R. Levy, S. Lifshits, E. Yohanan and Y. Ein-Eli, *ACS Appl. Energy Mater.*, 2020, **3**, 2585–2592.

164 L. Fan, H. Lu and J. Leng, *Electrochim. Acta*, 2015, **165**, 22–28.

165 Y.-J. Cho, I.-J. Park, H.-J. Lee and J.-G. Kim, *J. Power Sources*, 2015, **277**, 370–378.

166 P. Wu, Q. Zhao, H. Yu, Z. Tang, Y. Li, D. Huang, D. Sun, H. Wang and Y. Tang, *Chem. Eng. J.*, 2022, **438**, 135538.

167 T. H. Pham, W.-H. Lee, J.-H. Byun and J.-G. Kim, *Energy Storage Mater.*, 2023, **55**, 406–416.

168 S. Hosseini, T.-H. Xu, S. Masoudi Soltani, T.-E. Ko, Y.-J. Lin and Y.-Y. Li, *Int. J. Hydrogen Energy*, 2022, **47**, 501–516.

169 X. Li, J. Li, D. Zhang, L. Gao, J. Qu and T. Lin, *J. Mol. Liq.*, 2021, **322**, 114946.

170 H. Yu, P. Wu, D. Sun, H. Wang and Y. Tang, *Ind. Eng. Chem. Res.*, 2022, **61**, 12632–12640.

171 M. Wei, K. Wang, P. Pei, Y. Zuo, L. Zhong, N. Shang, H. Wang, J. Chen, P. Zhang and Z. Chen, *Appl. Energy*, 2022, **324**, 119690.

172 L. Guo, Q. Zhang, Y. Huang, S. Kaya, X. Zheng, R. Zhang, W. Shi and I. B. Obot, *J. Electroanal. Chem.*, 2023, **941**, 117535.

173 L. Luo, C. Zhu, L. Yan, L. Guo, Y. Zhou and B. Xiang, *Chem. Eng. J.*, 2022, **450**, 138175.

174 C. Lv, Q. Zhang, Y. Zhang, Z. Yang, P. Wu, D. Huang, H. Li, H. Wang and Y. Tang, *Electrochim. Acta*, 2022, **417**, 140311.

175 P. Gan, D. Zhang, L. Gao, Z. Xin and X. Li, *Colloids Surf., A*, 2023, **670**, 131530.

176 M. Wei, K. Wang, L. Zhong, T. H. M. Pham, Y. Zuo, H. Wang, P. Zhang, Z. Chen, S. Zhao and P. Pei, *Energy Storage Mater.*, 2023, **60**, 102812.

177 M. Wei, K. Wang, L. Kang, Y. Zuo, L. Zhong, P. Zhang, S. Zhang, P. Pei and J. Chen, *J. Power Sources*, 2022, **545**, 231974.

178 M. Wei, K. Wang, Y. Zuo, L. Zhong, A. Züttel, Z. Chen, P. Zhang, H. Wang, S. Zhao and P. Pei, *Adv. Funct. Mater.*, 2023, **33**(37), 2302243.

179 R. Revel, T. Audichon and S. Gonzalez, *J. Power Sources*, 2014, **272**, 415–421.

180 D. Gelman, B. Shvartsev and Y. Ein-Eli, *Top. Curr. Chem.*, 2016, **374**, 82.

181 K. L. Ng, Z. Lu, Y. Wang, C. V. Singh and G. Azimi, *J. Phys. Chem. C*, 2021, **125**, 15145–15154.

182 S. Choi, H. Go, G. Lee and Y. Tak, *Phys. Chem. Chem. Phys.*, 2017, **19**, 8653–8656.

183 D. Gelman, B. Shvartsev and Y. Ein-Eli, *J. Mater. Chem. A*, 2014, **2**, 20237–20242.

184 Y. Wang, W. Pan, K. W. Leong, S. Luo, X. Zhao and D. Y. C. Leung, *Green Energy Environ.*, 2023, **8**, 1117–1127.

185 S. Liu, J. Ban, H. Shi, Z. Wu, G. Shao, G. Cao and J. Hu, *Chem. Eng. J.*, 2022, **431**(3), 134283.

186 R. Mori, *RSC Adv.*, 2019, **9**, 22220–22226.

187 Y. Xu, Y. Zhao, J. Ren, Y. Zhang and H. Peng, *Angew. Chem., Int. Ed.*, 2016, **55**, 7979–7982.

188 Q. Zhang, L. Guo, Y. Huang, R. Zhang, A. G. Ritacca, S. Leng, X. Zheng, Y. Yang and A. Singh, *J. Power Sources*, 2023, **564**, 232901.

189 X. Wang, W. Liu, Y. Jin, X. Xie and Z. Yang, *ChemElectroChem*, 2023, **10**(10), e202300017.

190 V.-L. Nguyen, M. Ohtaki, V. N. Ngo, M.-T. Cao and M. Nogami, *Adv. Nat. Sci.: Nanosci. Nanotechnol.*, 2012, **3**, 025005.

191 Y.-J. Wang, B. Fang, D. Zhang, A. Li, D. P. Wilkinson, A. Ignaszak, L. Zhang and J. Zhang, *Electrochem. Energy Rev.*, 2018, **1**, 1–34.

192 J. X. Wang, H. Inada, L. Wu, Y. Zhu, Y. Choi, P. Liu, W.-P. Zhou and R. R. Adzic, *J. Am. Chem. Soc.*, 2009, **131**, 17298–17302.

193 M. Shao, Q. Chang, J.-P. Dodelet and R. Chenitz, *Chem. Rev.*, 2016, **116**, 3594–3657.

194 C. Wang, H. Daimon, T. Onodera, T. Koda and S. Sun, *Angew. Chem.*, 2008, **120**, 3644–3647.

195 J. Wu, A. Gross and H. Yang, *Nano Lett.*, 2011, **11**, 798–802.

196 Y. Xia, Y. Xiong, B. Lim and S. E. Skrabalak, *Angew. Chem., Int. Ed.*, 2009, **48**, 60–103.

197 S. J. Hwang, S. J. Yoo, J. Shin, Y.-H. Cho, J. H. Jang, E. Cho, Y.-E. Sung, S. W. Nam, T.-H. Lim, S.-C. Lee and S.-K. Kim, *Sci. Rep.*, 2013, **3**, 1309.

198 V. Mazumder, M. Chi, K. L. More and S. Sun, *J. Am. Chem. Soc.*, 2010, **132**, 7848–7849.

199 Y. Zhang, C. Ma, Y. Zhu, R. Si, Y. Cai, J. X. Wang and R. R. Adzic, *Catal. Today*, 2013, **202**, 50–54.

200 H. M. Song, D. H. Anjum, R. Sougrat, M. N. Hedhili and N. M. Khashab, *J. Mater. Chem.*, 2012, **22**, 25003.

201 R. Mori, *Electrochem. Energy Rev.*, 2020, **3**, 344–369.

202 Q. Hong and H. Lu, *Sci. Rep.*, 2017, **7**, 3378.

203 J. Wang, A. Wu, L. Xing, S. Ran, W. Yu, X. Dong and H. Huang, *J. Energy Chem.*, 2023, **86**, 217–226.

204 A. K. Ipadeola, K. Eid and A. M. Abdullah, *Curr. Opin. Electrochem.*, 2023, **37**, 101198.

205 K. Li, R. Cheng, Q. Xue, T. Zhao, F. Wang and C. Fu, *ACS Appl. Mater. Interfaces*, 2023, **15**(7), 9150–9159.

206 S. Vasudevan, D. Swathi Tharani, M. Manickam and R. Sivasubramanian, *Dalton Trans.*, 2024, **53**, 3713–3721.

207 Z. Shui, W. Zhao, H. Xiao, L. Zhu, Y. Liu, X. Deng and X. Chen, *J. Power Sources*, 2022, **523**, 231028.

208 A. P. Pandey, M. A. Shaz, V. Sekkar and R. S. Tiwari, *Int. J. Hydrogen Energy*, 2023, **48**, 21404–21411.

209 N. Senthilkumar, Md. A. Aziz, M. Pannipara, A. T. Alphonsa, A. G. Al-Sehemi, A. Balasubramani and G. Gnana kumar, *Bioprocess Biosyst. Eng.*, 2020, **43**, 97–109.

210 A. P. Pandey, B. Rani, M. Sharma, J. K. Yadav, P. Saini, S. Shalu and A. Dixit, *Energy Storage*, 2024, **6**(1), e549.

211 Y. Luo, Y. Chen, Y. Xue, J. Chen, G. Wang, R. Wang, M. Yu and J. Zhang, *Small*, 2022, **18**(2), 2105594.

212 X. Meng, X. Zhang, J. Rageloa, Z. Liu and W. Wang, *J. Power Sources*, 2023, **567**, 232988.

213 K. Hu, X. Wang, Y. Hu, H. Hu, X. Lin, K. M. Reddy, M. Luo, H. J. Qiu and X. Lin, *ACS Nano*, 2022, **16**, 19165–19173.

214 Y. Liu, M. Chen, M. Shah and Z. Liu, *J. Electrochem. Soc.*, 2023, **170**, 060531.

215 S. P. Qin, Y. Wang, Y. C. Li, W. W. Zhang, B. Yao and X. Y. Zhang, *J. Mater. Res. Technol.*, 2023, **24**, 4379–4389.

216 X. Wang, Z. Li, L. Liu, J. Hu, H. Shen, R. Li, Z. Geng, Z. Jin and C. Wang, *New J. Chem.*, 2024, **48**, 2269–2279.

217 K. Liu, X. Ye, A. Zhang, X. Wang, T. Liang, Y. Fang, W. Zhang, K. Hu, X. Liu and X. Chen, *RSC Adv.*, 2024, **14**, 5184–5192.

218 W.-X. Hong, W.-H. Wang, Y.-H. Chang, H. Pourzolfaghar, I.-H. Tseng and Y.-Y. Li, *Nano Energy*, 2024, **121**, 109236.

219 J. Wang, A. Wu, Z. Qiu, A. Li, W. Qin and H. Huang, *Appl. Surf. Sci.*, 2023, **608**, 155185.

220 S. Jeong, S. Kim, H. Son and O. L. Li, *Catal. Today*, 2023, **420**, 114025.

221 S. Kim, H. Yang, S. Jeong, T. Lee, S. Chae, J. H. Lee and O. L. Li, *J. Power Sources*, 2023, **566**, 232923.

222 T. Hu, W. Zhang, Z. Xia, Y. Zhu, Y. Liu, J. Zhang and L. Li, *Int. J. Energy Res.*, 2022, **46**, 11174–11184.

223 K. Hu, X. Wang, Y. Hu, H. Hu, X. Lin, K. M. Reddy, M. Luo, H.-J. Qiu and X. Lin, *ACS Nano*, 2022, **16**, 19165–19173.

224 W.-W. Tian, J.-T. Ren and Z.-Y. Yuan, *Appl. Catal., B*, 2022, **317**, 121764.

225 T. H. Nguyen, P. K. L. Tran, D. T. Tran, T. N. Pham, N. H. Kim and J. H. Lee, *Chem. Eng. J.*, 2022, **440**, 135781.

226 T. He, Y. Chen, Q. Liu, B. Lu, X. Song, H. Liu, M. Liu, Y. Liu, Y. Zhang, X. Ouyang and S. Chen, *Angewandte Chemie International Edition*, 2022, **61**(27), e202201007.

227 L. Cui, K. Xiang, X. Kang, K. Zhi, L. Wang, J. Zhang, X.-Z. Fu and J.-L. Luo, *J. Colloid Interface Sci.*, 2022, **609**, 868–877.

228 A. Sumboja, B. Prakoso, Y. Ma, F. R. Irwan, J. J. Hutani, A. Mulyadewi, M. A. A. Mahbub, Y. Zong and Z. Liu, *Energy Mater. Adv.*, 2021, **2021**, 7386210.

229 S. Liu, Z. Cao, Y. Meng, Y. Li, W. Yang, Z. Chang, W. Liu and X. Sun, *ACS Appl. Mater. Interfaces*, 2021, **13**, 26853–26860.

230 D. Liu, J. Tian, Y. Tang, J. Li, S. Wu, S. Yi, X. Huang, D. Sun and H. Wang, *Chem. Eng. J.*, 2021, **406**, 126772.

231 M. Jiang, C. Fu, R. Cheng, T. Liu, M. Guo, P. Meng, J. Zhang and B. Sun, *Chem. Eng. J.*, 2021, **404**, 127124.

232 R. Cheng, F. Wang, M. Jiang, K. Li, T. Zhao, P. Meng, J. Yang and C. Fu, *ACS Appl. Mater. Interfaces*, 2021, **13**, 37123–37132.

233 L. Huang, W. Zang, Y. Ma, C. Zhu, D. Cai, H. Chen, J. Zhang, H. Yu, Q. Zou, L. Wu and C. Guan, *Chem. Eng. J.*, 2021, **421**, 129973.

234 G. Li, D. Yu, J. Song, F. Hu, L. Li and S. Peng, *Mater. Lett.*, 2021, **296**, 129890.

235 A. P. Atencio, J. R. Aviles, D. Bolaños, R. Urcuyo, M. L. Montero, D. González-Flores and P. Ocón, *Electrochem. Sci. Adv.*, 2022, **2**(4), e2100125.

236 Y. Wang, H. Y. H. Kwok, W. Pan, Y. Zhang, H. Zhang, X. Lu and D. Y. C. Leung, *J. Power Sources*, 2020, **450**, 227685.

237 Y. Wang, H. Y. H. Kwok, W. Pan, Y. Zhang, H. Zhang, X. Lu and D. Y. C. Leung, *Electrochim. Acta*, 2019, **319**, 947–957.

238 Y. Wang, W. Pan, H. Kwok, X. Lu and D. Y. C. Leung, *Energy Procedia*, 2019, **158**, 522–527.

239 L.-L. Shen, G.-R. Zhang, M. Biesalski and B. J. M. Etzold, *Lab Chip*, 2019, **19**, 3438–3447.

240 Y. Zuo, Y. Yu, J. Feng and C. Zuo, *Sci. Rep.*, 2022, **12**, 9801.

241 W. Pan, Y. Wang, H. Y. H. Kwok and D. Y. C. Leung, *Green Energy Environ.*, 2023, **8**, 757–766.

242 T. Phusittananan, W. Kao-Ian, M. T. Nguyen, T. Yonezawa, R. Pornprasertsuk, A. A. Mohamad and S. Kheawhom, *Front. Energy Res.*, 2020, **8**, 189, DOI: **10.3389/fenrg.2020.00189**.

243 P. Sun, J. Chen, Y. Huang, J.-H. Tian, S. Li, G. Wang, Q. Zhang, Z. Tian and L. Zhang, *Energy Storage Mater.*, 2021, **34**, 427–435.

244 B. J. Hopkins, Y. Shao-Horn and D. P. Hart, *Science*, 2018, **362**, 658–661.

245 R. Mori, *RSC Adv.*, 2017, **7**, 6389–6395.

246 P. Teabnamang, W. Kao-Ian, M. T. Nguyen, T. Yonezawa, R. Cheacharoen and S. Kheawhom, *Energies*, 2020, **13**(9), 2275.

247 L. Wang, R. Cheng, C. Liu, M. C. Ma, W. Wang, G. Yang, M. K. H. Leung, F. Liu and S. P. Feng, *Mater. Today Phys.*, 2020, **14**, 100242.

248 S. Yang, *J. Power Sources*, 2002, **112**, 162–173.

249 X. Zhang, S. H. Yang and H. Knickle, *J. Power Sources*, 2004, **128**, 331–342.

250 W. Liu, T. Placke and K. T. Chau, *Energy Rep.*, 2022, **8**, 4058–4084.

251 P. Patel and A. Bonshtien, *MRS Bull.*, 2014, **39**, 214–215.

252 J. Turienzo, J. F. Lampón, R. Chico-Tato and P. Cabanelas, *Emerald Insight*, 2022, **15**, 191–210.

253 https://www.iocphinergy.in/news/hindalco-phinergy-and-iop-to-partner-on-revolutionary-aluminium-air-batteries-for-evs-and-energy-storage.

254 https://www.hindalco.com/media/press-releases/hindalco-phinergy-and-iop–partner-revolutionary-aluminium-air-batteries-evs-and-energy-storage.

255 https://idstch.com/technology/energy/.

256 J. J. Kang, W. Yang, G. Dermody, M. Ghasemian, S. Adibi and P. Haskell-Dowland, *IEEE Access*, 2020, **8**, 201498–201515.

257 NATO, https://www.sto.nato.int/publications/STOTechnical Reports/STO-TR-SET-173-Part-I/$TR-SET-173-Part-I-ALL.pdf.

258 B. M. L. Rao, R. Cook, W. Kobasz and G. D. Deuchars, in *IEEE 35th International Power Sources Symposium*, IEEE, pp. 34–37.

259 G. Fotouhi, C. Ogier, J.-H. Kim, S. Kim, G. Cao, A. Q. Shen, J. Kramlich and J.-H. Chung, *J. Micromech. Microeng.*, 2016, **26**, 055011.

260 X. Zheng, T. Zhang, H. Yang, Q. Zheng, Y. Gao, Z. Liu, W. Wang and K. Wang, *Electrochim. Acta*, 2020, **354**, 136635.

261 K. P. C. Yao, D. G. Kwabi, R. A. Quinlan, A. N. Mansour, A. Grimaud, Y.-L. Lee, Y.-C. Lu and Y. Shao-Horn, *J. Electrochem. Soc.*, 2013, **160**, A824–A831.

262 J. Jacas Biendicho, D. Noréus, C. Offer, G. Svensson, R. I. Smith and S. Hull, *Front. Energy Res.*, 2018, **6**, 69.

263 H. Ji, M. Wang, S. Liu, H. Sun, J. Liu, T. Qian and C. Yan, *Energy Storage Mater.*, 2020, **27**, 226–231.

264 T. Wang, M. Kunimoto, T. Mori, M. Yanagisawa, J. Niikura, I. Takahashi, M. Morita, T. Abe and T. Homma, *J. Power Sources*, 2022, **533**, 231237.

265 https://reports.valuates.com/market-reports/QYRE-Auto-34U15640/global-and-india-aluminum-air-battery.

266 https://www.researchnester.com/reports/aluminum-air-battery-market/3341.

267 J. K. Yadav, B. Rani, P. Saini and A. Dixit, *Energy Adv.*, 2024, **3**, 927–944.